

Experimental study of turbulent flows through pipe bends

by

Athanasia Kalpakli

April 2012
Technical Reports from
Royal Institute of Technology
KTH Mechanics
SE-100 44 Stockholm, Sweden

Akademisk avhandling som med tillstånd av Kungliga Tekniska Högskolan i Stockholm framlägges till offentlig granskning för avläggande av teknologie licentiatexamen den 3 maj 2012 kl 10.15 i sal D3, Lindstedtsvägen 5, Kungliga Tekniska Högskolan, Stockholm.

©Athanasia Kalpakli 2012

Universitetsservice US-AB, Stockholm 2012

Athanasia Kalpakli 2012, **Experimental study of turbulent flows through pipe bends**

CCGEx & Linné Flow Centre, KTH Mechanics, Royal Institute of Technology SE-100 44 Stockholm, Sweden

Abstract

This thesis deals with turbulent flows in 90 degree curved pipes of circular cross-section. The flow cases investigated experimentally are turbulent flow with and without an additional motion, swirling or pulsating, superposed on the primary flow. The aim is to investigate these complex flows in detail both in terms of statistical quantities as well as vortical structures that are apparent when curvature is present. Such a flow field can contain strong secondary flow in a plane normal to the main flow direction as well as reverse flow.

The motivation of the study has mainly been the presence of highly pulsating turbulent flow through complex geometries, including sharp bends, in the gas exchange system of Internal Combustion Engines (ICE). On the other hand, the industrial relevance and importance of the other type of flows were not underestimated.

The geometry used was curved pipes of different curvature ratios, mounted at the exit of straight pipe sections which constituted the inflow conditions. Two experimental set ups have been used. In the first one, fully developed turbulent flow with a well defined inflow condition was fed into the pipe bend. A swirling motion could be applied in order to study the interaction between the swirl and the secondary flow induced by the bend itself. In the second set up a highly pulsating flow (up to 40 Hz) was achieved by rotating a valve located at a short distance upstream from the measurement site. In this case engine-like conditions were examined, where the turbulent flow into the bend is non-developed and the pipe bend is sharp. In addition to flow measurements, the effect of non-ideal flow conditions on the performance of a turbocharger was investigated.

Three different experimental techniques were employed to study the flow field. Time-resolved stereoscopic particle image velocimetry was used in order to visualize but also quantify the secondary motions at different downstream stations from the pipe bend while combined hot-/cold-wire anemometry was used for statistical analysis. Laser Doppler velocimetry was mainly employed for validation of the aforementioned experimental methods.

The three-dimensional flow field depicting varying vortical patterns has been captured under turbulent steady, swirling and pulsating flow conditions, for parameter values for which experimental evidence has been missing in literature.

Descriptors: Turbulent flow, swirl, pulsation, pipe bend, hot-wire anemometry, cold-wire anemometry, laser Doppler velocimetry, stereoscopic particle image velocimetry.

Preface

This licentiate thesis in fluid mechanics deals with turbulent flows, with and without a swirling or pulsating motion superposed on the primary flow, in 90° curved pipes. The results in this thesis are from experimental work. The thesis is divided into two parts, with Part I including an introduction on the flows under focus and their applications, an extended literature review as well as an experimental set ups and techniques section where the set ups used for the measurements in the present work are presented and the experimental methods employed are described. Part I ends with a section where the results and conclusions from this study are summarized and a section where the respondent's contributions to all papers are stated. Part II consists of five papers, three of which are published and one is in print but are here adjusted to be consistent with the overall thesis format. Paper 5 is at present an internal report but it is planned to be extended and submitted in the future.

April 2012, Stockholm

Athanasia Kalpakli

Contents

Abstract	iii
Preface	iv
Part I. Overview and summary	
Chapter 1. Introduction	1
1.1. Towards increased engine efficiency: can fundamental research help?	1
1.2. Complex flows in nature and technology	2
Chapter 2. Flows in curved pipes	6
2.1. Dean vortices in steady flow	8
2.1.1. Mean flow development	8
2.1.2. Vortex structure in turbulent flows	14
2.2. Swirling flow	17
2.3. Pulsating flow with and without curvature effects	19
2.3.1. Pulsating flow in straight pipes	19
2.3.2. Pulsating flow through curved channels	20
2.4. Summary of previous studies	24
2.5. Flow parameters	25
Chapter 3. Experimental set ups & techniques	30
3.1. The rotating pipe facility	30
3.2. The CICERO rig	33
3.3. Hot/Cold-Wire Anemometry (HWA/CWA)	35
3.3.1. Hot-wire calibration	38
3.3.2. Temperature compensation	38
3.4. Particle Image Velocimetry (PIV)	40
3.5. Laser Doppler Velocimetry (LDV)	48
3.6. Experimental methods for the study of complex flows	49

Chapter 4. Main contribution and conclusions	55
4.1. Highly pulsating turbulent flow downstream a pipe bend–statistical analysis	55
4.2. Secondary flow under pulsating turbulent flow	55
4.3. Secondary flow development	56
4.4. The effect of curved pulsating flow on turbine performance	56
4.5. The effect of a swirling motion imposed on the Dean vortices	56
Chapter 5. Papers and authors contributions	58
Acknowledgements	61
References	63
Part II. Papers	
Paper 1. Experimental investigation on the effect of pulsations through a 90 degrees pipe bend	73
Paper 2. Turbulent flows through a 90 degrees pipe bend at high Dean and Womersley numbers	89
Paper 3. Dean vortices in turbulent flows: rocking or rolling?	103
Paper 4. Experimental investigation on the effect of pulsations on exhaust manifold-related flows aiming at improved efficiency	109
Paper 5. POD analysis of stereoscopic PIV data from swirling turbulent flow through a pipe bend	125

Part I

Overview and summary

CHAPTER 1

Introduction

“Science cannot solve the ultimate mystery of nature. And that is because, in the last analysis, we ourselves are part of nature and therefore part of the mystery that we are trying to solve.”

Max Planck (1858–1947)

1.1. Towards increased engine efficiency: can fundamental research help?

The Internal Combustion Engine (ICE) is still the most common source for powering both light and heavy-duty road vehicles. With the increasing cost and decreasing availability of fossil fuels as well as increasing concerns of green house gases on the climate, a large focus has recently been set on increasing the efficiency of the IC engine without sacrificing performance. Similar concerns are relevant also for engines running on alternative fuels, such as bio-fuels.

The gas exchange system has a prominent role in the development towards more efficient engines, where downsizing is, at least for light duty vehicles, the name of the game. The gas exchange system should efficiently provide the intake of fresh air to the engine as well as utilizing the energy (heat) in the exhaust gases, where an important, if not crucial, component is the turbocharger. However, the gas exchange system is always a compromise between performance and what is possible from a packaging viewpoint, e.g. the piping system cannot be designed with straight smooth pipes, the manifolds have complex geometry resulting in non-ideal flow profiles etc. The design of such systems is usually made with rather simple one-dimensional models although one knows *a priori* that such models cannot give an accurate description of the flow dynamics. Testing in engine test benches together with empirical knowledge, rather than scientifically based experimentation, are also used to a large extent for developing the design. Although one should not downgrade the importance of the experienced engineer, as stated in Manley *et al.* (2008): *“The challenge of internal combustion require a broad collection of research discoveries to make the transition from hardware intensive, experienced based fuel development and engine design to simulation intensive, science-based design”*.

In the present work certain aspects of the gas exchange system are approached from a basic scientific, rather than an engine application, viewpoint. Three specific aspects have been addressed, namely the steady flow through curved pipes as well as the effects of swirl and pulsations on such flows, all features that are apparent within the gas exchange system. As it will be mentioned in the coming section, such

aspects on flows in piping systems are not only dominant in internal combustion engines, but also in a number of other flow systems, and quite some efforts have been done earlier, but with other motivations, to investigate such conditions. On the other hand the parameter ranges for the IC engine flows are quite specific and it is therefore necessary to make studies for the relevant values of the parameters. The present studies have been performed through idealized experiments, and the fact that the quote from Manley *et al.* (2008) states that one should strive towards simulation intensive methods, such methods also need qualified boundary data and verification through quantitative scientific experiments. The aim of the present study is therefore to allow the reader mainly interested in IC engines *per se* to realize that it is both important and rewarding to go outside the immediate neighborhood of the engine aspects to get a better understanding of the physical processes important for engine performance.

1.2. Complex flows in nature and technology

Natural phenomena including those initiated from the motion of fluids have been the subject of many scientific studies and even though the mechanisms which trigger them remain to a large extent a mystery, science has succeeded to answer some of the questions regarding their existence and define the parameters which govern their dynamics.

One of the subjects from the area of fluid dynamics which still constitutes a “mystery” and is of vital importance is pulsating flow, i.e. the flow composed of a steady and a periodic component. Pulsating flow is a part of our own being, since it is the condition under which the human body operates. For instance, the heart is probably the most well-known pump in nature, it creates a periodic motion and distributes the blood to the whole body with a specific frequency rate. That causes also the distinct “beating” sound when listening to our hearts through a stethoscope (figure 1.1).

One should however not neglect the importance of pulsatile flow in the functioning of mechanical systems which in return might not be of vital importance but contribute to our well-being and have changed the way we experience life, such as the engine in the cars we drive.

On the other side of the spectrum, if we look around us (from heat exchangers to river banks and the human aorta), almost nothing is straight and how could that be with the confined space we have been given to live in, therefore most of the systems of any kind (natural, biological, mechanical) comprise of curved sections and conduits (figure 1.2).

Luckily or not, in many cases, the two aforementioned conditions are combined (i.e. pulsatile flows through curved pipes) and they can lead to complex flow phenomena. As stated in literature: “*pulsatile flow through a curved tube can induce complicated secondary flows with flow reversals and is very difficult to analyze*” (Kundu *et al.* 2012), “*unsteady flows in curved conduits are considerably more complex than those in straight conduits, and exhibit phenomena not yet fully understood*” (Hamakiotes & Berger 1988). This of course does not underrate the importance of the case of steady turbulent flow through a curved pipe on its own, which has not been fully explored yet and studies on its dynamics are being performed until nowadays (Hellström *et al.*

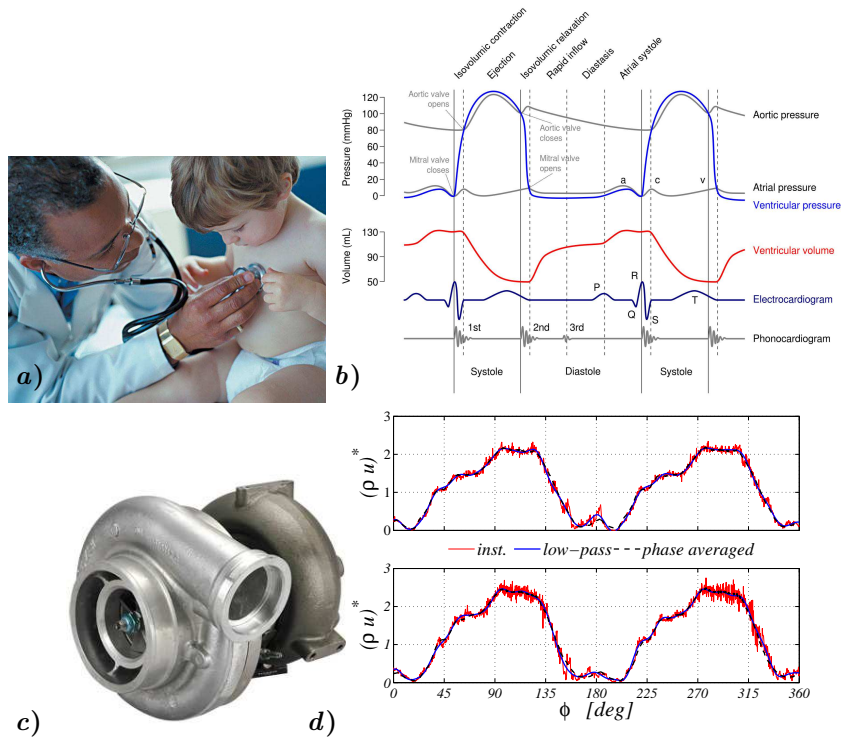


FIGURE 1.1. Examples showing how pulsating flows are greatly involved in our everyday life. *a)* A young patient having his heart examined by means of a stethoscope. (Source: <http://www.chatham-kent.ca>) *b)* A Wiggers diagram used in cardiac physiology to show the blood (aortic, ventricular and atrial) pressure variation, the ventricular volume and the electrocardiogram in a common plot. (Source: <http://www.enotes.com>) *c)* A turbocharger (Garrett). *d)* Mass flow rate density at the centreline (*top*) and wall (*bottom*) of a pipe. The flow is pulsating (40 Hz) in relevance to the inflow conditions into a turbine.

2011). The irregular motion of the vortical structures in that case may induce vibrations and cause fatigue in the pipes being part of e.g. the cooling systems of nuclear reactors. In such cases, the pressure drop caused by bends has to be estimated with high accuracy in order to achieve optimal plant safety (Ono *et al.* 2010; Shiraishi *et al.* 2009; Yuki *et al.* 2011; Spedding & Benard 2004).

Varying vortical patterns created by the counteraction between curvature and pulsation effects both in shape but also in time of appearance might lead to better or worse performance of systems. For example the role that pulsating flow plays in the causes of atherosclerosis or how it affects the performance of the turbocharger in the engine gas exchange system have not yet been clarified or in many cases have not even been considered. That is because, apart from the complexity of the flow itself with the corresponding difficulties investigating such complex flow experimentally or numerically, there is a substantial number of governing parameters to be considered.

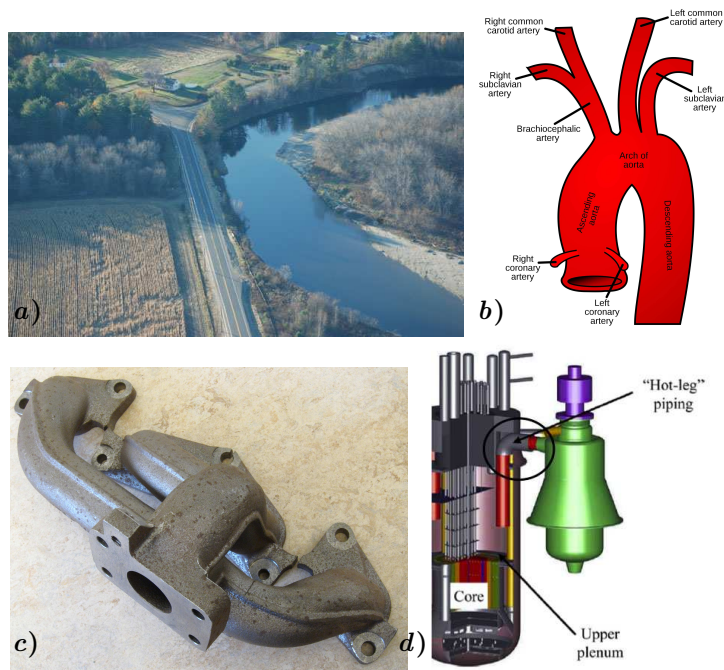


FIGURE 1.2. Examples showing how curved geometries are greatly involved in our everyday life. *a)* The *Sandy River* bank with the curve right next to the intersection of Whittier Road and Route 156 in Farmington, Franklin County, Maine, USA. (Source: www.dailybulldog.com) *b)* Illustration of the branches of the aortic arch. (Source: <http://howmed.net>) *c)* An exhaust manifold. *d)* Schematic of the cooling system of the *Japan Sodium-cooled Fast Reactor (JSFR)*. The “hot-leg” piping which is sharply bended and is used to transport the reactor coolant to a steam generator is circled. Image taken from Ono et al. (2010).

The present thesis is organized as follows: First, an extensive literature review is presented for flows in curved pipes as well as an introduction on the flow parameters. Thereafter the different experimental set ups and techniques used are described and in the last section of *Part I* a summary of the more important results and contributions is made. *Part II* of the thesis, contains the main results obtained so far, organized in the form of five papers, three of which have been already published and one is in print, whereas the fifth one is planned to be extended and submitted in the near future.

CHAPTER 2

Flows in curved pipes

“Learn from yesterday, live for today, hope for tomorrow. The important thing is not to stop questioning.”

Albert Einstein (1879–1955)

“The motion of the fluid as a whole can be regarded as made up of what are roughly screw motions in opposite directions about these two circular stream-lines”

Dean (1927)

If a fluid is moving along a straight pipe that after some point becomes curved, the bend will cause the fluid particles to change their main direction of motion. There will be an adverse pressure gradient generated from the curvature with an increase in pressure, therefore a decrease in velocity close to the convex wall, and the contrary will occur towards the outer side of the pipe (figure 2.1).

The centrifugal force ($\sim U^2/R_c$, where U is the velocity and R_c the radius of curvature) induced from the bend will act stronger on the fluid close to the pipe axis than close to the walls, since the higher velocity fluid is near the pipe axis. This gives rise to a secondary motion superposed on the primary flow, with the fluid in the centre of the pipe being swept towards the outer side of the bend and the fluid near the pipe wall will return towards the inside of the bend. This secondary motion is expected to appear as a pair of counter-rotating cells which bear the name of the British scientist Dean (1927) and are widely known today as *Dean vortices* (figure 2.2).

Being a pioneer in the study of fluid motion at low Reynolds numbers, Dean (1927) has been acknowledged for his work on the secondary motion in curved pipes for laminar flow (Binnie 1978). His work revealed the existence of the two symmetrical roll-cells but also introduced the parameter that dynamically defines such flows and is named after him, namely the *Dean number*¹:

¹This is how the Dean number is defined in this thesis, based on the mean axial velocity since it can be readily be measured but this is not always the variant used, especially in analytical or numerical studies. As mentioned in Berger & Talbot (1983)—where an extended section on the definition of the Dean number by various authors can be found—: *“This [authors using different forms of the Reynolds number or curvature ratio in their definition of the Dean number] makes for considerable confusion in reading and interpreting the literature”*. The relation between the rate of flow and curvature of the pipe for a given pressure gradient was given in Dean (1928) named as the parameter K (see also §2.1) and was later used in various forms (White 1929; Taylor 1929; McConalogue & Srivastava 1968).

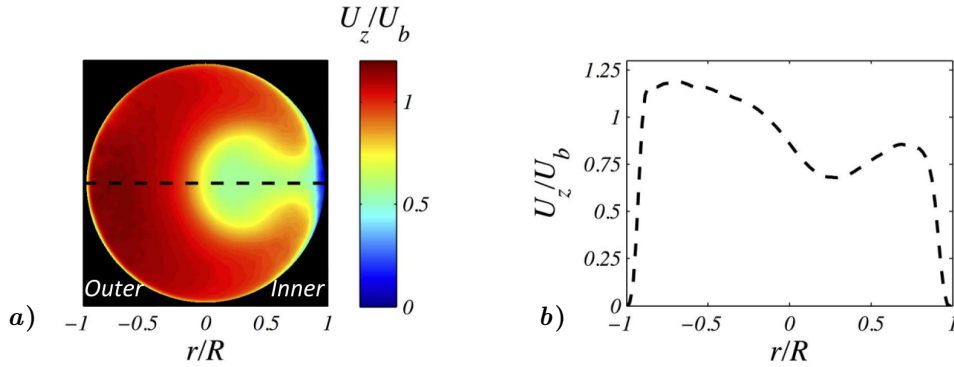


FIGURE 2.1. Example of the streamwise velocity (U_z) distribution at the exit of a 90° pipe bend *a)* Contour map of the streamwise velocity field at a pipe cross-section *b)* Profile of the streamwise velocity scaled by the bulk speed (U_b) along the horizontal axis.

$$De = Re \sqrt{\frac{R}{R_c}} \quad (2.1)$$

where $Re = \rho U_b D / \mu$ denotes the *Reynolds number*, with ρ being the fluid density, U_b the bulk velocity, $D = 2R$ the diameter of the pipe and μ the dynamic viscosity of the fluid.

In real life flow situations the flow through curved conduits may be further complicated being either laminar, transitional or turbulent (or a combination of these) and through the existence of swirl and/or pulsations. In this chapter a literature review summarizes some important aspects of such flows. The chapter is divided into five parts starting with a section dealing with *Dean vortices* in steady flow, probably the most characteristic feature of flows through bends. The second and third sections deal with studies with a swirling or pulsating motion superposed, respectively. Although this review cannot be complete, due to the large amount and diversity of past studies, there has been an effort to cover as much information as possible regarding both the variety of curved geometries (small curvature, 90° to U-bends and torus) and kinds of flows (laminar, steady, pulsating, swirling, turbulent). Section four provides an overview and summary of the references in a table. The chapter finishes with a section describing the parameters governing the types of flows investigated in this study.

One of the aims of this chapter is to learn from what has been achieved in the past and highlight the differences between the different flow conditions as well as the challenges researchers encounter with when studying (especially experimentally) complex flows.

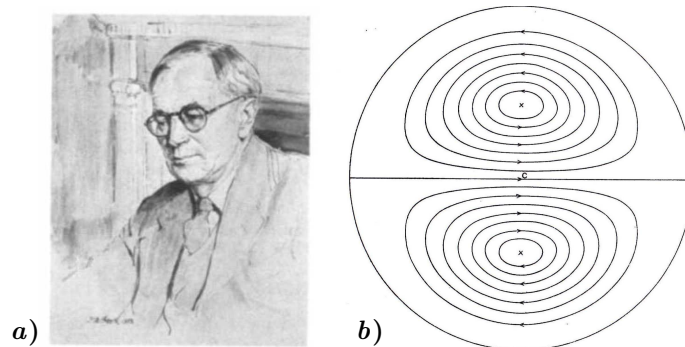


FIGURE 2.2. a) W. R. Dean (1896–1973) *Reprinted from Binnie (1978)*. b) A schematic of the Dean vortices. *Taken from Dean (1927)*.

2.1. Dean vortices in steady flow

“The water just rushes out against the outer bank of the river at the bend and so washes the bank away [...] it allows deposition to occur at the inner bank [...] the question arose to me: Why does not the inner bank wear away more than the outer one?”

Thomson (1876)

2.1.1. Mean flow development

Indeed many of us might have observed a similar behavior of the water flowing when sitting close to a river bank, as expressed by Thomson (1876) who explained theoretically the flow round a bend in a river². This simple example from nature as well as the circulatory systems of humans and other mammals that consist of rather curved veins, arteries and capillaries or the internal combustion engine with its branches and conduits, show how curved geometries are greatly involved in our everyday life and how important it is to study their impact on the functionality of both natural and industrial systems.

Noting in an early study (Eustice 1910) that even a small curvature can affect the quantity of flow of water through a pipe, Eustice (1911) introduced coloured liquid through capillary nozzles in various bent configurations made of glass, in order to visualize the stream fluid motion (figure 2.3). From the behaviour of the filaments he observed an uneven motion of the fluid compared to what had been known until that time for the motion of fluids in straight pipes³:

²His observations mainly concerned open-channel flow but is mentioned here for historical purposes.

³His experiments were later criticized by White (1929) for using non-fully circular sectioned pipes and by Taylor (1929) for introducing the dye early at the entrance of the curved pipe, therefore unable to detect a rise in the – as referred to the critical Reynolds number for which turbulence breaks in – “*Reynolds’ criterion*” – due to curvature.

“But in a curved pipe the water is continually changing its position with respect to the sides of the pipe, and the water which is flowing near the centre at one part approaches the sides as it moves through the pipe and flowing near the sides it exerts a ‘scouring’ action on the pipe walls”

Eustice (1911)

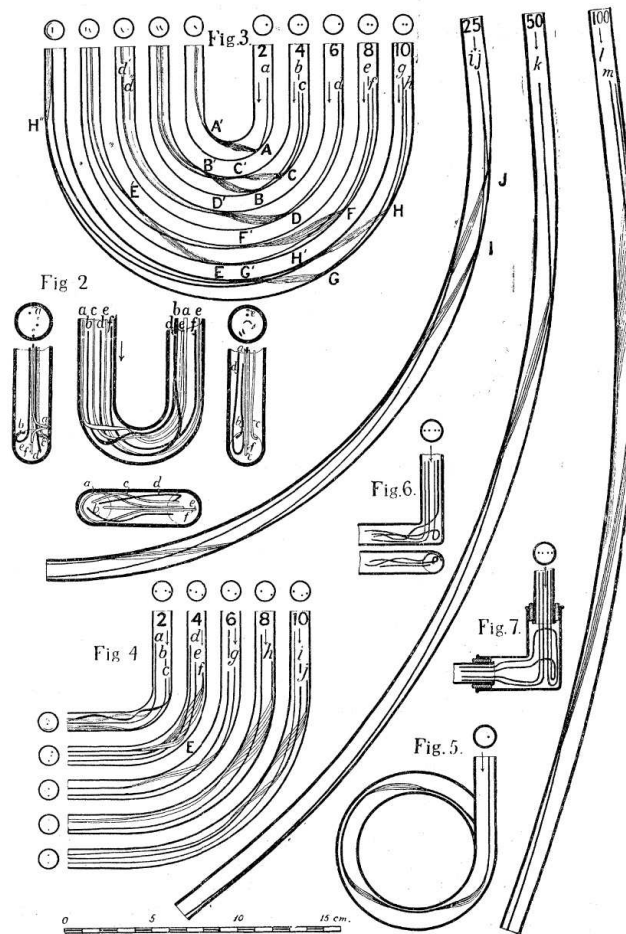


FIGURE 2.3. The different bend configurations used in the experiments by Eustice and the filaments showing the streamline motion. Reprinted from Eustice (1911).

Dean (1927, 1928) was the first to provide a theoretical solution of the fluid motion through curved pipes for laminar flow by using a perturbation procedure from a Poiseuille flow in a straight pipe to a flow in a pipe with very small curvature. He showed that the relation between the flow rate and the curvature of the tube depends on a single variable K defined as $K = 2Re^2(R/R_c)$, where the Reynolds number is defined here as: $Re = RU_o/\nu$ with U_o being the maximum velocity for a flow in a straight pipe of the same radius and with the same pressure gradient as in a curved pipe and ν is the kinematic viscosity. This relation is only valid for small curvature ratios R/R_c . He derived a series solution expanded in K to describe the fully developed, steady flow analytically in a tube with small K and demonstrated a flow field exhibiting a pair of symmetrical counter-rotating vortices. Since those findings many researchers have been intrigued to investigate the complicated flow field through pipe bends and the effect of the different parameters on the flow development.

By the late 1930's the flow through pipe bends was a topic of high interest including effects of curvature on the flow stability whereas characteristics of such flows *i.e.* the counter-rotating cells were already being reproduced in textbooks (Goldstein 1938). Other textbooks where information about pipe bends can be found are those by Schlichting (1955), Ward-Smith (1980) (where an extensive section on pipe bends including mitre bends, ducts with non-circular cross section and short circular arc-bends is available) but also in Kundu *et al.* (2012). This shows that the interest and the knowledge on flows through curved pipes has been expanding through the years and can be viewed as of fundamental importance to the field of fluid dynamics.

The work by Dean (1927) has been extended both theoretically and numerically over the years. McConalogue & Srivastava (1968) extended the work by Dean (1927) solving the equations numerically by Fourier-series expansion and showed that the secondary flow becomes prevalent for a higher value of the Dean number (defined as $D = 4\sqrt{K}$) up to which Dean (1927) extended his theory ($D \geq 96$, which was also their lower limit and whereas the upper was 600). This study was later extended by Greenspan (1973) by using a finite-difference technique and applying the problem to a wider Dean number range ($10 \leq D \leq 5000$). It was found that by increasing the Dean number the physical trends observed by McConalogue & Srivastava (1968) were still developing. Barua (1963) provided an asymptotic boundary-layer solution to the equations of motion for large Dean numbers when the viscous forces are significant only in a thin boundary layer and the motion outside that region is mostly confined to planes parallel to the plane of symmetry of the pipe. Analytical approximation methods for the flow in a curved pipe have been given in the more recent years by Topakoglu & Ebadian (1985) and Siggers & Waters (2005) by using series expansion of the curvature ratio and of the curvature ratio and Dean number, respectively.

White (1929) showed that the theory established by Dean (1927) can be valid for pipes of different curvatures. Somewhat unexpectedly, laminar flow can be maintained for larger Reynolds numbers (even by a factor of two for the highest curvature ratios studied) than for straight pipes, even though curvature is known to cause instability⁴.

⁴In Schmid & Henningson (2001) a short description on the Dean vortices as secondary instability can be found. Here the aim is to investigate the behavior of the Dean vortices in the turbulent flow regime, therefore the instability mechanisms are not the subject of this thesis and will not be further discussed.

Taylor (1929) verified those results (figure 2.4) by introducing a fluorescent colored band into the stream only after it had traversed at least one whole turn of the helix and confirmed also the existence of the Dean circulation as indicated by Dean (1927). He also observed that the flow was steady up to a certain speed at which the color band began to vibrate in an irregular manner that increased in violence with increasing speed until the flow became fully turbulent. Transition from laminar to turbulent flow has been also examined in a number of studies (Ito 1959; Srinivasan *et al.* 1970). Relations for the critical Reynolds number as proposed by different studies can be found in Ward-Smith (1980) and Spedding & Benard (2004) even though no universal solution exists since the parameter is highly dependent on the curvature ratio.

Kurokawa *et al.* (1998) examined the relaminarization mechanism in curved pipes by means of flow visualization and hot-film anemometry employing fully developed turbulent flow at the entrance of the bend. The secondary flow pattern was (once more) proved to depend on the magnitude of the Dean number and smoke images of the evolution of the secondary motions for different downstream positions and stations along the bend were presented. For the lowest Reynolds number ($Re = 2.2 \times 10^3$) a weak secondary flow was formed as two counter rotating vortices. For the higher Reynolds number ($Re = 5.3 \times 10^3$) no secondary motions were depicted and it was concluded that for the case of the 90° pipe bend the laminarization process is weak because of the short development distance. Smoke visualizations for bends of 180° (U-bend) and 360° (torus) as well as a 720 and a 1800° coiled pipe were additionally performed and weak secondary motions were captured for those cases as well. The presence of turbulent flow was related to the absence of the secondary motion from

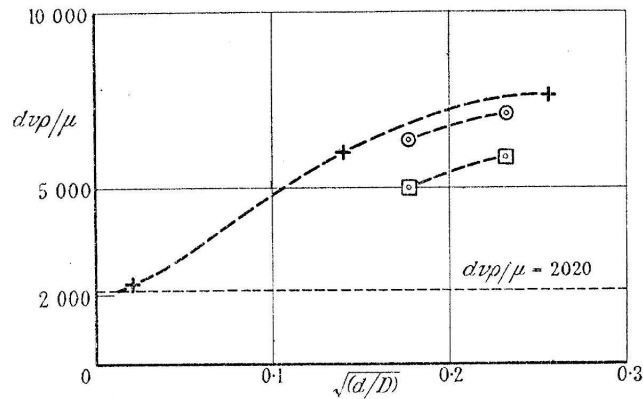


FIGURE 2.4. Reynolds number vs $\sqrt{d/D}$ where d the diameter of the pipe and D the diameter of the helix into which the pipe was wound. With + the data by White (1929) are shown. \odot indicates lowest Re at which flow appears completely turbulent in a helical glass tube. \square denotes highest Re at which flow is quite steady. *Image taken from Taylor (1929).*

the images due to smoke diffusion, therefore no secondary structures were captured under turbulent flow conditions in any of the aforementioned geometries.

Rowe (1970) measured the yaw angle relative to the pipe axis and the total pressure variation. It was indicated that the secondary motion is greatest at 30° from the inlet of the bend reducing afterwards its strength but still persisting until it reaches 90° . Later, Patankar *et al.* (1975) used the $k - \epsilon$ model to calculate the same cases as those of Rowe (1970) and obtained qualitative agreement of the mean flow profiles.

Azzola *et al.* (1986) investigated both experimentally and numerically the developing turbulent flow in a strongly curved 180° pipe bend. Mean velocity and Reynolds stress distributions indicated the existence of two cross stream flow reversals, as also shown in Rowe (1970). An additional symmetrical pair of counter-rotating vortices in the core of the flow was observed.

A few studies have also investigated the entry flow into curved pipes due to its importance in finding the distance required for the flow to reach the fully developed state or where the maximum shear stress appears. A pioneering study by Singh (1974) was made on the flow characteristics near the inlet of the pipe. A boundary layer is formed as the fluid enters the pipe where the viscous forces are confined while the core is inviscid, like in a straight pipe. Immediately downstream the entrance of the flow a considerable azimuthal flow is induced in the boundary layer from the outside to the inside of the bend due to the pressure gradient. The secondary flow generated by the curvature is therefore moving the slower fluid from the boundary layer inwards and the faster fluid at the core outwards. The inflow condition greatly affects the initial development of the flow with a non-uniformity in wall shear stress, i.e. the shear is largest at the inner wall before the maximum moves to the outer wall, appearing at two times larger distance for the first inlet condition than for the second one. It was shown that the smaller the curvature ratio the smaller the disturbances in the secondary motions and the entry condition affected the initial development of the flow but did not affect the flow significantly further downstream. Smith (1976) extended the work by Singh (1974) by applying more realistic inflow conditions, i.e. the distortion of the incoming flow is due to the curvature of the pipe and not due to the inflow profile. Yao & Berger (1975) theoretically investigated the development of the flow from a uniform velocity field at the entrance to a fully developed flow and for large Dean numbers. It was shown that in order to reach a fully developed state in the case of large Dean numbers, the entry length needs to be $\mathcal{O}(\sqrt{RR_cDe})$, (where the Dean number is defined here as: $De = 2\sqrt{R/R_c}(2RU_b/\nu)$). This value is smaller as compared to the case for a straight pipe.

Agrawal *et al.* (1978) performed LDV and hot-film anemometry measurements for the investigation of the flow in a curved pipe with a uniform motion as the inlet condition. Two semi-circular pipes with different curvature ratios were used for a Dean number range from 138 to 679. Comparison of their results to those of Singh (1974) and Yao & Berger (1975) gave poor agreement due to certain assumptions in the analytical procedure of the latter works (small effect of curvature, secondary flow streamlines parallel to the plane of symmetry). Enayet *et al.* (1982) also performed LDV measurements extending the effort by Agrawal *et al.* (1978) to turbulent flow. The results showed that the secondary flows were strongly dependent on the thickness

of the inlet boundary layer which in turn depends on the Reynolds number. For the turbulent case, the inlet boundary layers are much thinner than for the laminar case and the presence of a large central region of uniform velocity significantly influences the development of the secondary flow downstream the bend.

Soh & Berger (1984) investigated the laminar flow at the entrance of a bend for different Dean numbers and curvature ratios and observed secondary flow separation at the inner wall as the flow developed which proved to be highly dependent on the curvature ratio. Similarly to Agrawal *et al.* (1978) they showed a double peaked axial velocity profile at the plane of symmetry for large Dean numbers and both for the fully and non-fully developed flow cases. That phenomenon was explained due to the highly distorted vortex structure.

Bovendeerd *et al.* (1987) performed LDV measurements on the entry region of a 90° bend with a laminar parabolic profile as the inflow condition. The secondary flow at the entrance was directed towards the inner wall while disturbances were not observed downstream the inlet up to a distance of $\sqrt{RR_c}$. They provided a coherent description of the flow field throughout the bend, presenting the intensity of the secondary motions and the axial velocity profiles for different stations along the bend. It was shown that the secondary flow intensifies at an early stage but the axial flow pattern does not show any changes dominated by the inertial forces up to some distance. They compared their results with those by Soh & Berger (1984) and Agrawal *et al.* (1978) who used a uniform entry profile instead of a parabolic one and pointed out major differences in the flow development between the two conditions.

Sudo *et al.* (1998) investigated turbulent flow through a 90° curved pipe with long straight pipes both upstream and downstream at $Re = 6 \times 10^4$. Longitudinal, circumferential and radial components of mean and fluctuating velocities as well as Reynolds stresses were obtained by rotating a probe with an inclined hot-wire, extending the work by Azzola *et al.* (1986) and Enayet *et al.* (1982) who limited their investigations on measuring only the longitudinal velocity component. Past studies which showed that at the inlet the primary flow accelerates near the inner wall and a secondary flow moves from the outer towards the inner wall were confirmed. At 30° bend angle the secondary flow is formed as a pair of vortices but the primary flow stays deflected towards the inner wall until it becomes highly distorted at 75° and 90° bend angle. At some downstream distance from the bend the vortices start to break down but they persist up to a distance of ten pipe diameters.

The secondary motion of a fully developed turbulent flow in curved pipes was analyzed theoretically by Dey (2002) using the boundary-layer approach. Computational results of the boundary-layer thickness and the wall shear stress were presented for different Reynolds numbers and curvature ratios up to $De = 5 \times 10^5$. It was shown that the secondary boundary layer thickness along the outer pipe wall increases gradually but it starts growing rapidly near the point of the secondary boundary layer separation. The normalized thickness (over the radius of curvature) decreased with increasing Reynolds number while the wall shear stress increased with increasing radius near the outer wall until it reached some maximum value and then decreased to obtain its minimum at the separation point.

A summary on the studies performed on both curved pipes and elbow bends for laminar, transitional and turbulent flow (over 200 references) is given in Spedding

& Benard (2004), including their own results on the pressure drop in various bent geometries. They pointed out that the pressure drop is more significant due to flow separation at the inner wall in elbows as compared to bends.

2.1.2. Vortex structure in turbulent flows

The behavior of Dean vortices in turbulent flow, has not been studied extensively from an experimental point of view, but numerical simulations (mainly *Large-Eddy Simulations (LES)* and *Reynolds-Averaged Navier-Stokes (RANS)* modeling) have described a complex vortex pattern consisting of up to four or six cells under certain flow conditions (Hellström 2010).

Tunstall & Harvey (1968) found that in a sharp bend a unique vortex pattern exists for $Re = 4 \times 10^4$, consisting of a single vortex dominating the pipe cross section, switching its rotational direction from clockwise to counterclockwise. Three decades

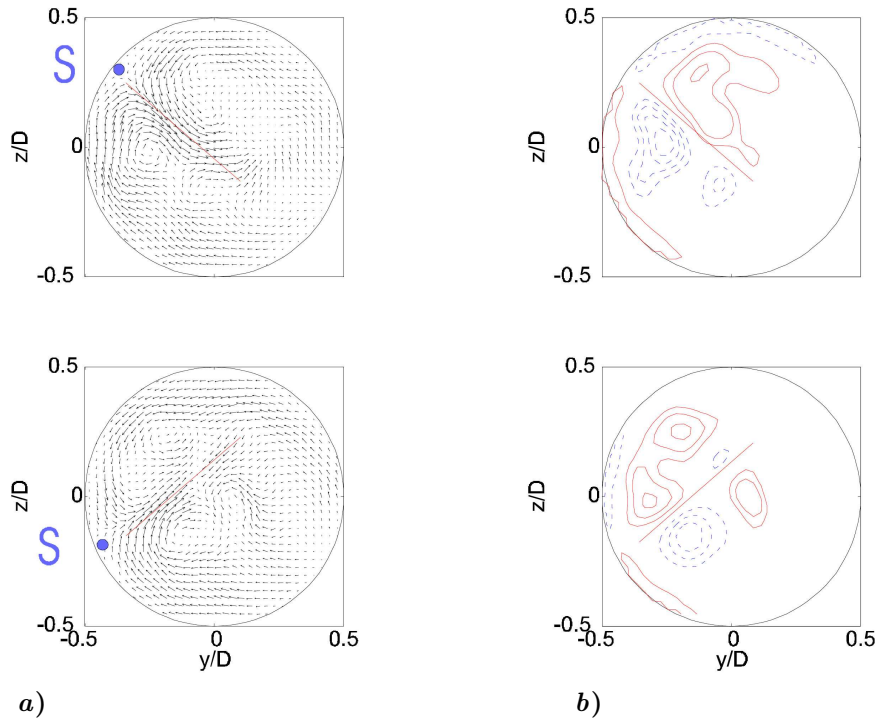


FIGURE 2.5. The “swirl switching” of the vortices at two instants. *a)* Velocity vector field (“S” marks the saddle point and the red line indicates the plane of symmetry). *b)* Contours of streamwise vorticity (blue dashed lines indicate negative value and red solid lines indicate positive value). *Reprinted from Brücker (1998).*

later, Brücker (1998) performed Particle Image Velocimetry (PIV) measurements to investigate this phenomenon further (figure 2.5). Some time later, Rütten *et al.* (2005) extended the analysis by means of LES for $Re = 5000 - 27000$ and proved the existence of the “swirl switching” that was first observed by Tunstall & Harvey (1968) and not only for the case of sharp bends where flow separation occurs. The same phenomenon was later captured also in Sakakibara *et al.* (2010) by means of Stereoscopic PIV (SPIV) for a higher Reynolds number ($Re = 12 \times 10^4$). A similar behavior of the vortices in turbulent flow was also observed by Ono *et al.* (2010) for $Re = 5.4 \times 10^5$ for a long elbow and more recently by Yuki *et al.* (2011) at the first section of a dual elbow by means of PIV at $Re = 5 \times 10^4$. Whereas a few possible explanations on the mechanism behind the swirl switching exist (Tunstall & Harvey 1968; Brücker 1998), it is still not fully understood.

An insight on how the secondary motions form due to different parameters was given in the numerical studies by So *et al.* (1991) and Lai *et al.* (1991) who focused on how the shape of different cells in the flow through a U-bend depends on the inlet flow profile, the Dean number and the curvature ratio. The flow patterns were shown to consist of four different vortex pairs: the Dean-type vortex pair, another pressure-driven pair near the pipe core as a consequence of local pressure imbalance (Rowe 1970; Azzola *et al.* 1986), a third separation cell near the inner bend (So *et al.* 1991) and a fourth one near the outer wall which is a turbulence driven secondary motion (Lai *et al.* 1991). For a uniform entry profile, small Dean numbers and curvature ratio

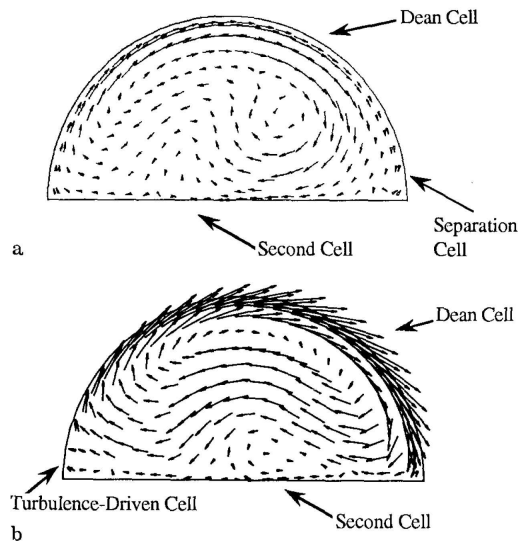


FIGURE 2.6. Secondary flows in a) Laminar flow with parabolic inlet profile at $De = 277.5$ b) Turbulent flow with fully developed inlet profile at $De = 13874$. Image taken from *Anwer & So (1993)*.

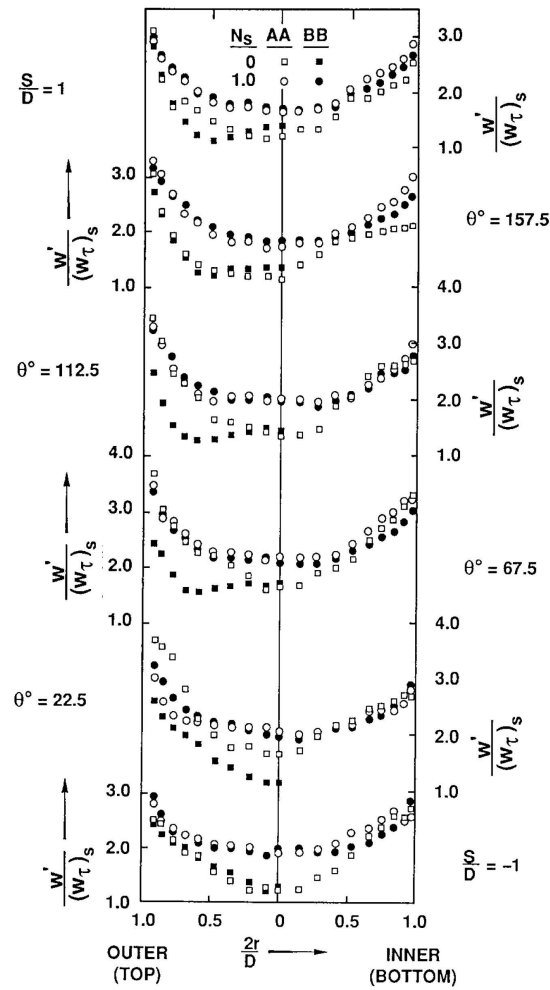


FIGURE 2.7. Velocity profiles of the streamwise velocity component for a non-swirling (open symbols) and a strongly swirling (black symbols) flow and for different bend stations. *Image taken from Anwer & So (1993).*

only the Dean-type cell is observed while when the entry flow profile to the bend is parabolic two additional cell structures can appear. For a fully developed turbulent inlet profile turbulence-driven secondary motion is induced due to anisotropy of the turbulent normal stresses and their radial and circumferential gradients (figure 2.6).

2.2. Swirling flow

Turbulent swirling flow is encountered in many industrial applications such as in hydraulic plants, combustion chambers and any machine that involves a turbine or fan. However, the effects of the swirl combined with effects from curved geometries, which are widely met in practice, on the turbulence and its structures have been studied only to a very limited extent.

The work by Binnie (1962) was among the first efforts to examine swirling flow in a 90° pipe bend, by means of flow visualization in water, though the experiments were limited to the movement of particles close to the wall. The flow pattern was explained by additional sketches which showed the existence of an air core, changing its position through the bend.

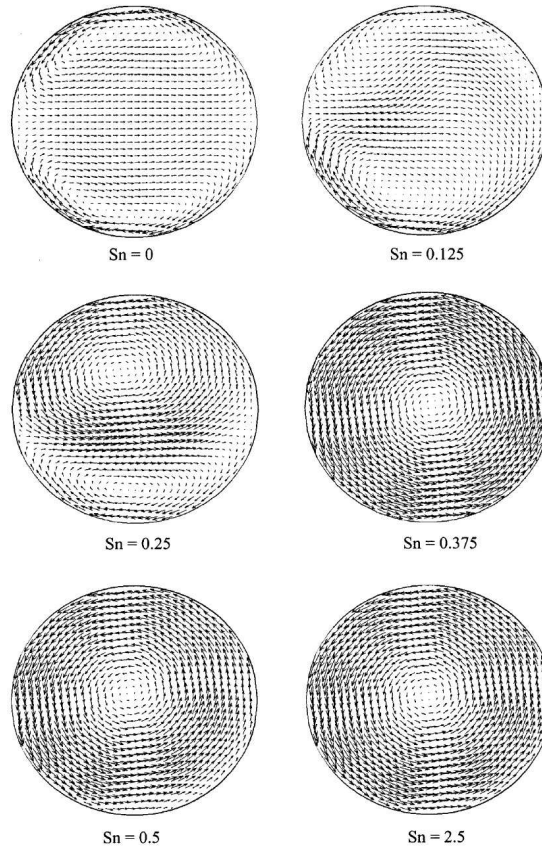


FIGURE 2.8. Flow structures at increasing swirl intensities.
Image taken from Pruvost et al. (2004).

The effect of swirling flow on hydraulic losses and the flow in U-bends was investigated experimentally by means of Pitot tubes in Shimizu & Sugino (1980). They also considered effects of wall roughness and the curvature ratio. Axial and peripheral velocity distribution plots and contours for a strong swirling flow revealed a close relation between the axial velocity and the vortex core center demonstrating that the maximum velocity moves to the opposite direction as the vortex core center. For the case of weak swirling flow, the vortex core was positioned at the inlet of the pipe and disappeared at some downstream angular station with the maximum velocity shifting towards the outer wall. A pressure difference pushed the fluid close to the wall in a counter-clockwise direction in that case, causing a reverse force which was stronger than the clockwise swirl motion existing in the upstream angular positions.

The case of a turbulent swirling flow through a curved pipe (two 90° pipes connected) was also examined experimentally by Anwer & So (1993) for $Re = 5 \times 10^4$ and for a high swirl intensity (defined in their study as: $N_s = \Omega D/2U_b$, where Ω the angular speed of the rotation section) of $N_s = 1$ by means of pressure taps, a hot-film gauge and a rotating hot-wire probe. From the mean velocity profiles (figure 2.7) along the horizontal and vertical planes it was shown that the profiles are not as skewed as in the non-swirling case which suggested that a single dominating cell exists here instead of multiple secondary structures. The extended work by So & Anwer (1993) showed that in swirling flow, the length needed for the flow to become fully developed is shorter than that needed in the case of a straight pipe and that the bend accelerates the decay of the swirl.

For the case when a swirling motion is superposed on the primary flow, CFD studies (Pruvost *et al.* 2004) have shown that the Dean cells merge as the swirl motion intensifies (figure 2.8) until the flow field becomes completely swirl dominated (the swirl intensity in that case was $S_n = 2.5$ where $S_n = \Omega R/2U_b$). Once again, the results so far concerning turbulent swirling flow through bends are based either on simulations (Pruvost *et al.* (2004) is one of the few studies considering turbulent swirling flow using CFD tools) or point-wise measurements (Anwer & So 1993) and therefore cannot provide an image of the vortices (or more specifically for the case of simulations a validated one). The work by Chang & Lee (2003) considered 2D-PIV measurements in turbulent swirling flow in a bend. Streamwise velocity profile plots showed negative velocity at the centre of the pipe at the inlet due to the strong swirl motion while later, increased in magnitude, it shifted towards the convex wall until it reached a bend angle of 45° where it allocated again to the concave wall. Additional turbulence intensity plots showed the existence of a two-cell phenomenon which for the case of the highest Reynolds number studied, remained distinguishable until the exit of the pipe.

2.3. Pulsating flow with and without curvature effects

"With each respiration, and to a lesser extent each heart beat, an arrest, or reversal of flow took place"

Helps & McDonald (1954)

2.3.1. Pulsating flow in straight pipes

Seminal studies on the fundamental characteristics of pulsating flows started truly in the mid '50s (Womersley 1955) with the early studies focusing mainly on the flow conditions in veins and arteries (McDonald 1952; Helps & McDonald 1954; Hale *et al.* 1955) and revealed some of the characteristics of pulsating flow such as *flow reversal*⁵ which would later be investigated both experimentally and numerically for a number of different applications. In pulsating flow inertia forces due to pulsations play an important role and their ratio with the viscous forces define the frequency parameter. Womersley (1955) has been credited for his work on pulsating flows and for providing a solution for the equations of motion for a viscous fluid in a circular pipe under a known oscillatory pressure gradient. He connected the viscous drag and flow rate by using a universal parameter, named today as the *Womersley number*, a dimensionless expression of the pulsatile flow frequency in relation to viscous effects:

$$\alpha = R\sqrt{\frac{n}{\nu}} \quad (2.2)$$

with R being the radius of the tube, n the circular frequency (i.e. $n = \omega = 2\pi f$ where f the frequency in cycles per second) and ν the kinematic viscosity of the fluid (see also § 2.5).

Pulsating flow can appear in different regimes: laminar, transitional and turbulent or depending on the nature of the flow in steady-state or transient form. On the other hand, steady-state pulsating flow is divided additionally into three categories due to the flow's own complexity. For $\alpha < 1.32$ (or as shown by Shemer & Kit (1984) for $\sqrt{St/Re} < 1.8 \times 10^{-2}$, where St is the *Strouhal number*, see § 2.5) the region is quasi-steady i.e. it can be treated as steady. At such low pulsation frequencies the turbulent structures have time to accommodate to the slowly varying flow rate and therefore the flow behaves similar to steady turbulent flow. For $1.32 < \alpha < 28$ the region is intermediate (passage between steady to pulsatile flow) and for $\alpha > 28$ it is inertia dominated, the pulsation frequency is so high that the turbulent structures cannot respond to the rapid changes. Hence the turbulence becomes independent of the phase angle of the pulsations (Carpinlioglu & Gündoğdu 2001).

Even though the transition of steady laminar flow to turbulence has been studied extensively, the case of transition of pulsating flow has only been studied to a certain extent. From what has been known so far, the passage between the different pulsating flow regimes can be rather complicated and the Reynolds number for the transition to turbulence or for which the flow remains fully turbulent under the full pulse cycle, there are no definite conclusions made. In general this is rather complicated since apart from the time-averaged critical Reynolds number (which constitutes the only criterion for transition in steady flows) the occurrence of turbulence and its persistence

⁵A flow of fluid in the opposite direction of its regular flow, known also as back flow.

throughout the whole pulse cycle depend also on the velocity amplitude ratio (U_{os}/U_m where U_{os} is the oscillatory velocity component and U_m the mean velocity) as well as the Womersley number (Ohmi *et al.* 1982; Kirmse 1979).

Tu & Ramaprian (1983) performed measurements at $Re = 5 \times 10^4$ and examined in detail the turbulence characteristics of steady, as well as quasi-steady and intermediate oscillatory flow. The time-mean velocity of quasi-steady turbulent flow was almost identical to the steady flow case but as the Womersley number increased, there was a phase lag between the velocity and the pressure gradient observed while mean axial flow profiles showed increased centerline velocity and an inflexion point was seen close to the wall. The turbulent flow was divided into the quasi-steady, low-frequency, intermediate-frequency, high-frequency and rapid-oscillation regimes according to the *turbulent Stokes number* introduced in Ramaprian & Tu (1983), see also § 2.5. Other studies on the effects of pulsations on turbulence are those by Gerrard (1971); Winter & Nerem (1984); Shemer & Kit (1984); Shemer *et al.* (1985).

2.3.2. Pulsating flow through curved channels

Under pulsating conditions the laminar vortices in a curved pipe can exhibit a highly varied pattern during one pulse cycle (Timité *et al.* 2010; Jarrahi *et al.* 2010) as illustrated in figure 2.9. Sudo *et al.* (1992) compared results from flow visualizations with numerical calculations and distinguished the secondary flows into five patterns according to different values of the flow parameters, see figure 2.10. *Type I* appears when the frequency parameter is so low that a large viscous layer forms near the wall and the vortices resemble those when the flow is steady for the full oscillation period. As the frequency parameter increases but remains in the moderate range ($\mathcal{O}(10)$), the viscosity effect reduces successively to the wall and the inertial effect increases in the pipe centre. This force imbalance favors the centrifugal effects in the core region of the pipe while at the outer wall the tangential velocity becomes larger than the radial velocity and the fluid at the centre moves towards the outer side of the pipe. Consequently, symmetrical, stretched vortices are formed with their centers moving to the top and bottom of the pipe cross-section. Furthermore, when the Womersley number increases further, the so-called Lyne instability sets in (see below).

The first pioneering study on oscillatory laminar flow through curved pipes is credited to Lyne (1970), almost 5 decades after the study by Dean (1927) on steady flow in a curved pipe. In this study small values of the parameter $\beta = \sqrt{2\nu/\omega R^2}$ were chosen so that the viscous effects were confined in a thin layer at the wall (Stokes layer⁶) and the rest of the flow was assumed to be inviscid in order to simplify the problem. It was shown that a secondary flow was confined in the Stokes layer due to centrifugal forces and in Lyne's words: “. . . the fluid is driven along the wall from the outer side of the bend to the inner, under the action of the pressure gradient which, in the Stokes layer, is no longer balanced by the centrifugal force associated with flow along the pipe; it returns centrifugally within, and at the edge of, the Stokes layer . . . ” (see figure 2.11). The secondary flow was shown to be governed by a conventional Reynolds number defined as:

⁶The boundary layer in oscillatory flows; its thickness is defined as: $\ell_s = \sqrt{2\nu/\omega}$ or in inner scaling: $\ell_s^+ = \ell_s u_\tau / \nu$, where u_τ the friction velocity, ω the angular frequency of pulsations and ν the kinematic viscosity.

$$R_s = \frac{W^2 R}{R_c \omega \nu} \quad (2.3)$$

where W is a typical velocity along the axis of the pipe. The analysis performed was valid for $R_s \ll 1$ or $R_s \gg 1$.

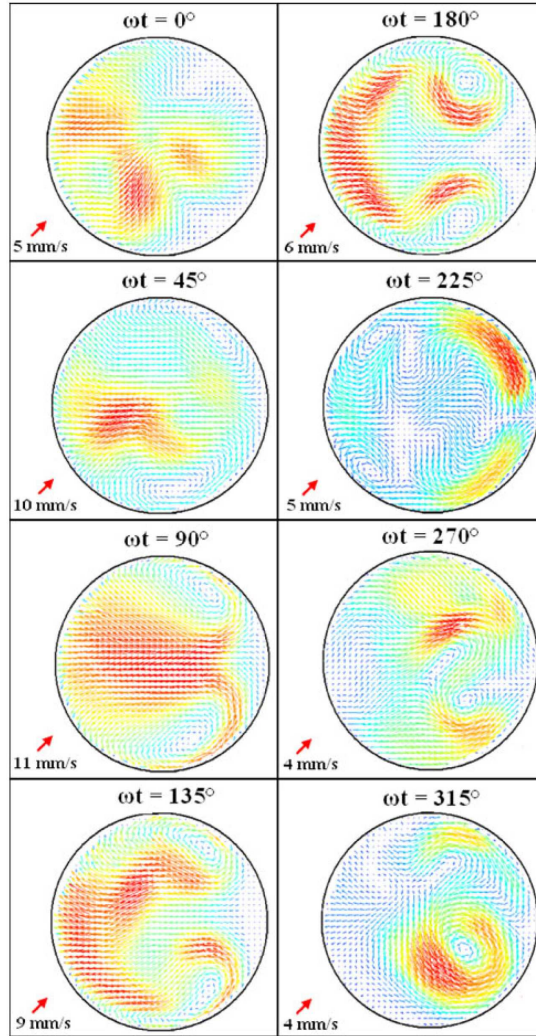


FIGURE 2.9. Secondary flow variation in an oscillation period at $\alpha = 10.26$. Highest velocity values (red vectors) are indicated to the left. *Image taken from Jarrahi et al. (2010).*

Smith (1975) further examined the counteraction between steady and oscillatory boundary layers. He also investigated when this inward-outward motion observed by Lyne (1970) occurs and distinguished the nature of primary and secondary flow depending on the Dean number and frequency parameter.

Zalosh & Nelson (1973) demonstrated the secondary motions for small values of the parameter $(R/R_c)(QR/\omega\nu)^2$ (where Q and ω are the amplitude and frequency of the pressure gradient, respectively) and for different pipe radii. Reversal of flow, confirming also observations by Lyne (1970) was observed. The theory was valid only for $R_s \ll 1$ but for arbitrary values of $\sqrt{2}\beta$. Bertelsen (1975) investigated experimentally the case when $\beta \ll 1$ and $R_s \lesssim 1$ (defined as in Lyne (1970); Zalosh & Nelson (1973)) and compared his results with the two aforementioned theories. He concluded that in practice the theories are valid for higher R_s than initially expected. The same observations on the outward-inward motion of the vortices in unsteady flow of small pulsatile frequency rate and mean Reynolds number were examined

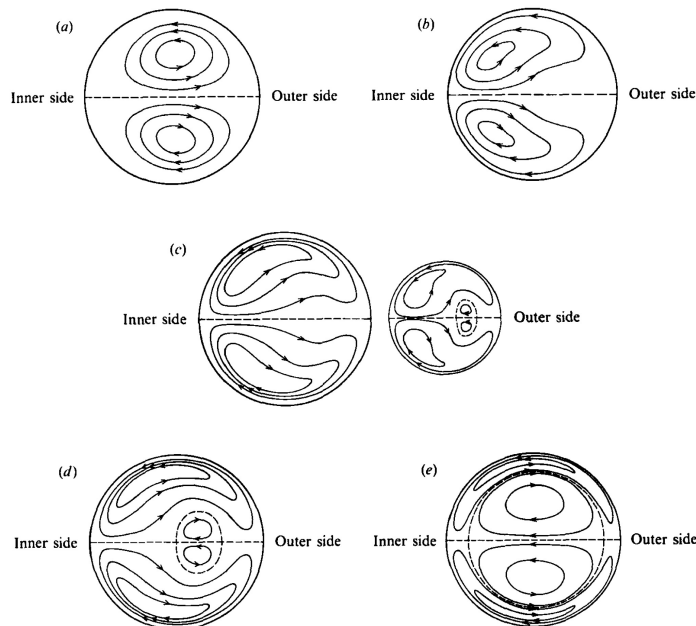


FIGURE 2.10. Schematic diagrams of the five secondary flow patterns *reprinted from Sudo et al. (1992)*. a) Dean circulation b) Deformed Dean circulation c) Intermediate circulation between Dean and Lyne circulations d) Deformed Lyne circulation e) Lyne circulation. Each type is distinguishable from the other by varying the Dean ($40 \leq De \leq 491$) and Womersley ($5.5 \leq \alpha \leq 28.2$) number.

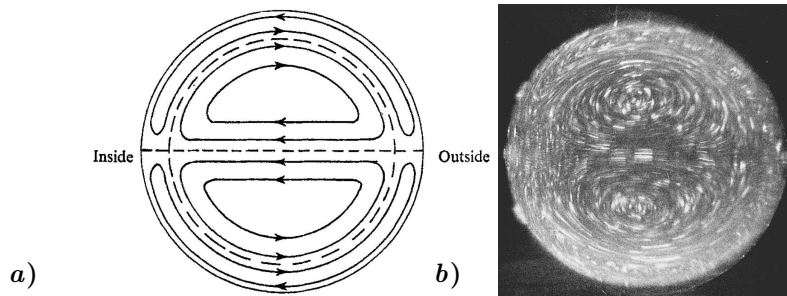


FIGURE 2.11. Lyne-type circulation. *a)* Reprinted from Lyne (1970) *b)* Reprinted from Bertelsen (1975).

numerically by Hamakiotes & Berger (1990) as well as the shear rates, which appeared to be larger at the peak of back flow located at the inner bend.

Studies has been focused, as in the steady flow case as well, on the entrance region of the bend. Singh *et al.* (1978), extending his work on the steady inlet flow conditions to a bend, performed a boundary-layer analysis using a pulsatile velocity profile as the inflow, relevant to blood flow. The study shows the slower moving fluid being drifted azimuthally from the outer bend to the inner as the secondary flow effect increases due to the curvature and induces a cross-flow of faster moving fluid from the inner bend to the outer. This results in a thinning of the boundary layer at the outer bend and a thickening at the inner. It was also shown that as the boundary layer grows during deceleration, back flow and negative wall shear stress develops.

Talbot & Gong (1983) performed an LDV study on the effects of different curvature ratio and Dean number and concluded that a similar classification as the one made by Smith (1975) for the regimes of fully-developed pulsatile flow in curved pipes may also be useful to distinguish between different entry-flow regimes.

Another study on the characteristics of the flow through curved geometries when pulsations are present with application to blood flow is the one by Chandran & Yearwood (1981). Back flow was observed close to the inner wall during early diastole which was delayed as the distance from the inner wall increased. Profiles of the axial, radial and tangential velocity components for both the vertical and horizontal plane were plotted showing that the reversal of flow in the central region of the vertical traverse coincides with the flow reversal observed in the same region in the horizontal traverse. Furthermore during early diastole, when back flow is located near the inner wall, both the tangential and radial components decrease in magnitude. The progressive reversal of the axial flow into the central core region as the diastole progresses is explained by the outward momentum caused by the movement of the radial velocity towards the outer wall. It is shown that tangential and radial components in the boundary layer of the inner wall are relatively large enough to enhance the rotational motions. Last, this study postulated one unique characteristic of pulsating flow in curved pipes in contrast to steady flow through similar geometries, namely that the maximum axial velocity in the entrance region is observed close to the outer wall and not the inner, as it has been known for the steady case.

The detailed nature of pulsatile laminar flow through a pipe bend was examined by Sumida *et al.* (1989) who, by means of visualization, provided snapshots of the secondary motions for a whole cycle. The results from the observations included the vortex core location and kinetic energy which were compared with numerical analysis. The effects of the frequency parameter ranging from 5.5 to 18 on the formation of the secondary structures were visualized. For the low Womersley number case, the flow appeared to be quasi-steady while at the highest, the axial velocity profile did not change with the cycle phase apart from the region where back flow occurred while in that case the core of the vortex did not change significantly. The results presented were referring to a Dean number of 200 and an amplitude ratio of 1. This work was later extended in Sumida (2007) where the Womersley and Dean numbers were 5.5 to 18 and 200 and 300, respectively. Results were obtained by means of LDV in order to examine the entrance length needed under those flow conditions for the flow to become fully developed. The flow field was found to be more complicated for moderate values of the Womersley number and the entrance length was shorter for pulsating flow than for steady flow.

The effect of the Womersley number was also examined numerically in Hamakiotes & Berger (1990) for a range between 7.5 and 25 and Reynolds numbers based on the mean velocity between 50 and 450. A Dean-type vortex was always present for the lower Reynolds number while at higher Re the Lyne-type motion was observed to occur earlier in the cycle for lower values of the Womersley number.

2.4. Summary of previous studies

In table 1 previous studies on flows through curved pipes have been summarized along with the parameter range that they investigated as well as the method applied (note in the various studies different forms of the parameters have been used, see previous paragraphs for details). A review of the studies on different kind of flows in curved pipes along with a separate section on experimental work can also be found in (Berger & Talbot 1983) with more than 130 references while textbooks dedicating sections on oscillatory flows in curved pipes are the – among others – ones by Ward-Smith (1980) and Pedley (1980). It can clearly be seen that whereas there has been given much consideration in laminar pulsating flow or turbulent steady flow, not many studies exist on turbulent pulsating or swirling flow and there is clear lack also of experimental work on highly pulsating or swirling turbulent flow, i.e. when both the Dean and Womersley numbers are high⁷.

⁷High enough so that turbulent flow is ensured throughout the whole pulsation cycle.

2.5. Flow parameters

It feels inherent to close this chapter on flows in curved pipes with a further discussion on the parameters governing such flows that have been presented in the previous sections. Most of them have already been mentioned but here a more detailed description on their definitions and physical meaning will be given.

The flow can in principle be described through the *conservation laws*, i.e. the conservation of *mass*, *momentum* and *energy*. As a reference the momentum equation in its general form (2.4) is given in tensor notation and in Cartesian coordinates. This will help us later in the section to understand the physical meaning of the flow parameters which will be presented.

$$\underbrace{\overbrace{\frac{\partial}{\partial t}(\rho u_i)}^{\text{unsteady acceleration}} + \overbrace{u_j \frac{\partial}{\partial x_j}(\rho u_i)}^{\text{convective acceleration}}}_{\text{Inertia}} = \underbrace{\frac{\partial \tau_{ij}}{\partial x_j} - \frac{\partial p}{\partial x_i}}_{\text{divergence stress}} + \underbrace{\rho f_i}_{\text{other forces}}, \quad (2.4)$$

where p is the pressure, τ_{ij} the viscous shear stress tensor which is defined as:

$$\tau_{ij} = \underbrace{\mu \left(\frac{\partial u_i}{\partial x_j} + \frac{\partial u_j}{\partial x_i} \right)}_{\text{viscous shear stress}} - \frac{2}{3} \delta_{ij} \frac{\partial u_k}{\partial x_k}. \quad (2.5)$$

The ratio of the inertia forces and the viscous forces acting on the fluid can be expressed in terms of the well-known non-dimensional *Reynolds number*:

$$Re \equiv \frac{\text{Inertia force}}{\text{Viscous force}} \propto \frac{\rho u \partial u / \partial x}{\mu \partial^2 u / \partial x^2} \propto \frac{\rho U^2 / L}{\mu U / L^2} = \frac{UL}{\nu}, \quad (2.6)$$

with ρ [kg/m³] denoting the fluid density, U [m/s] the characteristic velocity (e.g the bulk velocity U_b), L [m] the characteristic length (for pipe flows this is usually the radius R or diameter D of the pipe), μ [Pa·s] the dynamic and ν [m²/s] the kinematic viscosity, respectively. One may also note that the Reynolds number can be seen as the ratio between two time scales, a convective time scale (L/U) and a viscous one (ν/U^2).

In the case of curved pipes, the Reynolds number is still of great importance but here an additional force is added to the problem (equation 2.4), the centrifugal force introduced by the curvature of the pipe. This is expressed through the *curvature ratio* defined as:

$$\gamma \equiv \frac{\text{radius of pipe}}{\text{radius of curvature}} = \frac{R}{R_c}, \quad (2.7)$$

where R_c the centerline radius of the bent pipe.

Together the Reynolds number and the curvature ratio yield the *Dean number*, defined for the first time by Dean (1927):

$$De = \sqrt{\gamma} \times Re. \quad (2.8)$$

When an additional motion is superposed on the primary flow, the balance between the forces changes. For example when a swirling motion is added, a Coriolis force is acting on the fluid (in the rotating system) and the centrifugal forces weaken as the swirl intensity increases (see *paper 5*). This is expressed through the swirl number S for which different definitions exist in literature. In cases where the swirling motion is introduced by means of tangential injection of secondary flow or passive methods (guiding vanes) one needs to calculate the so called *integral swirl number*, the ratio between the fluxes of angular momentum to streamwise momentum (Örlü 2009). However, with the present experimental apparatus the mean velocity both in axial and tangential direction are well defined by rotating the whole pipe and the Swirl number can be defined as:

$$S = \frac{V_w}{U_b}, \quad (2.9)$$

where in the case of an axially rotating pipe, V_w is the angular speed of the pipe wall. This is a convenient way to define the swirl intensity since the wall velocity can be directly obtained by the rotational speed of the pipe (which is in this study can be monitored, see also § 3.1).

Last, when a pulsating motion is superposed on the flow, transient inertial forces act on the fluid in counteraction with viscous forces. This is expressed by the Womersley number:

$$\alpha = \frac{D}{2} \sqrt{\frac{\omega \rho}{\mu}}, \quad (2.10)$$

where $\omega = 2\pi f$ [rad/s] is the angular speed with f being the frequency of the pulsations. Sometimes the Womersley number⁸ is referred to in literature as the *dimensionless frequency parameter*: $\sqrt{\omega'}$.

Equation 2.10 shows that the Womersley number is a composition of the Reynolds number and the *Strouhal number*⁹:

$$St \equiv \frac{\text{unsteady acceleration}}{\text{advective acceleration}} \propto \frac{\partial u / \partial t}{u(\partial u / \partial x)} \propto \frac{\omega U}{U^2 / L} = \frac{\omega L}{U} \quad (2.11)$$

where L the characteristic length, in our case the diameter of the pipe. Similar to the Reynolds number the non-dimensional Strouhal number can be seen as a ratio between two time scales, the time scale inherent to the flow motion (L/U) and the time scale of oscillatory motion (ω^{-1}).

For small Womersley numbers the flow behaves quasi-steady since decreasing α means increasing viscous effects which become dominant when $\alpha < 1$. With increasing Womersley number on the other hand the inertial forces become more and more

⁸It should be mentioned here that even though not used within the context of this study an inner scaled frequency parameter can also be defined (*inner scaled Strouhal number*) as $\omega^+ = \omega \nu / u_\tau^2$ where u_τ the friction velocity, for more details see He & Jackson (2009).

⁹It is more frequently used to describe the shedding frequency of a vortex behind a cylinder since it was introduced by Vincenc Strouhal (1850–1922), a Czech physicist, after experimenting with vortex shedding behind wires. It is therefore defined as $St = fL/U$, based on the vortex shedding frequency, f .

important and the velocity starts to show phase lag with respect to the pressure gradient. This phase lag becomes 90° for laminar flow but less than 90° for turbulent flow (Ramaprian & Tu 1983). In literature sometimes the *Stokes number* is used which for laminar oscillatory flow reads:

$$Sto = R\sqrt{\frac{\omega}{8\nu}} \quad (2.12)$$

and in turbulent flow as explained in Ramaprian & Tu (1983) becomes:

$$Sto = \frac{\omega D}{U_b}, \quad (2.13)$$

The turbulent Stokes number is much smaller than the equivalent laminar one for the same frequency rates and it can be seen as the ratio of two characteristic length scales, the pipe radius and the viscous scale $\sqrt{2\nu/\omega}$. The Stokes number was named after *G. G. Stokes (1819–1903)*¹⁰ in honour for his study on the boundary layer in laminar oscillatory flows.

An important parameter for pulsating flows which together with the Womersley and Dean number define the different regimes of the pulsating flow (*quasi-steady, intermediate, inertia dominant*, see also § 5) is the velocity amplitude ratio:

$$A = \frac{Q_o}{Q}, \quad (2.14)$$

where Q_o is the flow rate amplitude of the oscillatory component and Q is the amplitude of the mean flow rate.

Throughout the thesis, the aforementioned numbers are going to be mentioned several times since they are the governing parameters of the flows in focus and from now on the reader will be referred to this section for their definitions.

¹⁰Physicist and mathematician who has been known for his great contribution to fluid dynamics, including the *Navier-Stokes equations* on the fluid motion and the *Stokes' law* on the frictional forces acting on a spherical object e.g. a particle with small Reynolds number in a viscous fluid.

Author(s) (year)	Type of flow	Superposed motion	Type of approach	Measurement technique(s)	Range of		
					De	α	S
Dean (1927)	laminar	–	analytical	–	up to 96	0	0
White (1929)	transitional	–	experimental	Visualization	50–1950	0	0
Taylor (1929)	transitional	–	experimental	Visualization	886–1647	0	0
Tunstall & Harvey (1968)	turbulent	–	experimental	Visualization, hot-wire, gold-shim flag	28280–153440	0	0
McConalogue & Srivastava (1968)	laminar	–	numerical	–	96–600	0	0
Rowe (1970)	turbulent	–	numerical & experimental	yawmeter, pitot tube	47200	0	0
Lyne (1970)	laminar	oscillating	analytical & experimental	photographs	6.57	0.05	0
Greenspan (1973)	laminar	–	numerical	–	10–5000	0	0
Bertelsen (1975)	laminar	oscillating	experimental	tracer method	22.8–1840	8.69–22	0
Agrawal <i>et al.</i> (1978)	laminar	–	experimental	LDV	138–679	0	0
Chandran & Yearwood (1981)	laminar	pulsating	experimental	hot-film	320 & 1140	20.76	0
Enayet <i>et al.</i> (1982)	laminar & turbulent	–	experimental	LDV	212, 463 & 18243	0	0
Talbot & Gong (1983)	laminar	pulsating	experimental	LDV	120 & 372	8 & 12.5	0
Soh & Berger (1984)	laminar	–	numerical	–	108.2–680.3	0	0

TABLE 1. Previous studies on flows through pipe bends.

Author(s) (year)	Type of flow	Superposed motion	Type of approach	Measurement technique(s)	Range of		
					De	α	S
Bovendeerd <i>et al.</i> (1987)	laminar	–	experimental	LDV	286	0	0
Hamakiotes & Berger (1988)	laminar	pulsating	numerical	–	0.7–756	15	0
Sumida <i>et al.</i> (1989)	laminar	pulsating	numerical & experimental	Visualization	90 & 200	5.5–18	0
Hamakiotes & Berger (1990)	laminar	pulsating	numerical	–	38–340	7.5–25	0
So <i>et al.</i> (1991)	laminar	–	numerical	–	277.5–1360	0	0
Lai <i>et al.</i> (1991)	turbulent	–	numerical	–	13875	0	0
Sudo <i>et al.</i> (1992)	laminar	pulsating	numerical & experimental	photographs	40–500	5.5–28	0
Anwer & So (1993)	turbulent	swirling	experimental	hot-film gauge, rotating-wires & pressure taps	13875	0	1
Sudo <i>et al.</i> (1998)	turbulent	–	experimental	hot-wire	30000	0	0
Brücker (1998)	turbulent	–	experimental	PIV	1400 & 3500	0	0
Pruvost <i>et al.</i> (2004)	turbulent	–	numerical	–	14000 & 30000	0	0.125, 0.25, 0.5 & 2.5
Rütten <i>et al.</i> (2005)	turbulent	–	simulations (LES)	–	1400, 2000, 3500 4000, 11000 & 19000	0	0
Ono <i>et al.</i> (2010)	turbulent	–	experimental	PIV	100000, 250000, 318000 & 381000	0	0
Timité <i>et al.</i> (2010)	laminar	pulsating	numerical & experimental	LDV & Visualization	286–1144	1–20	0
Jarrahi <i>et al.</i> (2010)	laminar	pulsating	experimental	PIV	126.6–301.5	8.37–24.5	0

CHAPTER 3

Experimental set ups & techniques

“A scientist in his laboratory is not a mere technician: he is also a child confronting natural phenomena that impress him as though they were fairy tales”

Marie Curie (1867–1934)

“No amount of experimentation can ever prove me right; a single experiment can prove me wrong”

Albert Einstein (1879–1955)

In the following chapter the experimental set ups and techniques that have been used for the purposes of the current study are going to be presented. Two experimental set ups have been used, one where a swirling motion could be generated by rotating a long pipe upstream the pipe bend in order to study effects of a swirling motion on the vortical structures and one where pulsating flow could be created by rotating a valve in order to study pulsatile effects on the flow structures downstream the curved pipe. Due to the complexity of the flow, different techniques had to be used in order to fully investigate the flow field both in terms of statistical quantities and large scale structures. Therefore, PIV was employed to visualize and quantify the coherent structures while combined HWA/CWA was used to statistically analyze the flow field. Finally, LDV has also been applied for further investigation of some of the results from the two aforementioned techniques. Their principles and how they have been applied in the present study are explained in details in the following sections.

3.1. The rotating pipe facility

One of the aims of the current study is to visualize the Dean vortices in turbulent flow and examine the effect of a swirling motion, superposed on the primary flow, on their behaviour. For that purpose Time-resolved Stereoscopic Particle Image Velocimetry (TS-PIV) measurements were conducted at the *rotating pipe facility* in the Fluid Physics Laboratory at KTH Mechanics. Here a general description of the facility (figure 3.1) will be provided, for further details on the set up the reader is referred to (Facciolo 2006; Örlü 2009).

Figure 3.2 shows a schematic of the main experimental set up. The air is provided by a centrifugal fan and the mass flow rate can be controlled by means of a butterfly valve monitored through the pressure drop across an orifice plate. A distribution chamber is implemented in order to minimize the vibrations created by the fan while a



FIGURE 3.1. Close-up of the set up showing the rotating pipe mounted within a triangular shaped framework and connected to the stagnation chamber covered by an elastic membrane in order to further reduce pressure fluctuations.

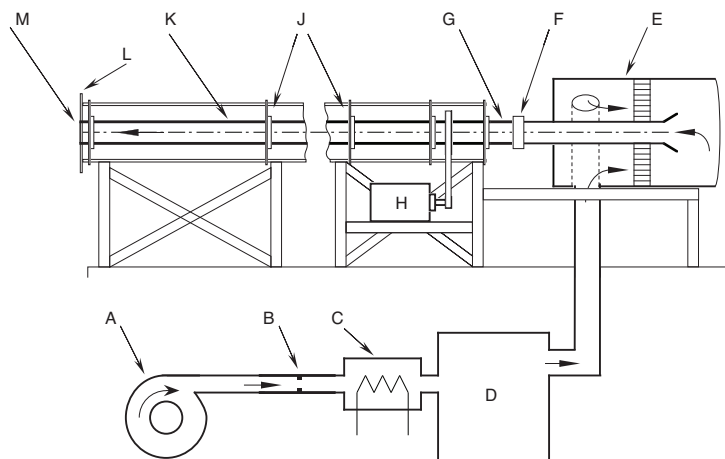


FIGURE 3.2. Schematic of the experimental set up. **A)** Centrifugal fan, **B)** flow meter, **C)** electrical heater, **D)** distribution chamber, **E)** stagnation chamber, **F)** coupling between stationary and rotating pipe, **G)** honeycomb, **H)** DC motor, **J)** ball bearings, **K)** rotating pipe, **L)** circular end plate, **M)** pipe outlet.

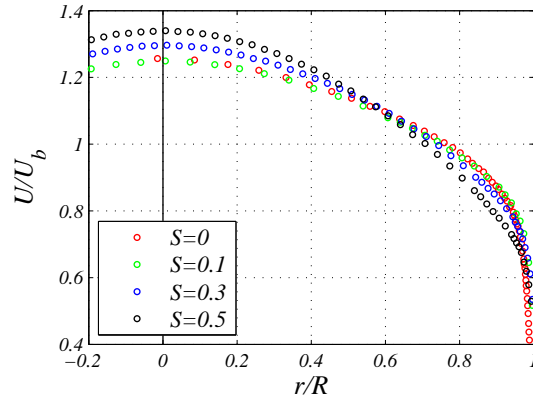


FIGURE 3.3. Mean velocity profiles at the exit of the $100 D$ pipe (see point **M** in figure 1) for $Re_D = 24000$ and for different swirl numbers ($S = 0, 0.1, 0.3, 0.5$). Repr. from Sattarzadeh (2011)

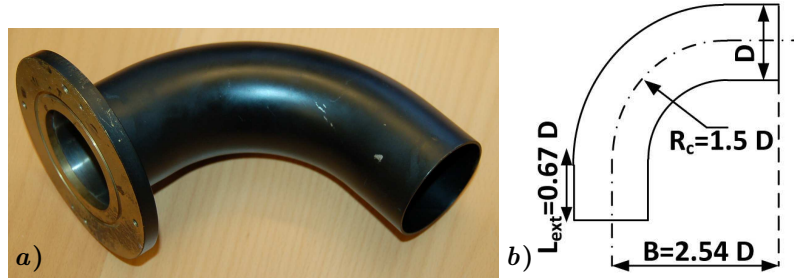


FIGURE 3.4. a) Pipe bend that was mounted at the exit of the $100 D$ long straight pipe. b) Dimensional details of the pipe bend.

honeycomb installed inside a stagnation chamber, where the air is fed into, distributes the air evenly. The air is first led into a one meter long stationary section which is connected to the rotating pipe, which has at its entrance a 12 cm long honeycomb and brings the flow into more or less solid body rotation. The pipe can rotate to speeds up to 2000 rpm by means of DC motor which is connected to the pipe through a belt. The total length of the pipe section is $100 D$ where D denotes the inner diameter of the pipe, equal to 60 mm. Figure 3.3 shows the mean velocity profiles for different swirl intensities at a Reynolds number based on the pipe diameter, $Re_D = 24000$ at the exit of the pipe. The profile for the non-swirling case, depicts very closely what is known for fully-developed turbulent flow while as the swirl number increases the profile shape approaches that of the laminar pipe flow (Sattarzadeh 2011). This constitutes also

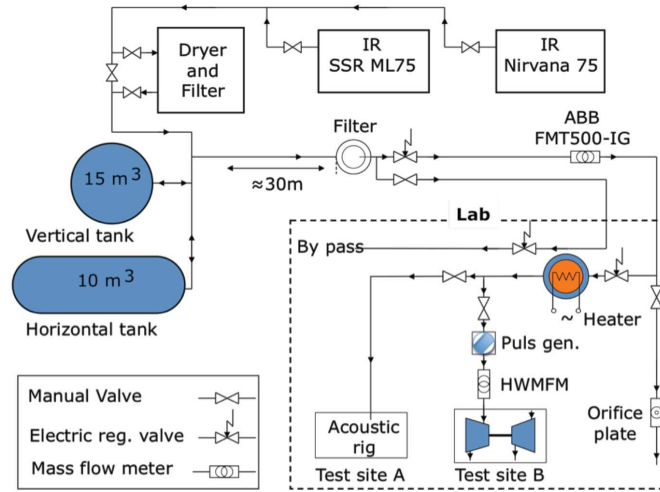


FIGURE 3.5. Layout of the Cicero rig. *Image taken from Laurantzon et al. (2010b).*

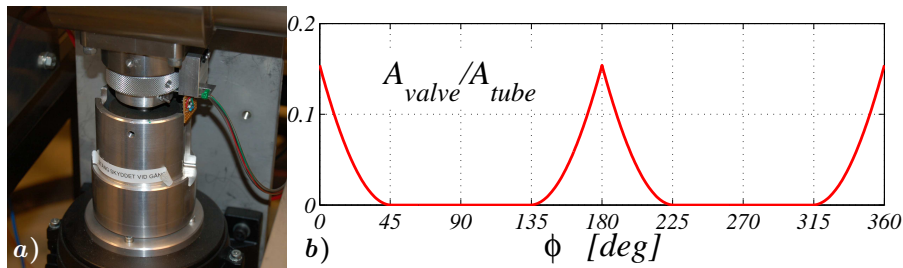


FIGURE 3.6. *a)* The rotating valve (its housing is also shown). *b)* Relative open area change caused by the rotating valve as function of the revolution angle.

the entrance length for the flow which is fed into the bent pipe (figure 3.4). Note that while the straight pipe is rotating, the bend is remaining still. The curved pipe has an inner diameter of $D = 60.3$ mm and curvature radius of $R_c = 95.3$ mm, giving a curvature ratio ($\gamma = D/2R_c$) of 0.31. The length of the straight section after the 90° curvature is $0.67 D$.

3.2. The CICERO rig

The main goal of the current work is to investigate the flow field under the counteraction between centrifugal, inertial and viscous forces and for that purpose the case of a turbulent pulsating flow downstream a pipe bend is considered.



FIGURE 3.7. The two bend pipes used for the measurements performed in the CICERO laboratory. *a)* Bend I *b)* Bend II with the $1 D$ extension mounted on it.

Three experimental techniques have been utilized (see § 3.3-3.5) in order to fully examine the complex flow field and stress the applicability of classical and state-of-the-art experimental methods under harsh flow conditions. The measurements took place at the *CICERO Laboratory* at *KTH CCGEx (Competence Centre for Gas Exchange)*, where a compressor installation facility (two *Ingersoll Rand* screw compressors) has been developed (Laurantzon *et al.* 2010b) that can deliver up to 500 g/s air flow at 6 bar. The *CICERO rig* (see figure 3.5) can be operated under both steady and pulsating flow conditions while the mass flow rate is being monitored by a hot-film type mass flow meter (ABB Thermal Mass Flowmeter FMT500-IG) which is located around 10 m upstream from the measurement site. The pulsations are being supplied by a rotating valve, consisting of a sphere with a tight fitting in a 55 mm pipe, which is located upstream of the pipe test section. The sphere is cut off at two sides, thereby the valve opens twice per revolution (Figure 3.6 depicts the relative open area change caused by the rotating valve as function of the revolution angle). The rotation rate of the valve can be set by a frequency-controlled AC motor and the maximum open area is approximately 15% of the pipe area.

The total entrance length before the flow is fed into the pipe bend (Figure 3.7) is approximately $20 D$, therefore the flow reaching the pipe bend is not fully developed; a condition which is met in most industrial applications (for example in the internal combustion engine which is the focal point in this study, due to packaging constraints the pipe sections connecting the different bends are quite short). Two pipe bends have been used for the experiments performed in the CICERO laboratory and are shown in Figure 3.7 with their geometrical details listed in table 1. At the exit of *Bend II* straight pipe extensions were connected in order to study the flow evolution, which were 0.2 , 1 , 2 and $3 D$ long each. Both bends are considered to be sharp, in accordance with the geometrical characteristics of bent sections found in the engine.

In order to study the effect of the steady and pulsatile flow through a sharp curved bend on the turbine map of a turbocharger an additional set of measurements was performed (see *paper 4* for more details) with the pipe *Bend II* having the $0.2 D$ extension mounted upstream of the turbocharger (Garrett). Figure 3.8 shows the experimental configuration used for these measurement run tests and has been designed,

TABLE 1. Geometrical details of the pipe bends used in the *Cicero Laboratory*. The diameter of the pipe, the curvature radius and the length of the extension downstream the bend are shown.

	D [mm]	R_c [mm]	L_{ext}/D
Bend I	39	45.8	1
Bend II	40.5	51	0.2, 1, 2, 3

built and taken into operation in connection with the work in Laurantzson *et al.* (2012). Instantaneous pressure and mass flow rate measurements were performed across the turbocharger by means of fast response pressure transducers (Kistler) and the vortex mass flow meter introduced in Laurantzson *et al.* (2012), respectively.

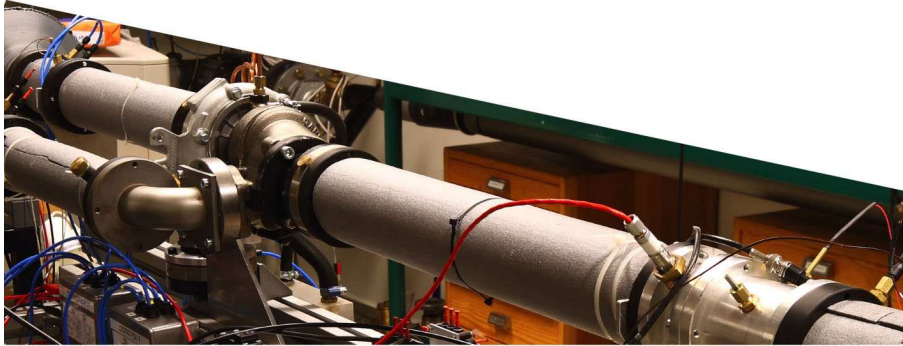


FIGURE 3.8. Set up for the instantaneous pressure and mass flow rate measurements across the turbocharger. Hot wire probes (see next section) comprising the vortex flow meter were placed downstream and upstream of the turbocharger (Garrett).

3.3. Hot/Cold-Wire Anemometry (HWA/CWA)

The use of a heated wire with temperature dependent resistance exposed in air flow to measure the fluid velocity is the basic principle of hot-wire anemometry. It is a relatively cheap, easy-to use technique with high frequency response and has greatly contributed to develop our understanding of turbulence, probably more than any other technique¹. Evidence of interest on the hot-wire principle is traced back to

¹This is referring mostly to the long time that hot-wire anemometry has been available (over a century) to study turbulence compared to other techniques which have also contributed (each one in different ways) to our understanding of turbulence and its structures but they have only been used the last few decades (§ 3.4, 3.5).

Oberbeck (1895) and King (1914), with the first hot-wire sensor being 10 cm long with a diameter of a few tenths of a millimeter (Oberbeck 1895). This shows the great improvements that the technique has gone through, since today subminiature wires down to 0.6 micron diameter can be operated to study the smaller scales of turbulence (Ligrani & Bradshaw 1987).

A few textbooks have been devoted to hot-wire anemometry and its principles such as: Perry (1982); Lomas (1986); Bruun (1995). The aim of the current section is therefore to introduce the reader to the technique and highlight the usability of the method for the purposes of the current study, for more details about the progresses on the method through the years and its applicability on various flows the reader is referred to Comte-Bellot (1976) and Stainback *et al.* (1996).

The hot-wire is simply made by a probe which holds the metal prongs on which the sensor element is soldered or welded on (see also figure 3.9). The number of prongs/sensors as well as the way they are manufactured may vary depending on the applications and/or number of velocity components that need to be measured. The wire element is usually made of tungsten or platinum and the diameters or lengths vary depending on the frequency and spatial resolution required. Typically, a 1 mm long sensor with a diameter of a few microns is used.

The wire is connected to an electrical circuit, so-called Wheatstone bridge, and different operation modes are available. The most common modes are the CTA (Constant Temperature Anemometry) and the CCA (Constant Current Anemometry) mode. The names speak for themselves, i.e. in CTA mode the wire is operated under constant temperature by means of a servo amplifier. This keeps the bridge in balance by controlling the current to the sensor and keeps the resistance constant, independent from the cooling of the element due to the fluid flow. The change in voltage gives a measure of the fluid velocity (indirectly through the heat transfer). The resistance of the hot-wire is given by:

$$R_w = R_0[1 + \alpha_0(T_w - T_0)] \quad (3.1)$$

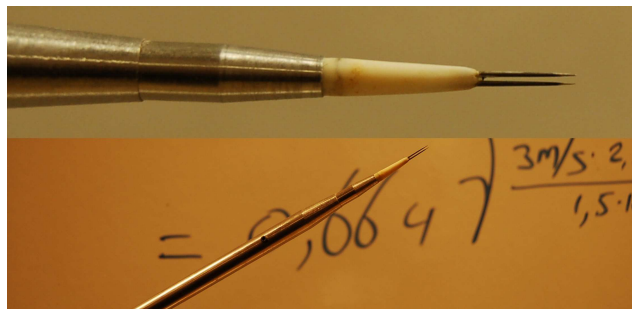


FIGURE 3.9. A single hot-wire with diameter $d = 2.5\mu\text{m}$ and length $l = 0.5$ mm. The probe has been manufactured at the Fluid Physics Laboratory, KTH Mechanics.

and is a function of the wire temperature, T_w . Usually the reference temperature is chosen as $T_0 = 20^\circ\text{C}$ and the temperature coefficient of resistivity of the wire, α_0 , can be determined through an iterative method (see § 3.3.2). The resistance overheat ratio $a_R = (R_w(T_w) - R_0(T_0))/R_0(T_0)$ is a function of the temperature overheat ratio: $a_T = (T_w - T_0)/T_0$ and determines the velocity sensitivity of the wire.

In CCA mode the current is kept constant and the decreasing voltage with increasing effective cooling velocity is measured. This has been the first mode of operation for hot-wires but due to the thermal inertia of the wire element the frequency response is limited and it is today mainly used for temperature measurements. This requires that the response from the wire (cold-wire in that case) is only due to temperature variations, therefore the current in CCA mode should be set by the user high enough to get satisfactory temperature resolution but small enough so that the sensitivity to velocity variations is negligible.

One of the main drawbacks of hot-wire anemometry for measurements in highly pulsating flows is the so-called “forward-reverse ambiguity” (Bruun 1995) as well as its fragility. A few techniques have been developed through the years in order to measure reverse flow with a hot-wire but they are cumbersome and have certain limitations (Moulin *et al.* 1997; Günkel *et al.* 1971). Furthermore, flows through bends are three-dimensional and even though there is the possibility of measuring all three velocity components, this is a complicated and time-consuming procedure. Last but not least, another disadvantage of the technique is the need for compensation for the temperature variations which can be quite large depending on the amplitude of the periodic component in a pulsating flow. Measurements performed in the *CI-CERO Laboratory* (Laurantzon *et al.* 2010*b*) have shown temperature variations of up to 6° which correspond to underestimation of the flow speed by around 20 m/sec. Therefore, hot-wire measurements in a highly pulsating environment should always be corrected for temperature variations, consequently cold-wire measurements should be performed simultaneously with the hot-wire measurements (see also § 3.3.2). For a more detailed usability of the hot-wire technique under pulsating flow conditions, the reader is referred to Berson *et al.* (2010). One can not neglect though, even under those limitations, the advantages of the hot-wire compared to non-intrusive techniques (see also § 3.4 and 3.5), namely its high frequency response and temporal resolution. When studying turbulence statistics for example or the small scales of turbulence, hot-wires cannot be easily replaced.

In the present study both a manual and a semi-automatic traversing mechanism for the movement of the hot-wire probe have been used (figure 3.10). In the case of the manual traverse (see also *Paper 1*) the measurements were performed by means of a single hot-wire, neglecting the effects from temperature variations with the aim to get a first impression of the velocity profile at high Reynolds and Womersley numbers. The semi-automatic traverse was later designed in order to rotate a combined HW/CW probe controlled by a DC motor and map the whole cross-sectional area of the curved pipe. The reader should keep in mind that when comparing the results in the present study from the different experimental techniques employed, the geometry was slightly different, as apparent from figure 3.10, i.e. due to technical restrictions a $6 D$ long straight pipe had to be mounted downstream the measurement plane. The effects of such a configuration are planned to be examined in the future. Typically

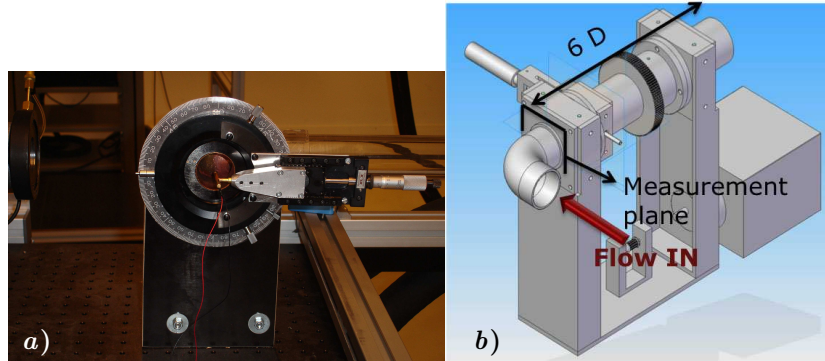


FIGURE 3.10. *a)* The manual traversing system with the single wire probe mounted. *b)* Automatic traversing mechanism showing the direction of flow and the combined HW/CW probe being positioned upstream of a $6 D$ long straight pipe.

a $5 \mu\text{m}$ hot-wire with $\ell/d = 200$ was used in both cases while a cold-wire of $2.5 \mu\text{m}$ diameter and $\ell/d = 600$ (where ℓ and d are the length and diameter of the wire, respectively) was used in the case where hot/cold-wire measurements were performed simultaneously in accordance to Bruun (1995).

3.3.1. Hot-wire calibration

Since with the hot-wire we can only measure velocity indirectly, a calibration procedure in order to translate the measured voltage into velocity is required. The calibration can be done either *in situ*, which is of course recommended but also in some cases where this is not possible, the calibration can be done outside of the measurement site.

The hot-wire is here calibrated in a nozzle facility where a differential pressure transducer gives the dynamic pressure. The voltage acquired from the hot-wire is plotted against the velocity of the flow (the dynamic pressure is translated in velocity) for the whole range of the expected velocities during the measurements, therefore a complete mapping between voltage of sensor and flow velocity is obtained by fitting a curve between the acquired points using the following equation introduced by King (1914), therefore named after him as *King's law*:

$$E^2 = A + B(\rho U)^n \quad (3.2)$$

A typical calibration curve is shown in figure 3.11².

3.3.2. Temperature compensation

As mentioned already, the temperature varies under one cycle in pulsating flows. This will lead to considerable errors when measuring the velocity by means of a

²Note that the voltage here is amplified as well as in figure 3.12

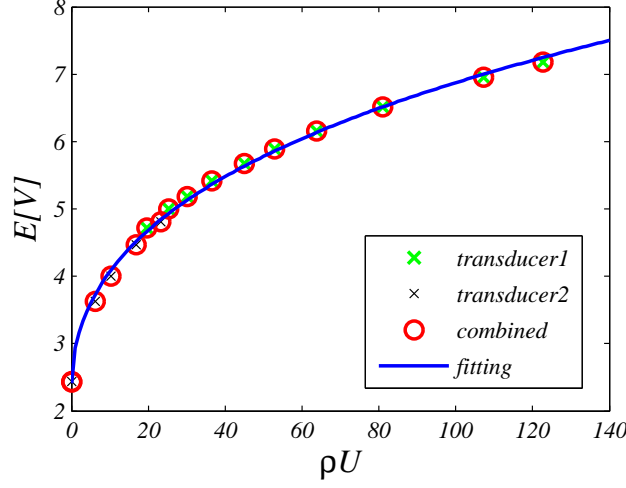


FIGURE 3.11. Calibration curve for a hot-wire (E vs ρU). The calibration points have been acquired in reference with two pressure transducers for two speed ranges.

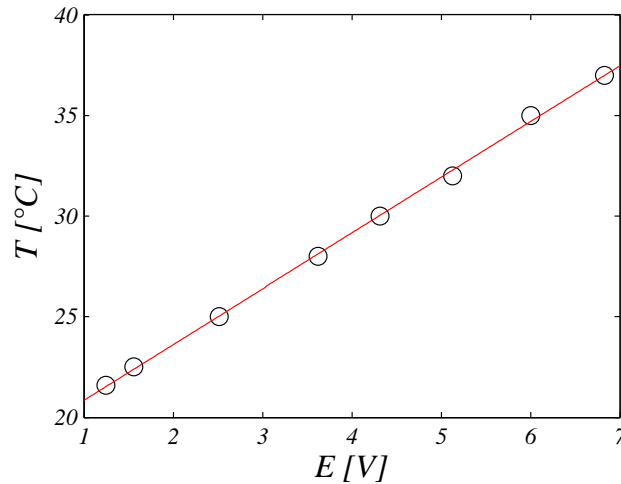
hot-wire in CTA mode (Bruun 1995; Berson *et al.* 2010). In the present study, cold-wire measurements were performed simultaneously with the hot-wire measurements in order to compensate the voltage readings for temperature variations according to equation:

$$E_c^2 = E^2 \left(1 - \frac{T - T_0}{\alpha_R / \alpha_0} \right)^{-1} \quad (3.3)$$

where E_c the compensated voltage, T_0 the reference temperature and α_0 the temperature coefficient of resistivity of the wire.

The calibration of the cold-wire provides a linear relation between the voltage and the temperature since the resistance of the wire is proportional to the voltage and therefore to the temperature (T). A typical calibration curve for a cold-wire is shown in figure 3.12.

For the determination of the temperature coefficient of resistivity of the wire, α_0 in relation 3.3, the hot-wire is calibrated first under ambient room temperature and then calibrated in heated flow. The temperature variations are monitored by means of a thermocouple. The two calibration curves obtained for the two cases are thereafter fitted using King's law as described above and the value of α_0 for which the two calibration curves collapse on top of each other is chosen. The values found in the present measurements were $\alpha_0 = 0.0015K^{-1}$ when platinum-rhodium was used as the hot-wire material and $\alpha_0 = 0.0039K^{-1}$ when platinum was used. These values are quite close to those reported in Bruun (1995) at 20°C.

FIGURE 3.12. Calibration curve for a cold-wire (T vs E)

3.4. Particle Image Velocimetry (PIV)

“Any sufficiently advanced technology is indistinguishable from magic.”

Arthur C. Clarke (1917–2008)

“A picture shows me at a glance what it takes dozens of pages of a book to expound.” (in Fathers and Sons)

Ivan Sergeevich Turegev (1818–1883)

Phrases that people use in everyday life such as: “*A picture is worth a thousand words*”³ (figure 3.13), “*I believe only what i see*” etc, express perfectly how a complex idea or a large amount of data can be conveyed by a single image as well as the tendency of humans to believe what their eyes can evince.

Those facts but also human curiosity led to the progress of visualization. The first efforts of visualizing natural phenomena and the people who mastered them can be found in Nakayama & Aoki (2001), including—among others— scientists such as the avant-garde *Leonardo DaVinci (1452–1519)*, the innovative *Osborne Reynolds (1842–1912)* and the father of modern aerodynamics *Ludwig Prandtl (1875–1953)*.

³This adage is believed to have its origins in an article promoting the use of images in advertisements that appeared on the sides of streetcars. The article was published in 1921 and had the title “One look is worth a thousand words” but a few years later the quote appeared in the same journal rephrased to “One picture is worth ten thousand words” and was credited to Confucius (551 BC–479 BC). It is also sometimes attributed to Napoleon Bonaparte (1769–1821) who used to say “A good sketch is better than a long speech” (“*Un bon croquis vaut mieux qu’un long discours*”). Nevertheless, the adage expresses perfectly the aim of visualization.

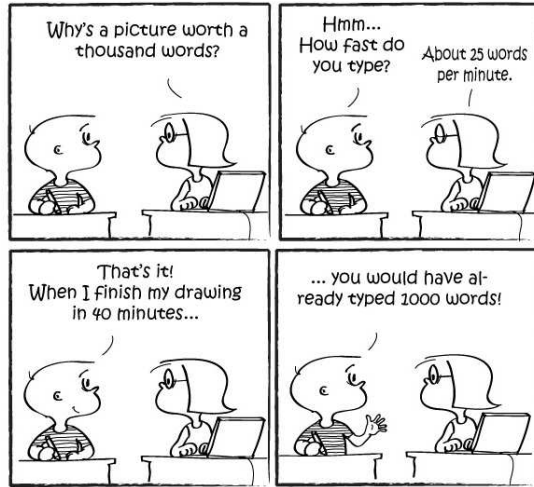


FIGURE 3.13. Comical illustration of the famous quote.
 (Source: <http://cartoosh.com/gigglebites>)

The need to not only visualize but also determine quantitatively flow phenomena, led to the development of particle image velocimetry. Making possible one of the great challenges of the 20th century in fluid mechanics, to both determine flow structures with high accuracy and visualize them at the same time, established PIV one of the “hot topics” the past few years in experimental techniques. Being a relatively new method (“making an entrance” in the fluid mechanics community almost a century after HWA) it has developed rapidly taking into account the cost of operation and complexity of components involved.

The principle of PIV is quite simple (figure 3.14). The flow is seeded with particles matching the density of the fluid medium so that they follow the flow ideally. This of course is never perfectly the case so one has to make the assumption that the distribution of particles is uniform and that they track the flow truly. How well the particles follow the flow can be indicated by the particle response time: $\tau_p = d_p^2(\rho_p/18\mu)$ (where the transcript p denotes *particle*), and is a convenient measure of the tendency of particles to follow the flow, even if the acceleration of the fluid is not constant or if the Stokes’ drag law⁴ does not apply. Also the ratio of τ_p to the *Kolmogorov time scales* in turbulent flows can be used and in that case a ratio value less than 0.1 is desired to assume that the particles follow the flow satisfactorily.

After the flow is seeded homogeneously, the measurement plane is illuminated twice by some light source (usually a powerful laser) in a very short interval of time Δt and the light scattered by the particles is recorded either on a single frame or sequence of frames. Here we will consider the double-frame/single-exposure recording technique

⁴In 1851, G. G. Stokes derived an expression for the frictional force exerted on spherical objects with very small Reynolds numbers ($Re \ll 1$) in a continuous viscous fluid making the assumptions of laminar flow, spherical particles which do not interact with each other.

which preserves the temporal order of the PIV recordings and is usually preferred if appropriate equipment is available (for a description of all the possible PIV recording techniques the reader is referred to c.f. (Raffel *et al.* 2007)). Since the aim of PIV is not only to visualize the flow but estimate it quantitatively, the post-processing and evaluation of the images and the methods used to reach a high accuracy level is of great importance. The basis of the analysis of PIV data is cross-correlation. The images taken at the two different instances are divided in small interrogation windows (or areas or spots) and thereafter for each one of those areas a correlation peak is obtained which gives the particle (pixel) displacement. Sophisticated algorithms to increase resolution and accuracy have been developed such as multi-pass processing of the images with adaptive interrogation window sizes as well as window deformation. The fundamentals of PIV as well as information on data validation algorithms to increase accuracy and minimize the measurement error can be found in Westerweel (1994, 1997). Thereafter, knowing the time between the illuminations and determining the displacement of the particles within that time as described above, one can “simply” obtain the flow velocity.

The accuracy and the resolution of PIV data can be limited due to technical restrictions of the PIV hardware as well as the noise which is apparent when electronics are involved in the measurements. Furthermore the Signal-to-Noise ratio (S/N) can be affected from velocity gradients (for example in pulsating flows or flows after curvatures) or particles which move outside the interrogation window between one frame and the next. Nevertheless, technological advances have made it possible to succeed high enough spatial resolution in order to resolve small scale structures and record

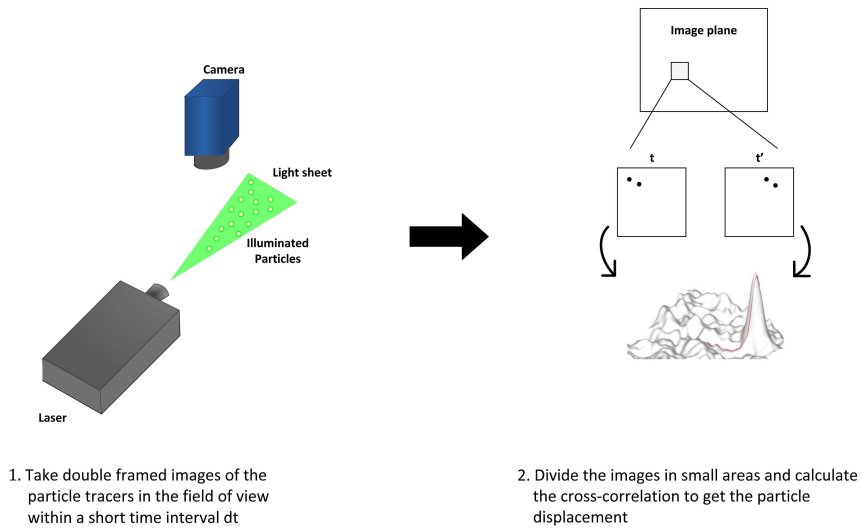


FIGURE 3.14. Basic principle of planar 2D PIV.

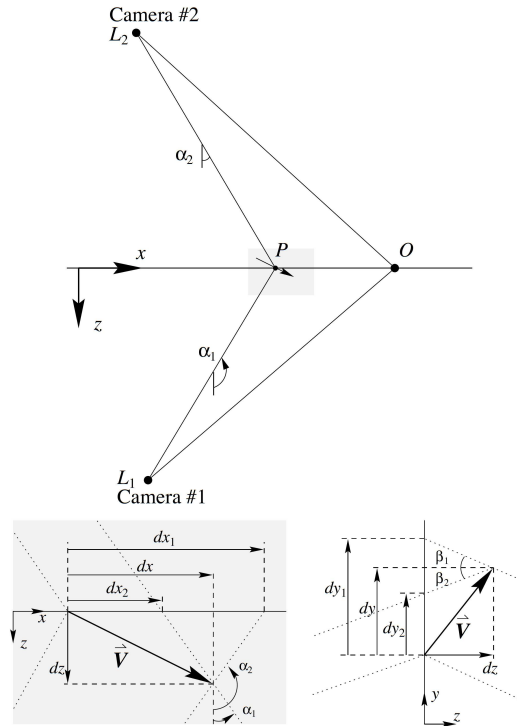


FIGURE 3.15. Geometric description used for reconstruction of the three-dimensional displacement vector. *Image taken from Willert (1997).*

flows at supersonic speeds with acceptable noise levels⁵ while there exists a rule to choose the time between the two illuminations so that the particle displacement d_s is: $0.1 \text{ pixel} < d_s < 1/4$ (where 0.1 pixel equals the accuracy of the system) the interrogation area size to avoid particle image pair losses.

A typical 2D-PIV set up to measure two velocity components consists of one camera and one light source. Stereoscopic PIV (SPIV) with two cameras set at a known angle in-between them (typically 90°) can be performed and the third displacement field can be reconstructed i.e. the displacements from each image plane are mapped to the object plane and by combining them the three-dimensional velocity vectors is

⁵Today, CMOS (Complementary Metaloxide Semiconductor) cameras allow acquisition of images with a few kHz frequency with an interframing of less than $1 \mu s$ and diode pumped lasers (e.g. Nd:YLF) operate at repetition rates of tenths of kHz.

obtained⁶ (Willert 1997; Prasad 2000; Calluaud & David 2004; Doorne & Westerweel 2007).

The reconstruction geometry is simple, here the imaging geometry shown in Willert (1997) is considered but the following formulae can be adapted to any other case. If an origin point O in the light sheet has coordinates (x_0, y_0, z_0) and assuming the coordinate system shown in figure 3.15 we place two cameras at any angle in-between them (note here both cameras are placed on either side of the laser sheet i.e. in forward scatter mode), the displacement vector at a point P (x_p, y_p, z_p) within the light sheet is given by:

$$dx = \frac{dx_2 \tan \alpha_1 - dx_1 \tan \alpha_2}{\tan \alpha_1 - \tan \alpha_2} \quad (3.4)$$

$$dy = \frac{dy_2 \tan \beta_1 - dy_1 \tan \beta_2}{\tan \beta_1 - \tan \beta_2} \quad (3.5)$$

$$dz = \frac{dx_2 - dx_1}{\tan \alpha_1 - \tan \alpha_2} = \frac{dy_2 - dy_1}{\tan \beta_1 - \tan \beta_2} \quad (3.6)$$

where:

$$\begin{aligned} \tan \alpha_1 &= \frac{x_p - x_1}{z_p - z_1} & \tan \alpha_2 &= \frac{x_p - x_2}{z_p - z_2} \\ \tan \beta_1 &= \frac{y_p - y_1}{z_p - z_1} & \tan \beta_2 &= \frac{y_p - y_2}{z_p - z_2} \end{aligned}$$

with dx_1 and dx_2 being the displacements in the x -direction as viewed from the two cameras (which here are assumed to be the points $L1(x_1, y_1, z_1)$ and $L2(x_2, y_2, z_2)$). α_1 and α_2 compose the angle enclosed by the viewing ray and the light sheet parallel to the z -axis for the respective viewing directions projected onto the xz -plane. Accordingly, the same can be defined by projecting the yz -plane and therefore the angles between the cameras are β_1 and β_2 and the displacement components are dy_1 and dy_2 .

In the case when the cameras are set in the same vertical position as the field of view the angles β_1 and β_2 become small, therefore equation 3.5 must be rewritten to:

$$dy = \frac{dy_1 + dy_2}{2} + \frac{dz}{2}(\tan \beta_2 - \tan \beta_1) = \quad (3.7)$$

$$\frac{dy_1 + dy_2}{2} + \frac{dx_2 - dx_1}{2} \left(\frac{\tan \beta_2 - \tan \beta_1}{\tan \alpha_1 - \tan \alpha_2} \right) \quad (3.8)$$

The aforementioned reconstruction (Willert 1997) requires that the displacement data set is translated to true displacements in the global coordinate system. Additionally, in the case of stereo PIV special adapters (Scheimpflug) should be used on

⁶It should be mentioned here that nowadays it is also possible to perform tomo-PIV, i.e. to directly measure the three velocity components in a volume instead of a plane (Elsinga *et al.* 2006) but this technique is far beyond the scopes of this thesis.

the lenses so that the image, lens and object plane intersect in a common line (Prasad & Jensen 1995)(figure 3.16). This however introduces a strong perspective distortion since the factor of magnification is no longer constant across the complete field of view. Therefore calibration of the cameras is essential to tackle the above issues and different approaches exist in literature (Prasad 2000).

In the present study, Time-resolved Stereo-PIV (TS-PIV) has been used to measure turbulent flow with and without a swirling or pulsating motion superposed at high velocities, that requires a high-speed PIV system. Two high-speed C-MOS cameras (Fastcam APX RS, Photron, 3000 fps at 1024×1024 pixels) were positioned at an angle of approximately 90° (figure 3.17) and at forward-backward scatter mode at the vicinity of the pipe bend exit and 105 mm Nikon Nikkor lenses were adjusted using a Scheimpflug adapter. A laser light sheet of approximately 1 mm thickness was produced by a Nd-YLF laser (Pegasus, 10 kHz maximum frequency, New Wave Research) and a water-based solution (Jem Pro Smoke Super ZR-Mix) was atomized using a high volume liquid seeding generator (10F03 Seeding Generator, DANTEC). A calibration-based reconstruction approach that also provides information about the viewing direction of the cameras was undertaken. Images of a two level⁷ calibration plate (figure 3.18) which has equally spaced marks and is coincident with the laser sheet, are acquired and thereafter the information from those images are used to map the object plane to the measurement plane. In the present study the calibration is done using the pinhole model in order to fit the dewarping mapping function to the marks found in each image, using the DaVis 7.2 software by LaVision GmbH. The images are first dewarped and then the 2D2C vectors are computed at the correct world grid but the dewarping and image deformation is done here once before each step of the multi-pass iterative scheme. In the end, a self-calibration procedure to eliminate errors from misalignment of the laser light sheet with the calibration target

⁷Multiple-level calibration plates with reference targets at different heights are essential if information on the viewing angle of the cameras is needed to be obtained to reconstruct the three-component displacement vector in the case of SPIV.

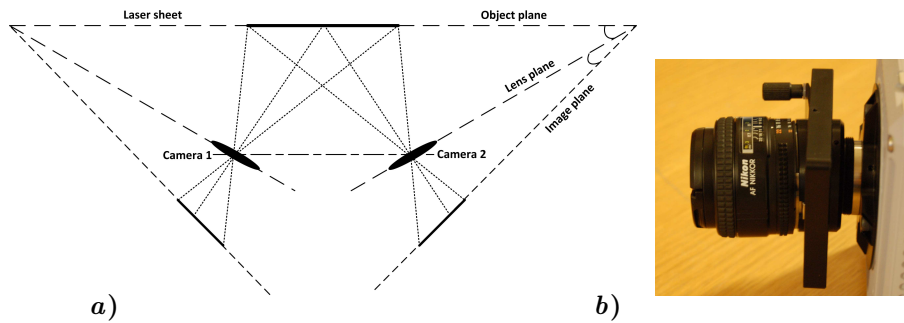


FIGURE 3.16. *a)* The cameras in an angular position and according to the Scheimpflug condition. *b)* The camera lens (Nikon Nikkor, 60 mm shown here) having the Scheimpflug adapter mounted on it.

is being performed. Disparity correction of the recordings is advised in general when performing SPIV since considerable errors in PIV measurements might arise if the

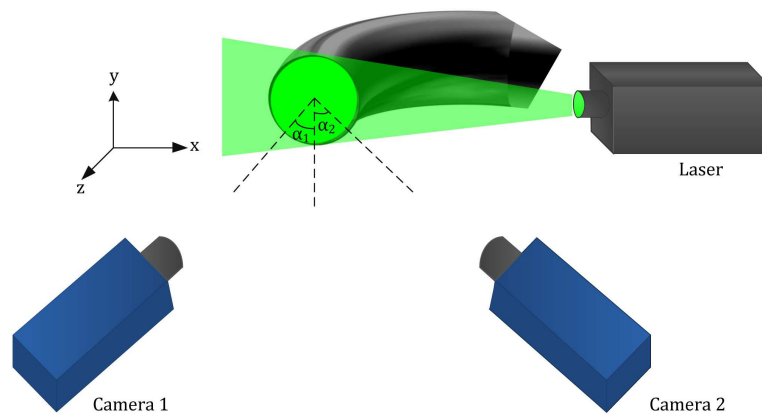


FIGURE 3.17. Set up of the PIV system at the vicinity (≈ 0.5 mm from the pipe exit) of the pipe bend exit.



FIGURE 3.18. Two-level calibration plate provided by LaVision GmbH. Levels are separated by 2 mm, dots are equally spaced within 15 mm from each other.

light sheet does not coincide with the $z = 0$ plane. Details about the aforementioned approach can be found in Wieneke (2005).

For details on the post-processing of the data the reader is referred to the corresponding papers in *Part II* of the thesis. In all the cases a median test⁸ has been used to detect *outliers*, i.e. data deviating strongly from neighboring data and replaced by a linear interpolation of the neighboring vectors.

⁸A median vector is computed from eight neighboring vectors and the middle vector is compared with this median vector. The center vector is rejected when it is outside the allowed range of the average vector. For details see Westerweel (1994)

3.5. Laser Doppler Velocimetry (LDV)

The first work on LDV was done in the early '60's (Yeh & Cummins 1964) and now almost 50 years later it is a well used single-point technique to determine the flow velocity. An extended description on the principle of LDV and its applications is found in Zhang (2010). The flow is seeded here as well and two coherent beams of monochromatic light intersect at a point in the measurement volume creating a fringe pattern. The transmitter (laser) light impinges on the moving particle and light is scattered and received by a stationary detector (figure 3.19). By knowing the Doppler-equivalent frequency of the laser beam and the frequency of the scattered light the velocity of the particle and therefore the flow velocity can be determined.

In the present study LDV measurements were performed with a single component DANTEC FlowLite system and a BSA 60 processor. The emitting light source is a 10 mW He-Ne laser with wavelength of 632.8 nm. The lens mounted on the laser is 400 mm in focal length. The liquid used for seeding is a *Shell Odina 27* oil.

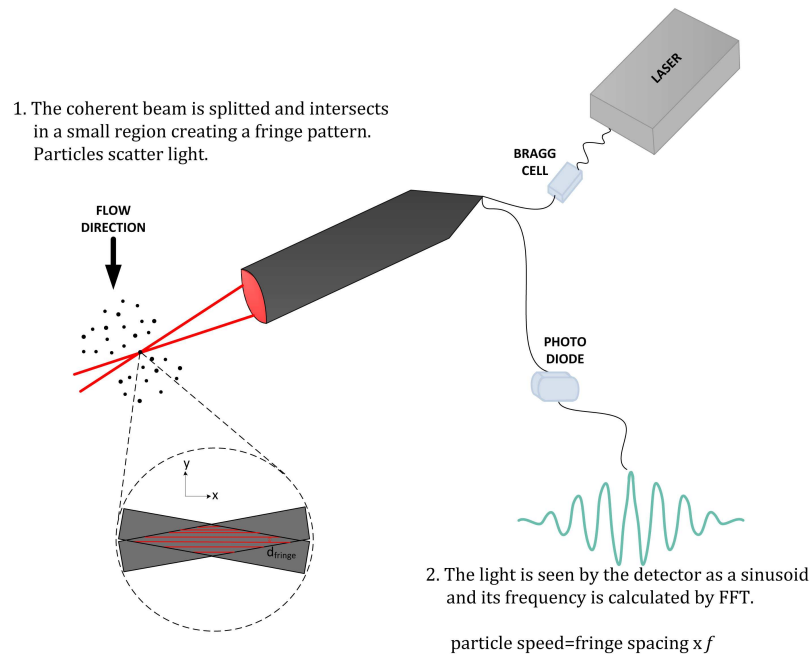


FIGURE 3.19. Laser Doppler Velocimetry set up

3.6. Experimental methods for the study of complex flows

The techniques mentioned in § 3.3-3.5 are three of the most commonly employed techniques nowadays in experimental fluid mechanics for the measurement of the unsteady flow velocity. Each one of them has its own unique capabilities which can be exploited to gain specific information depending on the flow under study and the aim of the respective work. A comparison between the three techniques is quite revealing (table 2) and from a first impression it is obvious that the decision on which technique to choose for the experiment relies greatly on the nature of the flow and which features need to be investigated (e.g. structures, statistics). PIV for example, provides extreme possibilities for the study of structures but it is still limited when studying statistics, where the hot-wire is unrivaled due to its much higher spatial and temporal resolution. On the other hand, to consider mapping a pipe cross-section for all velocity components with a single-point technique is time-consuming and complicated (e.g. manufacturing of multiple-probe hot-wires, calibration and so on).

In the case of a complex flow, that might be described by three-dimensionality, flow skewness, streamline curvature, adverse and favorable pressure gradients, temperature and velocity variations in time and so on, a combination of the experimental methods is necessary. In such cases, errors or limitations of each technique cannot be neglected in a highly complex flow as maybe done in simpler flows. For example, in low speed steady flows through straight pipes, the temperature variations or the secondary flow are normally not large and their effect on the hot-wire readings can be disregarded or the time resolution needed for statistical analysis of the flow can be covered satisfactorily by the features of the present PIV hardware available.

TABLE 2. Typical properties of experimental techniques for the measurement of flow velocity

	HWA	LDV	PIV
Type	single-point	single-point	multiple point
Spatial resolution	$5 \mu\text{m} \times 1 \text{ mm}$	$100 \mu\text{m} \times 1 \text{ mm}$	$32 \times 32 \text{ px}$ for $2048 \times 2048 \text{ px}$ image
Intrusive	✓	×	×
Dynamic Range	12-16 bit	16-bit	6-10 bit
Frequency response	up to 50 kHz	up to 30 kHz	

Within the framework of this project a data base including hot-wire, LDV and PIV data has been obtained with the aim to further study the features of each technique in a highly complex flow environment (curved and pulsating flow). Preliminary results will be presented here, however future analysis is intended to be performed.

TABLE 3. Flow parameter range considered in the present project.

	Re ($\times 10^4$)	γ	α	z/D
HWA	4.2	0.4	0	1
	4.2	0.4	0	2
	4.2	0.4	40	3
	2.7	0.4	40	3
	8.7	0.4	40	3
LDV	2.7	0.4	0, 40, 70	0.2
	2.7	0.4	0, 40, 70	3
PIV	2.7	0.4	0, 40, 60, 70	0.2
	2.7	0.4	0, 60	1
	2.7	0.4	0, 60	2
	4.2	0.4	0, 40	3
	2.7	0.4	0, 40, 70	3
	4.2	0.4	0	3

The hot-wire data have been acquired by means of the semi-automatic traversing mechanism described in § 3.3 while for the PIV and LDV the respective set ups are described in § 3.4 and 3.5.

Table 1 shows the parameters for which data have been acquired with each technique. In this section results will be shown only for the data sets which are highlighted in blue.

The parameter range varies depending on the technique used. The reader should note that the aim of the study is not to compare the data obtained with the different techniques but rather emphasize the necessity of combining them to exploit the features each one offers for the study of complex flows like the ones considered here. Therefore, the Reynolds and Womersley numbers were higher for the hot-wire measurements than for the PIV. At such high speeds the particles leave the thin laser sheet while the time between the laser pulses can not be easily adjusted since the velocity gradient is becoming larger after the bend with increase in speed and pulsation frequency. On the other hand at low speeds and pulsation frequencies, the PIV was employed in order to visualize the secondary structures. Finally, LDV was used to check the dynamic range capabilities of the PIV (in pulsating flow conditions where the velocity might range from negative velocities to a few times the bulk velocity) and the falsifying effects of the temperature variations and back flow on the hot-wire readings.

TABLE 4. Sampling conditions for the experiments.

	Sampling time [s]	Sampling frequency [kHz]	Number samples
HWA	20	20	400000
LDV	30	1 (average)	30000 (average)
PIV	1 & 0.66	1 (steady flow) & 1.5 (pulsating flow)	1000

Table 4 shows the different conditions under which the data for the present study were acquired for each experimental method. The sampling differences are quite remarkable due to the different features of each method and they should be kept in mind when evaluating the results from each one of them. Also as mentioned already in § 3.3, for the hot-/cold-wire data due to technical restrictions, the experimental set up was quite different than for the PIV and LDV measurements.

Figure 3.20 shows contour plots of the mass flow rate density (denoted here as ρW) sensed by the hot-wire. The asterisk denotes scaling by the bulk mass flow rate density obtained with the ABB mass flow meter (see also § 3.3). The flow development for three downstream stations (1, 2 and 3 D) from the pipe bend exit is shown and for $De = 2.7 \times 10^4$. All the hot-/cold-wire data shown here have been obtained by rotating the probe by means of the semi-automatic traversing mechanism. The development of the flow is illustrated, with the flow field being highly skewed at the 1 D station depicting the faster moving fluid positioned distinctively near the outer wall and the slower fluid close to the inner. However, traveling further downstream, the flow slowly starts to recover from the bend effects and a more homogeneous flow field is being formed at the 3 D station. The development of the flow at different stations downstream the pipe bend has also been studied by means of PIV (papers 2 and 3) and the same flow behavior was depicted. The advantage of using PIV compared to hot-wires in this case is the much less acquisition time but most important, the development of the secondary flow could additionally be obtained. To serve as an indication of the complexity involved in the mapping of a pipe cross-section by means of single-point techniques, it should be mentioned that the sampling frequency for the hot-/cold-wire measurements was 20 kHz and the number of samples 400000, which yields a sampling time of $T_s = 20$ s for each measurement point. This translates into a total acquisition time of more than one hour for the positions taken (8 positions along the axis and 24 angular positions). This underlines the large differences in the acquisition time, needed to map a pipe cross-section between single- and multi-point measurement techniques. Similar experiments performed with the PIV (see papers 2 and 3) provided the velocity field across a pipe cross-section in a total time of one second. Nevertheless, the high temporal resolution of the hot-wire data will be used in the future for further statistical analysis of the flow, similarly to what has been done before (*Paper 1*) but for the whole cross-sectional area and for correcting the

hot-wire readings for temperature variations which has not been done in the previous work.

A surface plot of the phase-averaged mass flow rate density for different phase angles and for $De = 1.5 \times 10^4$ and $\alpha = 40$ is shown in figure 3.21. It can be seen that even though at the end of acceleration the velocity reaches three times the bulk velocity, the effect of the secondary flow is still evident from the skewed shape of the velocity field.

In figure 3.22 both the instantaneous and phase-averaged signals at the centerline of the pipe are shown for $De = 1.5 \times 10^4$ and $\alpha = 40$ and for data obtained with the three experimental methods, i.e. hot-/cold-wire, PIV and LDV. Here, the differences between the three techniques are highlighted for a complex flow (curved and pulsating). From the instantaneous data it can be seen that the samples from the LDV are not equidistant, especially in low velocities (this is due to the random arrival of seeding particles to the measuring volume which might bias statistical quantities that depend on the time resolution) while the temporal resolution of the hot-wire can not be rivaled by any of the other two techniques. The dynamic range of the PIV seems to be quite broad, expanding from almost zero velocity to three times the bulk and agreeing satisfactorily with the results from LDV. The low temporal resolution of the PIV can clearly be seen in both figures, especially when comparing with the hot-wire where the phase-averaged signal was calculated for many more valve cycles than for the PIV where only a few could be used for the number of images available.

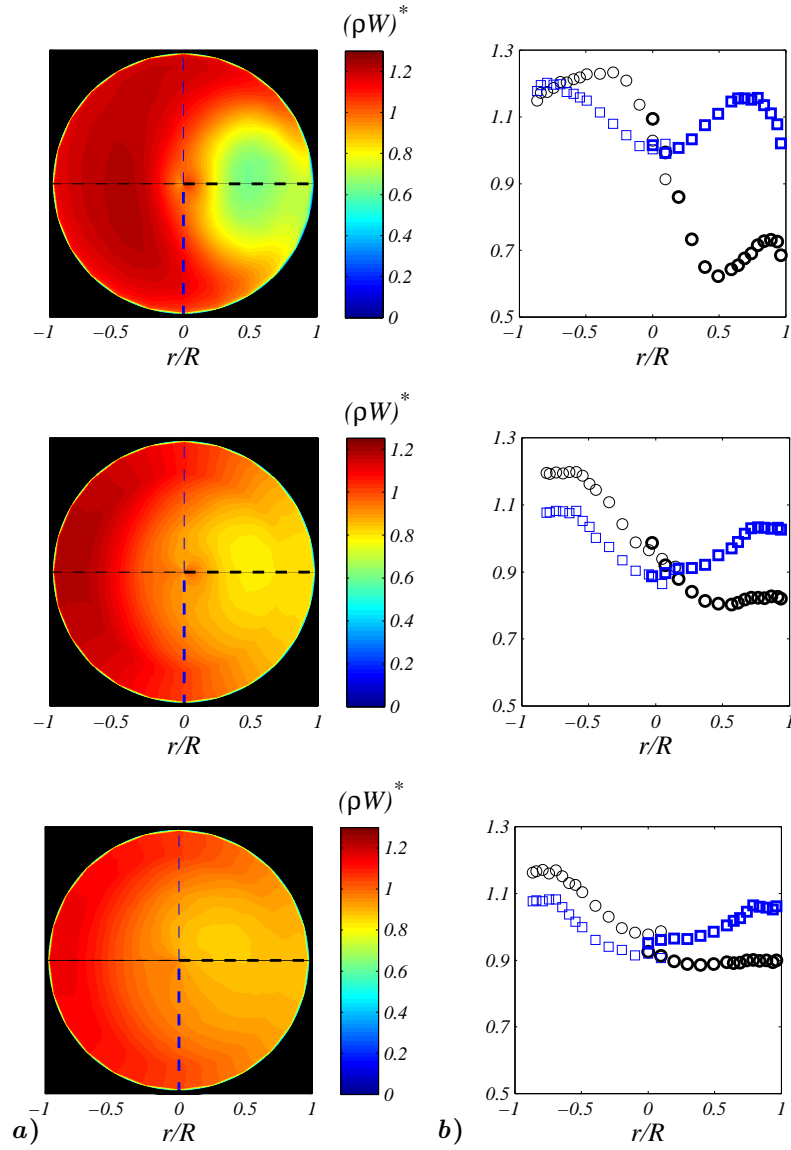


FIGURE 3.20. Contour plots (a) and velocity profiles of the streamwise component along the horizontal (o) and vertical (□) pipe axis (b) from hot-wire data acquired at three downstream stations (1, 2 and 3 D from top to bottom) from the bend exit. The mass flow rate density (ρW) has been scaled by the bulk mass flow rate density obtained with the ABB mass flow meter. $De = 2.7 \times 10^4$.

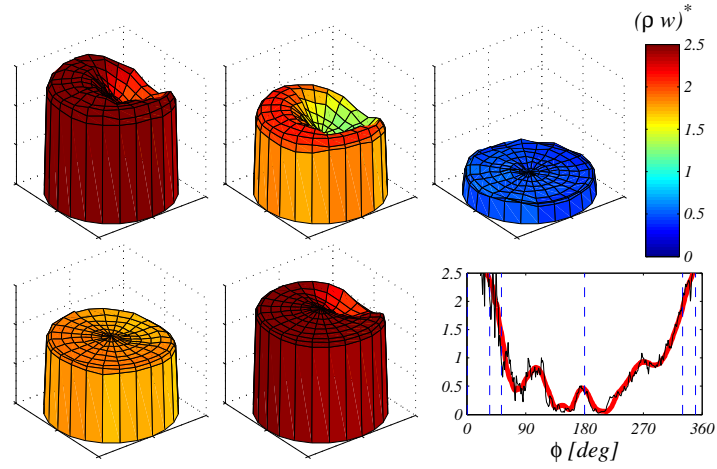


FIGURE 3.21. Surface plots of phase-averaged mass flow rate density for four different phase angles from hot-wire data acquired three diameters downstream from the bend exit. $De = 1.5 \times 10^4$ and $\alpha = 40$. Insert depicts the phase averaged (—) and instantaneous (---) signal at the centerline of the pipe with blue dashed lines indicating the phase angle at which the surface plots correspond to.

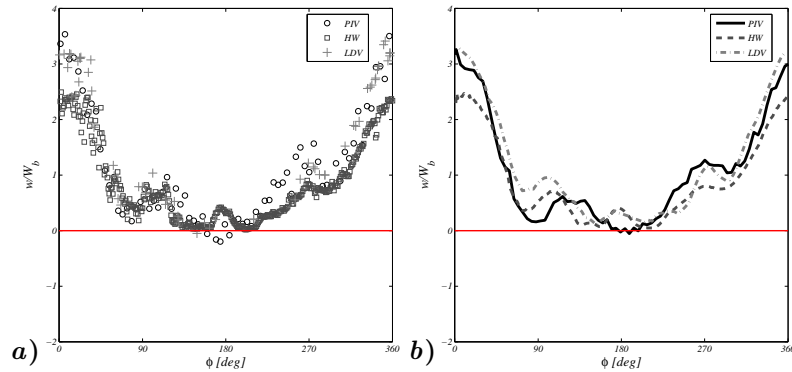


FIGURE 3.22. Instantaneous (a) and phase-averaged (b) signal of the streamwise velocity component at the centerline of the pipe, $3 D$ downstream distance from the bend exit. PIV (—), hot-/cold-wire (---) and LDV (-.-). Velocities are scaled with the bulk speed. $De = 1.5 \times 10^4$ and $\alpha = 40$.

CHAPTER 4

Main contribution and conclusions

In this chapter the main contributions and conclusions from the papers presented in *Part II* are given. For details on the results the reader is referred to the appended papers.

4.1. Highly pulsating turbulent flow downstream a pipe bend—statistical analysis

- Highly pulsating ($\alpha = 80$) turbulent flow 1 D distance downstream a pipe bend ($De = 1.5 \times 10^5$) has been examined by means of a single hot-wire probe traversed along the symmetry axis of the pipe from the inner to the outer side. The investigation of the effects of the pulsatile motion on turbulent flow was done by means of statistical analysis and through comparison with the steady flow case.
- The mean velocity profile is not significantly affected by the pulsations (compared to the steady flow case) while the r.m.s. is dominated by the pulsations which is furthermore supported by a trimodal PDF distribution due to the pulsations.
- Back flow (a well-known phenomenon in pulsating flows) has been encountered as well and it has been indicated from the weighted PDF distributions towards zero and also from the phase-averaged signal at the pipe centerline where a mirrored “dimple” is depicted. Additional LDV measurements (since the hot-wire cannot sense direction of flow) were performed and back flow of a magnitude of almost 50% of the bulk velocity was substantiated.
- The pulsatile flow has been decomposed by means of a high- and low-pass filter and it has been shown that the pulsatile motion is superposed on the turbulence with the high-pass filtered signal being not only qualitatively, but also to some degree quantitatively identical to the r.m.s. distribution of the steady flow.

4.2. Secondary flow under pulsating turbulent flow

- Pulsating and steady turbulent flow ($\alpha = 72$, $De = 1.5 \times 10^4$) was visualized and measured quantitatively by means of TS-PIV 3 D downstream a sharp pipe bend ($\gamma = 0.4$). The flow field at a pipe cross-section under steady conditions exhibits two vortices which on average appear symmetrical to each other whereas instantaneously their behavior is unsteady, oscillating between three states, viz. a clockwise, an anti-clockwise and a symmetrical one.

- During high pulsations, the vortical pattern appears to depend highly on the cycle phase, with no secondary motions being evident during acceleration while symmetrical vortical structures are formed during deceleration and a strong back flow sets in.

4.3. Secondary flow development

- The three-dimensional flow field development at three different stations downstream a sharp pipe bend was captured by means of TS-PIV for $De = 1.5 \times 10^4$. A highly skewed velocity field was depicted at the closest to the bend station. For that case, symmetrical vortices smaller in size as for the other bend stations were confined on the most upper and lower pipe walls and depicted the same behavior both on average and instantaneously. For the more downstream positions the flow field starts to recover from the curvature effects, even though secondary motion is still evident with a more unsteady behavior instantaneously as observed according to a previous work.
- The development of the secondary motions was captured also for the case of a pulsating turbulent flow ($\alpha = 30$). For the station closest to the bend, similar vortical structures as those appearing in the steady flow case were depicted during deceleration and acceleration (where the streamwise velocity reaches almost four times the bulk velocity) while at the end of deceleration they change shape into more rounded roll cells which vanish soon after the onset of reversed flow.

4.4. The effect of curved pulsating flow on turbine performance

- Turbine maps at two different mass flow rates and at a pulsation frequency of 40 Hz are plotted for the case when a sharp bend, as the one used for the PIV measurements, is mounted upstream the turbine in order to account for effects of the presence of curvature on the turbocharger performance. The hysteresis loop due to the filling and emptying of the turbine under a pulse period, was observed to expand to greater magnitudes as the mass flow rate increased. A slight effect of the presence of the bend at the inlet of the turbine was shown on the average quantities but a significant change was observed in the instantaneous results with the hysteresis loop significantly damped due to the presence of the bend.

4.5. The effect of a swirling motion on the vortices

- Fully developed turbulent flow at different Reynolds numbers through a curved pipe bend with $R_c/D = 1.6$ was examined by means of TS-PIV. The effect of Reynolds number on the secondary flow appeared to be insignificant, at least for the range that was considered in this study.
- The unsteady behavior of the Dean vortices was visualized and the so-called “swirl-switching” phenomenon was studied through the POD reconstructed fields from the TS-PIV measurements. The analysis showed that only a few modes were needed to reconstruct the flow field and reveal the unsteady vortical motion while the inhomogeneous filtering that the POD is applying on

the flow field helped in order to study the phenomenon further by means of spectral analysis.

- Turbulent swirling flow through the bend was studied for a wide range of swirl numbers. The Dean vortices become perturbed even for a weak swirl motion imposed, with the lower vortex being more sensitive to the motion since it is rotating at the opposite direction (counter-clockwise) as compared to the applied motion (clockwise direction). The upper vortex grows in strength and size as the swirl number increases until the flow becomes fully swirl dominated with a single vortex located at the centre of the pipe. Velocity profiles of the streamwise component for the different swirl numbers show that the flow field gradually becomes symmetrical and the centrifugal effects become weaker as the swirl number increases.
- The effect of the swirling motion on the secondary flow has been further examined by means of POD. It was shown that the swirling motion contributes mostly to the total energy of the flow field, being the most energetic structure. The energy percentage of the 0-mode (mean field) increases from 60% for the lowest swirl number to almost 90% for the swirl dominated flow field. From the first two spatial modes (considering only the fluctuating part of the flow field) it is shown that coherent structures, constituting the most energetic features (regardless the 0-mode which shows the swirling motion) resemble the Dean vortices for all the swirl number cases studied. These structures are not as well structured as the Dean vortices but show the existence of other large scale features in the flow field, co-existing with the swirling motion.
- The effect of swirl and curvature on the very-large-scale motions (VLSM) has been examined. Both instantaneous and reconstructed streamwise velocity fluctuations by using the most energetic POD modes were visualized, constructed using Taylor's hypothesis. Elongated meandering structures, as described in literature were observed spanning a streamwise extent of about $5R$. Nevertheless, the effect of curvature was seen as an inclination of the structures as compared to the case of a corresponding flow case in a straight pipe, considered in the literature. Moreover, in a swirling motion the structures are tilted due to the change in the mean flow direction while for the swirl dominated flow motion they are teared up into shorter and wider structures.

CHAPTER 5

Papers and authors contributions

Paper 1

Experimental investigation on the effect of pulsations on turbulent flow through a 90 degrees pipe bend

A. Kalpakli (AK), R. Örlü (RÖ), N. Tillmark (NT) & P. H. Alfredsson (HAL).
3rd Int. Conf. on Jets, Wakes & Separated Flows.

This work deals with hot-wire measurements on pulsating turbulent flow downstream a pipe bend in order to assess the effects of pulsations on the statistics of turbulence. The experiments were performed by AK under the supervision of RÖ & NT. The data analysis and the writing was done jointly by AK & RÖ with help by HAL. The work has been presented in Cincinnati, OH, USA, 2010.

Paper 2

Pulsatile turbulent flow through pipe bends at high Dean and Womersley numbers

A. Kalpakli (AK), R. Örlü (RÖ), N. Tillmark (NT) & P. H. Alfredsson (HAL).
J. Phys.: Conf. Series, 318, 092023

The three-dimensional flow field at a cross-section at the exit of a pipe bend under pulsating turbulent flow conditions has been captured by means of Particle Image Velocimetry (PIV). The experiments were done by AK in the facility designed by NT. The data analysis was done by AK with help by RÖ. The writing was done by AK with input from RÖ & HAL. The work has been presented at the *13th European Turbulence Conference (ETC13)*, 12-15 Sept., in Warsaw, Poland, 2011.

Paper 3

Dean vortices in turbulent flows: rocking or rolling?

A. Kalpakli (AK), R. Örlü (RÖ) & P. H. Alfredsson (HAL).

J. Visualization, **15**, 37-38, 2011

This work presents clear snapshots of the secondary motions as well as the mean three-dimensional flow field at a cross-section downstream a curved pipe. The experiments were done by AK. The data analysis and the writing was done jointly by AK & RÖ with input from HAL. This work has been published in *Journal of Visualization*. Part of this work has been presented at the *64th Annual Meeting of the American Physical Society (DFD)*, 20-22 Nov., Baltimore, MD, USA, 2011 and has been selected to appear online at the *APS Gallery of fluid motion, Virtual Pressroom* (<http://www.aps.org/units/dfd/pressroom/gallery/kalpakli11.cfm>).

Paper 4

Experimental investigation on the effect of pulsations on exhaust manifold-related flows aiming at improved efficiency

A. Kalpakli (AK), R. Örlü (RÖ), N. Tillmark (NT) & P. H. Alfredsson (HAL).

10th Int. Conf. on Turbochargers and Turbocharging

This work is a continuation of paper 2. Additional measurements to examine the effect of a pipe bend at the inlet of a turbocharger have been performed. The experiments were done by AK. The set up for the turbocharger measurements was designed by NT¹. The data analysis was done by AK (PIV data) & RÖ (turbine maps). The writing was done by AK with input from RÖ and HAL. This work has been accepted for presentation at *Institute of Mechanical Engineers (IMEchE)*, 15-16 May, London, 2012 and will be published in the conference proceedings.

Paper 5

POD analysis of stereoscopic PIV data from swirling turbulent flow through a pipe bend

A. Kalpakli (AK)

Internal Technical Report

This work deals with swirling turbulent flow downstream a pipe bend. The report is a work in progress and is planned to be submitted.

¹Fredrik Laurantzon is also greatly acknowledged for his help with this set up and for providing the LabView code for the turbocharger measurements

Acknowledgements

This research was started within the competence centre CICERO and is since 2011 supported by its successor CCGEx (Competence Centre for Gas Exchange). Both centres were/are supported by the Swedish Energy Centre, Swedish vehicle industry and KTH. The Linné FLOW Centre at KTH has also provided support through extensive use of their infrastructure in terms of flow instrumentation (hot-wire anemometry, LDV and PIV).

First of all I would like to express my gratitude to my main supervisor Prof. P. Henrik Alfredsson not only for accepting me as his student but also for his always friendly attitude. His active involvement in all parts of my work by sharing and initiating ideas as well as his support and encouragement for my participation in international conferences are greatly acknowledged.

Special thanks go to both my co-advisors. Dr. Nils Tillmark for keeping the CICERO lab up and running and for having a solution for any kind of technical matter whenever needed. Credit for designing and bringing the HW/CW semi-automatic traversing system into life goes also to him. Dr. Ramis Örlü is greatly acknowledged not only for being available “24/7” to discuss any kind of research related topic but mostly for transmitting his enthusiasm on fluid dynamics and teaching me (probably without his awareness) how a researcher should think and approach problems. The help and guidance I received from you in my first steps as a PhD student, from building hot-wires to setting up a whole experiment is invaluable.

Our skillful toolmakers, Joakim Karlström and Göran Rådberg deserve special thanks for being there whenever I had problems in the laboratory but also for providing many times advice and guidance for the building of set ups.

Many thanks go to Dr. Gabriele Bellani for helping me in my “first PIV steps” but also for passing along his enthusiasm on the technique. The set up of the PIV experiments would have taken a much longer time if it wasn’t for your advice.

Tekn.Lic. Onofrio Semeraro is acknowledged for spending time the last few weeks, while the writing of this thesis, on fruitful discussions about modal analysis.

MSc. Markus Pastuhoff deserves many thanks for the designing of the DC motor used as part of the semi-automatic traversing mechanism as well as for being a great office mate.

Tekn.Lic. Fredrik Laurantzson is acknowledged for his help with the turbocharger measurements and the vortex flowmeter as well as for creating a nice atmosphere in the CICERO lab.

MSc. Sohrab Sattarzadeh is thanked for providing the hot-wire data for validation of the PIV measurement technique as well as for being a nice colleague.

Everyone at the Fluid Physics lab but also at OB18 are acknowledged for creating a nice and cheerful working environment. Special thanks go to: Bengt, Antonio, Alexandre, Renzo, Julie, Shahab, Johan, Malte, Karl, Matthias, Emma, Olle, Enrico. Shintaro Imayama and Alexander Sakowitz are thanked for creating a friendly and fun atmosphere in the office and for all the nice discussions (technical and non).

Dr. Mihai Mihaescu is thanked for reading and providing comments on this thesis.

I would like to devote a small part of this section and thank the people from whom I get support outside work. Miriam, thank you for an incredible summer time in Sicily and for all the nice times spent in Stockholm. But mostly thank you for being a true friend and for “propagating” your inexhaustible energy every time I’m tired from work. *Grazie.*

All my love and thoughts go to the people without whom I wouldn’t be here. My mum and dad for always being by my side supporting me by any means and for letting me always choose my own path. My sister for all the love and support but also for sharing her knowledge and enthusiasm on art and different cultures. Last but definitely not least all my love goes to the one person who shares his days and nights with me and has made Sweden feel like home. *Tack Johan.*

References

- AGRAWAL, Y., TALBOT, L. & GONG, K. 1978 Laser anemometer study of flow development in curved circular pipes. *J. Fluid Mech.* **85**, 497–518.
- ANWER, M. & SO, R. M. C. 1993 Swirling turbulent flow through a curved pipe. Part 1: Effect of swirl and bend curvature. *Exp. Fluids* **14**, 85–96.
- AZZOLA, J., HUMPREY, J. A. C., IACOVIDES, H. & LAUNDER, B. E. 1986 Developing turbulent flow in a U-bend of circular cross-section: measurement and computation. *J. Fluids Eng.* **108**, 214–221.
- BARUA, S. N. 1963 On secondary flow in stationary curved pipes. *Quart. J. Mech. Appl. Math.* **16**, 61–77.
- BERGER, S. A. & TALBOT, L. 1983 Flow in curved pipes. *Annu. Rev. Fluid Mech.* **15**, 461–512.
- BERSON, A., BLANC-BENON, P. & COMTE-BELLOT, G. 2010 On the use of hot-wire anemometry in pulsating flows. A comment on 'A critical review on advanced velocity measurement techniques in pulsating flows'. *Meas. Sci. Technol.* **21**, 128001.
- BERTELSEN, A. F. 1975 An experimental investigation of low Reynolds number secondary streaming effects associated with an oscillating viscous flow in a curved pipe. *J. Fluid Mech.* **70**, 519–527.
- BINNIE, A. M. 1962 Experiments on the swirling flow of water in a vertical pipe and a bend. *Proc. Roy. Soc.*, **270**, 452–466.
- BINNIE, A. M. 1978 Some notes on the study of fluid mechanics in Cambridge, England. *Annu. Rev. Fluid Mech.* **10**, 1–11.
- BOVENDEERD, P. H. M., STEENHOVEN, A. A. V., VOSSE, F. N. V. D. & VOSSERS, G. 1987 Steady entry flow in a curved pipe. *J. Fluid Mech.* **177**, 233–246.
- BRÜCKER, C. 1998 A time-recording DPIV study of the swirl switching effect in a 90° bend flow. *Proc. 8th Int. Symp. Flow Vis., 1-4 Sept., Sorrento (NA), Italy* pp. 171.1–171.6.
- BRUUN, H. 1995 Hot-wire anemometry. Principles and signal analysis. *Oxford Univ. Press*.
- CALLAUD, D. & DAVID, L. 2004 Stereoscopic particle image velocimetry measurements of the flow around a surface-mounted block. *Exp. Fluids* **36**, 53–61.
- CARPINLIOĞLU, M. Ö. & GÜNDOĞDU, M. Y. 2001 A critical review on pulsatile pipe

- flow studies directing towards future research topics. *Flow Meas. Instrum.* **12**, 163–174.
- CHANDRAN, K. B. & YEARWOOD, T. L. 1981 Experimental study of physiological pulsatile flow in a curved tube. *J. Fluid Mech.* **111**, 59–85.
- CHANG, T. H. & LEE, H. S. 2003 An experimental study on swirling flow in a 90 degree circular tube by using Particle Image Velocimetry. *J. Vis.* **6**, 343–352.
- COMTE-BELLOT, G. 1976 Hot-wire anemometry. *Annu. Rev. Fluid Mech.* **8**, 209–231.
- DEAN, W. R. 1927 Note on the motion of fluid in a curved pipe. *Phil. Mag.* **4**, 208–223.
- DEAN, W. R. 1928 The stream-line motion of fluid in a curved pipe. *Phil. Mag.* **5**, 671–695.
- DEY, S. 2002 Secondary boundary layer and wall shear for fully developed flow in curved pipes. *Proc. Roy. Soc.* **458**, 283–298.
- DOORNE, C. W. H. & WESTERWEEL, J. 2007 Measurement of laminar, transitional and turbulent pipe flow using Stereoscopic-PIV. *Exp. Fluids* **42**, 259–279.
- ELSINGA, G. E., SCARANO, F., WIENEKE, B. & OUDHEUSDEN, B. W. 2006 Tomographic particle image velocimetry. *Exp. Fluids* **41**, 933–947.
- ENAYET, M. M., GIBSON, M. M., TAYLOR, A. & YIANNESKIS, M. 1982 Laser-doppler measurements of laminar and turbulent flow in a pipe bend. *Int. J. Heat Fluid Flow* **3**, 213–219.
- EUSTICE, J. 1910 Flow of water in curved pipes. *Proc. Roy. Soc.* **84**, 107–118.
- EUSTICE, J. 1911 Experiments on stream-line motion in curved pipes. *Proc. Roy. Soc.* **85**, 119–131.
- FACCILOLO, L. 2006 A study on axially rotating pipe and swirling jet flows. *PhD thesis, KTH Mechanics, Stockholm, Sweden*.
- GERRARD, J. H. 1971 An experimental investigation of pulsating turbulent water flow in a tube. *J. Fluid Mech.* **46**, 43–64.
- GOLDSTEIN, S. 1938 Modern developments in fluid mechanics. *Oxford Univ. Press*.
- GREENSPAN, D. 1973 Secondary flow in a curved tube. *J. Fluid Mech.* **57**, 167–176.
- GÜNKEL, A. A., PATEL, R. P. & WEBER, M. E. 1971 A shielded hot-wire probe for highly turbulent flows and rapidly reversing flows. *Ind. Eng. Chem. Fundamentals* **10**, 627–631.
- HALE, J. F., McDONALD, D. A. & WOMERSLEY, J. 1955 Velocity profiles of oscillating arterial flow, with some calculations of viscous drag and the Reynolds number. *J. Physiol.* **128**, 629–640.
- HAMAKIOTES, C. C. & BERGER, S. A. 1988 Fully developed pulsatile flow in a curved pipe. *J. Fluid Mech.* **195**, 23–55.
- HAMAKIOTES, C. C. & BERGER, S. A. 1990 Periodic flows through curved tubes: the effect of the frequency parameter. *J. Fluid Mech.* **210**, 353–370.
- HE, S. & JACKSON, J. D. 2009 An experimental study of pulsating turbulent flow in a pipe. *Eur. J. Mech.-B/Fluids* **28**, 309–320.
- HELLSTRÖM, F. 2010 Numerical computations of the unsteady flow in turbochargers. *PhD thesis, KTH Mechanics, Stockholm, Sweden*.
- HELLSTRÖM, L. H. O., ZLATINOV, M. & SMITS, A. 2011b Turbulent pipe flow through a 90° bend. *7th Int. Symp. on Turbulence and Shear Flow Phenomena, 28-31 July, Ottawa, Canada*.

- HELPS, E. P. W. & McDONALD, D. A. 1954 Observations on laminar flow in veins. *J. Physiol.* **124**, 631–639.
- ITO, H. 1959 Friction factors for turbulent flow in curved pipes. *J. Basic Eng.* **82**, 123–134.
- JARRAHI, M., CASTELAIN, C. & PEERHOSSAINI, H. 2010 Secondary flow patterns and mixing in laminar pulsating flow through a curved pipe. *Exp. Fluids* **50**, 1539–1558.
- KING, L. V. 1914 On the convection of heat from small cylinders in a stream of fluid: determination of the convection constants of small platinum wires with applications to hot-wire anemometry. *Phil. Trans. Roy. Soc.* **214**, 373–432.
- KIRMSE, R. E. 1979 Investigations of pulsating turbulent pipe flow. *J. Fluids Eng. Trans. ASME* **101**, 436–442.
- KUNDU, K. P., COHEN, M. I. & DOWLING, R. D. 2012 Fluid mechanics. *Elsevier Inc., 5th ed.*
- KUROKAWA, M., CHENG, K. C. & SHI, L. 1998 Flow visualization of Relaminarization phenomena in curved pipes and related measurements. *J. Vis.* **1**, 9–28.
- LAI, Y., SO, R. M. C. & ZHANG, H. S. 1991 Turbulence-driven secondary flows in a curved pipe. *Theoret. Comput. Fluid Dyn.* **3**, 163–180.
- LAURANTZON, F., ÖRLÜ, R., SEGALINI, A. & ALFREDSSON, P. H. 2010a Time-resolved measurements with a vortex flowmeter in a pulsating turbulent flow using wavelet analysis. *Meas. Sci. Technol.* **21**, 123001.
- LAURANTZON, F., SEGALINI, A., ÖRLÜ, R., TILLMARK, N. & ALFREDSON, P. H. 2012 Experimental analysis of turbocharger interaction with a pulsatile flow through time-resolved flow measurements upstream and downstream the turbine. *10th Int. Conf. on Turbochargers and Turbocharging (IMEchE), UK.*
- LAURANTZON, F., TILLMARK, N. & ALFREDSSON, P. H. 2010b A pulsating flow rig for analyzing turbocharger performance. *9th Int. Conf. on Turbochargers and Turbocharging (IMEchE)* pp. 363–372.
- LIGRANI, P. M. & BRADSHAW, P. 1987 Subminiature hot-wire sensors: development and use. *J. Phys. E: Scient. Instrum.* **20**, 323–332.
- LOMAS, G. C. 1986 Fundamentals of Hot Wire Anemometry. *Cambridge Univ. Press.*
- LYNE, W. H. 1970 Unsteady viscous flow in a curved pipe. *J. Fluid Mech.* **45**, 13–31.
- MANLEY, D. K., MCLLROY, A. & TAATJES, C. 2008 Research needs for future internal combustion engines. *Physics Today* **11**, 47–52.
- MCCONALOGUE, D. J. & SRIVASTAVA, R. S. 1968 Motion of a fluid in a curved tube. *Proc. Roy. Soc.* **307**, 37–53.
- MCDONALD, D. A. 1952 The occurrence of turbulent flow in the rabbit aorta. *J. Physiol.* **118**, 340–347.
- MOULIN, A. M., GASTER, M., WOODBURN, C. N., BARNES, J. R. & WELLAND, M. E. 1997 A directionally sensitive hot-wire anemometer. *Exp. Fluids* **22**, 458–462.
- NAKAYAMA, Y. & AOKI, K. 2001 Progress of visualization. *J. Vis.* **4**, 9–18.
- OBERBECK, A. 1895 Ueber die abkühlende Wirkung von Luftströmen. *Ann. der Physik* **292**, 397–411.
- OHMI, M., IGUCHI, M. & URAHATA, I. 1982 Transition to turbulence in a pulsatile

- pipe flow. Part 1: Waveforms and distribution of pulsatile velocities near transition region. *Bull. JSME* **25**, 182–189.
- ONO, A., KIMURA, N., KAMIDE, H. & TOBITA, A. 2010 Influence of elbow curvature on flow structure at elbow outlet under high Reynolds number condition. *Nuclear Eng. Design* **241**, 4409–4419.
- ÖRLÜ, R. 2009 Experimental studies in jet flows and zero pressure-gradient turbulent boundary layers. *PhD thesis, KTH Mechanics, Stockholm, Sweden*.
- PATANKAR, S. V., PRATAP, V. S. & SPALDING, D. B. 1975 Prediction of turbulent flow in curved pipes. *J. Fluid Mech.* **67**, 583–595.
- PEDLEY, T. J. 1980 Fluid mechanics of large blood vessels. *Cambridge Univ. Press*.
- PERRY, A. E. 1982 Hot-wire anemometry. *Clarendon Press Oxford*.
- PRASAD, A. K. 2000 Stereoscopic particle image velocimetry. *Exp. Fluids* **29**, 103–116.
- PRASAD, A. K. & JENSEN, K. 1995 Scheimpflug stereocamera for particle image velocimetry in liquid flows. *Appl. Optics* **34**, 7092–7099.
- PRUVOST, J., LEGRAND, J. & LEGENTILHOMME, P. 2004 Numerical investigation of bend and torus flows, part I: effect of swirl motion on flow structure in U-bend. *Chem. Eng. Sc.* **59**, 3345–3357.
- RAFFEL, M., WILLERT, C., WERELEY, S. & KOMPENHANS, J. 2007 Particle image velocimetry. A practical guide. *Springer Verlag, 2nd ed.*
- RAMAPRIAN, B. R. & TU, S. W. 1983 Fully developed periodic turbulent pipe flow. Part 2. The detailed structure of the flow. *J. Fluid Mech.* **137**, 59–81.
- ROWE, M. 1970 Measurements and computations of flow in pipe bends. *J. Fluid Mech.* **43**, 771–783.
- RÜTTEN, F., SCHRÖDER, W. & MEINKE, M. 2005 Large-eddy simulation of low frequency oscillations of the Dean vortices in turbulent pipe bend flows. *Phys. Fluids* **17**, 035107.
- SAKAKIBARA, J., SONOBE, R., GOTO, H., TEZUKA, H., TADA, H. & TEZUKA, K. 2010 Stereo-PIV study of turbulent flow downstream of a bend in a round pipe. *14th Int. Symp. Flow Vis., 21-24 June, EXCO Daegu, Korea* pp. 1–11.
- SATTARZADEH, S. S. 2011 Experimental study of complex pipe flows. *MSc. thesis, KTH Mechanics, Stockholm, Sweden*.
- SCHLICHTING, H. 1955 Boundary-layer theory. *McGraw-Hill, 7th ed.*
- SCHMID, P. J. & HENNINGSON, D. S. 2001 Stability and transition in shear flows. *Springer Verlag*.
- SHEMER, L. & KIT, E. 1984 An experimental investigation of the quasisteady turbulent pulsating flow in a pipe. *Phys. Fluids* **27**, 72–76.
- SHEMER, L., WYGNANSKI, I. & KIT, E. 1985 Pulsating flow in a pipe. *J. Fluid Mech.* **153**, 313–337.
- SHIMIZU, Y. & SUGINO, K. 1980 Hydraulic losses and flow patterns of a swirling flow in U-bends. *JSME* **23**, 1443–1450.
- SHIRAIISHI, T., WATAKABE, H., SAGO, H. & YAMANO, H. 2009 Pressure fluctuation characteristics of the short-radius elbow pipe for FBR in the postcritical Reynolds regime. *J. Fluid Sci. Technol.* **4**, 430–441.

- SIGGERS, J. H. & WATERS, S. L. 2005 Steady flows in pipes with finite curvature. *Phys. Fluids* **17**, 077102.
- SINGH, M. P. 1974 Entry flow in a curved pipe. *J. Fluid Mech.* **65**, 517–539.
- SINGH, M. P., SINHA, P. C. & AGGARWAL, M. 1978 Flow in the entrance of the aorta. *J. Fluid Mech.* **87**, 97–120.
- SMITH, F. T. 1975 Pulsatile flow in curved pipes. *J. Fluid Mech.* **71**, 15–42.
- SMITH, F. T. 1976 Fluid flow into a curved pipe. *Proc. Roy. Soc.* **351**, 71–87.
- SO, R. M. C. & ANWER, M. 1993 Swirling turbulent flow through a curved pipe. Part 2: Recovery from swirl and bend curvature. *Exp. Fluids* **14**, 169–177.
- SO, R. M. C., ZHANG, H. S. & LAI, Y. G. 1991 Secondary cells and separation in developing laminar curved-pipe flows. *Theoret. Comput. Fluid Dyn.* **3**, 141–162.
- SOH, W. Y. & BERGER, S. A. 1984 Laminar entrance flow in a curved pipe. *J. Fluid Mech.* **148**, 109–135.
- SPEDDING, P. L. & BENARD, E. 2004 Fluid flow through 90 degree bends. *Dev. Chem. Eng. Mineral Process* **12**, 107–128.
- SRINIVASAN, P. S., NANDAPURKAR, S. S. & HOLLAND, F. A. 1970 Friction factors for coils. *Trans. Inst. Chem. Eng* **48**, 156–161.
- STAINBACK, P. C. & NAGABUSHANA, K. A. 1996 Review of Hot-Wire Anemometry Techniques and the Range of their Applicability for Various Flows. *Electro. J. Fluid Eng. Trans. ASME*.
- SUDO, K., SUMIDA, M. & HIBARA, H. 1998 Experimental investigation on turbulent flow in a circular-sectioned 90-degree bend. *Exp. Fluids* **25**, 42–49.
- SUDO, K., SUMIDA, M. & YAMANE, R. 1992 Secondary motion of fully developed oscillatory flow in a curved pipe. *J. Fluid Mech.* **237**, 189–208.
- SUMIDA, M. 2007 Pulsatile entrance flow in curved pipes: effect of various parameters. *Exp. Fluids* **43**, 949–958.
- SUMIDA, M., SUDOU, K. & WADA, H. 1989 Pulsating Flow in a curved pipe. *JSME* **32**, 523–531.
- TALBOT, L. & GONG, K. O. 1983 Pulsatile entrance flow in a curved pipe. *J. Fluid Mech.* **127**, 1–25.
- TAYLOR, G. I. 1929 The criterion for turbulence in curved pipes. *Proc. Roy. Soc.* **124**, 243–249.
- THOMSON, J. 1876 On the origin of windings of rivers in alluvial plains with remarks on the flow of water round bends in pipes. *Proc. Roy. Soc.* **25**, 5–8.
- TIMITÉ, B., CASTELAIN, C. & PEERHOSSAINI, H. 2010 Pulsatile viscous flow in a curved pipe: Effects of pulsation on the development of secondary flow. *Int. J. Heat Fluid Flow* **31**, 879–896.
- TOPAKOGLU, H. C. & EBADIAN, M. A. 1985 On the steady laminar flow of an incompressible viscous fluid in a curved pipe of elliptical cross-section. *J. Fluid Mech.* **158**, 329–340.
- TU, S. W. & RAMAPRIAN, B. R. 1983 Fully developed periodic turbulent pipe flow. Part 1. Main experimental results and comparison with predictions. *J. Fluid Mech.* **137**, 31–58.
- TUNSTALL, M. J. & HARVEY, J. K. 1968 On the effect of a sharp bend in a fully developed turbulent pipe-flow. *J. Fluid Mech.* **34**, 595–608.

- WARD-SMITH, A. J. 1980 Internal Fluid Flow. The fluid dynamics of flow in pipes and ducts. *Clarendon Press*.
- WESTERWEEL, J. 1994 Efficient detection of spurious vectors in particle image velocimetry data. *Exp. Fluids* **16**, 236–247.
- WESTERWEEL, J. 1997 Fundamentals of digital particle image velocimetry. *Meas. Sci. Technol.* **8**, 1379–1392.
- WHITE, C. M. 1929 Streamline flow through curved pipes. *Proc. Roy. Soc.* **123**, 645–663.
- WIENEKE, B. 2005 Stereo-PIV using self-calibration on particle images. *Exp. Fluids* **39**, 267–280.
- WILLERT, C. 1997 Stereoscopic digital particle image velocimetry for application in wind tunnel flows. *Meas. Sci. Technol.* **8**, 1465–1479.
- WINTER, D. C. & NEREM, R. M. 1984 Turbulence in pulsatile flows. *Ann. Biomed. Eng.* **12**, 357–369.
- WOMERSLEY, J. 1955 Method for the calculation of velocity, rate of flow and viscous drag in arteries when the pressure gradient is known. *J. Physiol.* **127**, 553–563.
- YAO, L. S. & BERGER, S. A. 1975 Entry flow in a curved pipe. *J. Fluid Mech.* **67**, 177–196.
- YEH, Y. & CUMMINS, H. Z. 1964 Localized fluid flow measurements with an HeNe laser spectrometer. *Appl. Phys. Letters* **4**, 176–178.
- YUKI, K., HASEGAWA, S., SATO, T., HASHIZUME, H., AIZAWA, K. & YAMANO, H. 2011 Matched refractive-index PIV visualization of complex flow structure in a three-dimensionally connected dual elbow. *Nuclear Eng. Design* **241**, 4544–4550.
- ZALOSH, R. G. & NELSON, W. G. 1973 Pulsating flow in a curved tube. *J. Fluid Mech.* **59**, 693–705.
- ZHANG, Z. 2010 LDA Application methods. Laser Doppler Anemometry for Fluid Dynamics. *Springer Verlag*.

Part II

Papers

“A new scientific truth does not triumph by convincing its opponents and making them see the light, but rather its opponents eventually die, and a new generation grows up that is familiar with it.”

Max Planck (1858–1947)

Paper 1

Experimental investigation on the effect of pulsations on turbulent flow through a 90 degrees pipe bend

By Athanasia Kalpakli, Ramis Örlü, Nils Tillmark & P. Henrik Alfredsson

Linné Flow Centre & CCGEx, KTH Mechanics, SE-100 44 Stockholm, Sweden

Published in *Proc. of 3rd Int. Conf. on Jets, Wakes & Separated Flows* 2010

Pulsatile turbulent flows in curved pipes at high Dean numbers are prevalent in various components of internal combustion engines, particularly the intake of exhaust manifolds. Despite their technological importance, there is a clear lack of experimental data. The present paper provides preliminary, albeit unique, data from an experimental investigation, thereby addressing this gap and depicts impressions of the phase evolution of the complex flow including a back flow region. It is also shown, that due to the scale separation of the pulsations and the turbulence, the pulsatile flow can statistically be decomposed into its large-scale pulsations and the steady case.

1. Introduction

The gas flow in the exhaust system of an internal combustion engine (ICE) is quite complex due to several complications such as complex geometry, pulsating flow, compressibility, high temperatures, partly transonic conditions etc. Numerical simulations of such flow systems are generally favored, however these need to be validated against experiments in which the main physical features of interest are captured, in order to assess the accuracy and limitations of the simulations.

Besides the importance of gas flows in ICE, pulsatile flows in curved pipes are also present in e.g. respiratory flows and blood flows. This explains why most of the past studies reported in the literature are restricted to laminar (Sumida 2007) and incompressible (Mullin & Greated 1980) flows under low pulsation frequencies (Sudo *et al.* 1992). Although there are studies dealing with the flow in exhaust manifolds (Capobianco *et al.* 1993), these are mainly focused on straight pipes or the heat transfer in pipe bends (Bauer *et al.* 1998). Hence, there is a need for experimental data in pulsating turbulent flows in curved pipes at high Dean (De) and Womersley (α) numbers, defined by equations (1) and (2), respectively.

$$De = \sqrt{\gamma} Re, \tag{1}$$

$$\alpha = \frac{D}{2} \sqrt{\frac{\omega \rho}{\mu}}. \quad (2)$$

Hereby $Re = \rho U D / \mu$ and $\gamma = D / (2R_2)$ denote the Reynolds number and the curvature ratio, respectively, with R_2 being the bend centreline radius (see also figure 1).

In the present work the turbulent flow through a straight pipe and 90 degree pipe bend has been studied both under steady and pulsating conditions.

Mean and turbulence intensity profiles, probability density distributions, as well as phased-averaged statistics will be presented together with evolution snapshots from the mean flow development under a cycle. It will be shown, that despite the complexity of the flow under pulsating conditions in curved pipes, a simple scale decomposition of the pulsating flow can be performed to reveal the statistics of the steady case. This consequently suggests that the turbulence is merely superposed on the large-scale pulsating motion. Furthermore, back flow during the deceleration phase has been observed not only for the bend pipe, but also for the straight pipe section.

2. Experimental set-up

The experiments were performed at the Laboratory of KTH CICERO (*Centre for Internal Combustion Engine Research Opus*) in a newly developed flow rig that can be used both under steady and pulsating conditions. The set up, sketched in figure 1, consists of a long steel pipe (I) and a transparent Plexiglas (II) pipe section. The long pipe ends with either a straight pipe section (III) or a 90 degrees pipe bend (II). A rotating valve (V) in the pipe provides the pulsations and its frequency is controlled by means of a frequency regulated AC motor, which sets the rotation rate. The air is supplied through a compressor rig installation that can deliver up to 500 g/s at 6 bar. For details of the CICERO flow rig the reader is referred to Laurantzon *et al.* (2010).

Fluctuating mass flow rate density (ρu) measurements were performed with a hot-wire probe with a welded 5 micron tungsten wire of 1 mm length. The hot-wire was operated by means of a *DISA 55M01* main frame with a *55M10* standard CTA channel. The hot-wire was manually traversed across the horizontal and vertical axes, i.e. the y - and z -axes respectively, as indicated in figure 1. The mass flow was furthermore monitored by a hot-film type ABB mass flowmeter, that was mounted upstream the rotating valve. This was done to ensure steady inflow conditions to the flow rig as well as to provide a correct bulk mean mass flow rate for the non-dimensionalisation of the hot-wire readings.

Measurements were performed both under steady and pulsating conditions. The pipe has an inner diameter (D) of 39 mm, while the curved pipe section has a curvature ratio (γ) of 0.6¹. The results presented here were obtained at a mean mass flow rate of 120 g/s, corresponding to a Reynolds and Dean number of around 2×10^5 and

¹Note that due to an error the curvature ratio depicted here and the centerline pipe bend radius in figure 1 have been misprinted in the original paper. The correct values are: $\gamma = 0.42$ and $R_2 = 1.17D$.

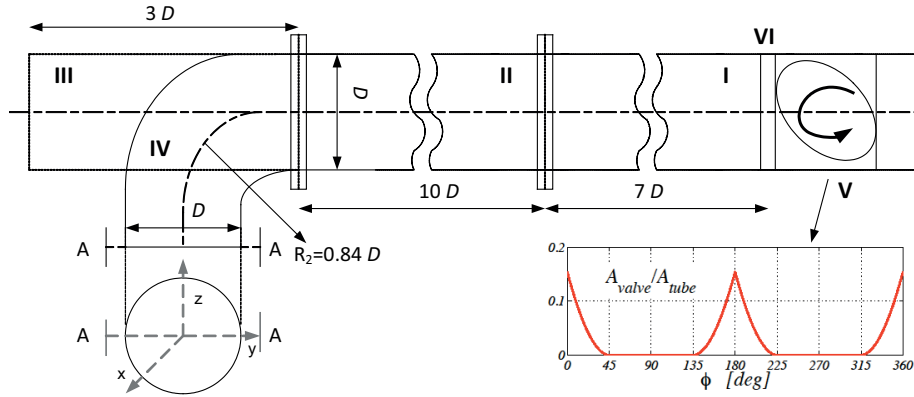


FIGURE 1. Schematic of the pipe bend configuration: I) Steel pipe section, II) Plexiglas pipe section, III) interchangeable straight brass pipe section, IV) interchangeable 90 degrees brass pipe bend, V) rotating valve, VI) smoke injection muff. The insert depicts the relative open area change caused by the rotating valve as function of revolution angle.

1.5×10^5 , respectively. In the case of pulsating flow, a pulsation frequency of 40 Hz was chosen, giving a Womersley number of 80.

Although the flow under pulsating conditions is non-isothermal, the hot-wire readings presented here were not corrected for pulsatile temperature variations, due to missing instantaneous temperature measurements. Secondary flows in curved pipes are additionally present and falsify the hot-wire readings as well. However, based on the concept of effective velocity, the secondary components will not assert a too strong effect on the readings of a single hot-wire probe (Bruun 1995). Hence the primary goal of the present investigation is not to provide an accurate quantitative assessment of the mass density rate, but rather to illuminate the qualitative effects of the pulsation and the curvature on the turbulent flow itself.

To ensure the correctness of the conclusions based on hot-wire measurements during the low speed phases, supplementary laser Doppler velocimetry (LDV) measurements have been performed for the straight pipe section at the pipe centreline. The LDV system is a single component *DANTEC FlowLite* system comprising a backscatter fibre optics probe, a 400 mm lens and a BSA F/P 60 processor. The source is a He-Ne laser of 10 mW emitting light with a wave length of 632.8 nm. The seeding particles were atomized oil (*Shell Ondina 27*) that was injected through an opening in a muff (VI) interconnecting the steel pipe section (I) and the pulse generator (V).

All measurements, both with the hot-wire and the LDV, were taken directly at the outlet of the straight pipe and the pipe bend, respectively.

3. Results & Discussion

3.1. General flow description

In figure 2 we show the mass flow rate measured by the hot-wire both in terms of the probability density distribution (pdf) as the colored band as well as the corresponding mean and rms-distributions (red and blue dots, respectively). Under steady conditions (left figure), despite the relatively short length of the straight pipe section between the pulse generator and the pipe outlet, the flow at the pipe outlet exhibits a well developed axi-symmetry, as evident from the mean and rms-distributions. Also the skewness and flatness distributions as well as profiles taken along the z -axis show axi-symmetry. Quantities with an asterisk in the superscript indicate non-dimensionalisation with the bulk mass flow rate density obtained from the ABB flowmeter. Furthermore the quantitative values agree well with what is known from fully developed turbulent pipe flow studies (Schlichting 1955).

Under pulsating conditions the mean profile changes only slightly towards a more top-hat like profile, however the rms distribution exhibits quantitative and qualitative differences with respect to the steady counterpart. Here the rms is calculated on the full signal and is clearly dominated by the pulsating motion which is furthermore supported by the trimodal probability density function (pdf), which occurs due to the pulsatile motion. The time traces of the signal at two different radial positions are seen in figure 3. The trimodal behaviour of the pdf is apparent from the signals, there are three plateau-like regions, one just above zero (as will be discussed below

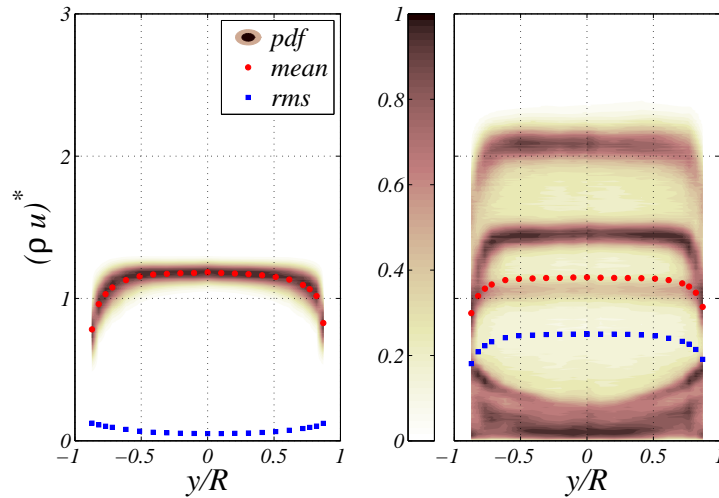


FIGURE 2. Contour plots of the probability density function of the mass flow rate density along the y -axis at the exit of the straight pipe together with its mean and root mean square value. *Left*: steady conditions, *right*: pulsating conditions (40 Hz).

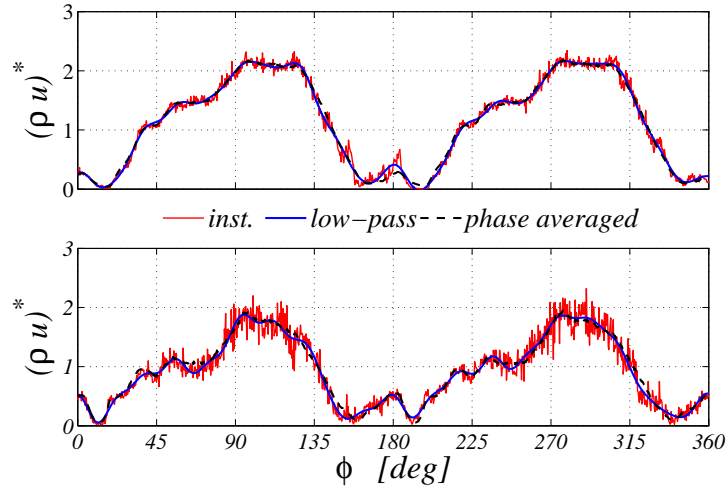


FIGURE 3. Instantaneous signal of the mass flow rate density at the exit of the straight pipe together with its low-pass filtered ($f_c = 400$ Hz) and phase-averaged (≈ 200 valve cycles) counterpart. *Top*: $y/R = 0$, *bottom*: $y/R = 0.87$.

this includes a region of back flow) and two at higher values. As can be seen both the latter have higher instantaneous flow rate than the mean value for the steady case. As expected the turbulence fluctuations, that seem to be merely superposed on the large scale pulsating motion, are higher closer to the wall as compared to the centreline, although this is not reflected in the rms-distribution.

In the case of the steady flow in the pipe bend, the mean profile, shown in the left part of figure 4, indicates that the fluid is strongly accelerated near the outer wall but also on the centreline the mass flow rate is higher, while simultaneously, it is decelerated near the inner wall, which is a result of an adverse pressure gradient generated by flow over a curved surface (Chandran & Yearwood 1981). The pdf shows large fluctuations near the inner wall and the local turbulence level here is of the order of 50% or higher. Under pulsating conditions (right part of figure 4) the rms distribution resembles again very closely the one of the mean profile, similar to the steady case. In the outer part of the bend the pdf also resembles that of the straight pipe with three (or maybe even four) different plateaus.

Considering the pulsating flow cases, both in the straight pipe and pipe bend, it becomes evident that the pdf is particularly weighted towards the lower mass flow rate density side, and in particular it seems to have been squeezed towards zero. Recalling the inability of a hot-wire to sense the flow direction, the so called forward-reverse ambiguity (Bruun 1995), it seems plausible that instantaneous back flow is sensed as an equally strong velocity in the mean streamwise direction, i.e. x -direction. This can furthermore be observed when inspecting the instantaneous signals for the pulsating flow, as depicted in figures 3 and 5, for the straight pipe and pipe bend, respectively.

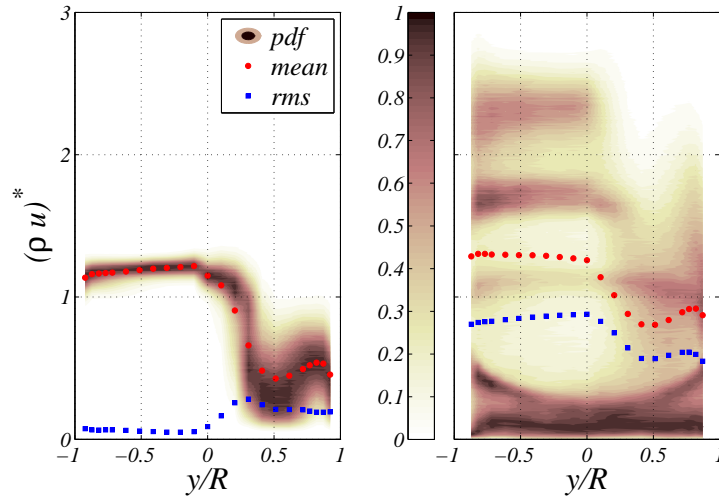


FIGURE 4. Contour plots of the probability density function of the mass flow rate density along the y -axis at the exit of the pipe bend together with its mean and root mean square value. *Left*: steady conditions, *right*: pulsating conditions (40 Hz).

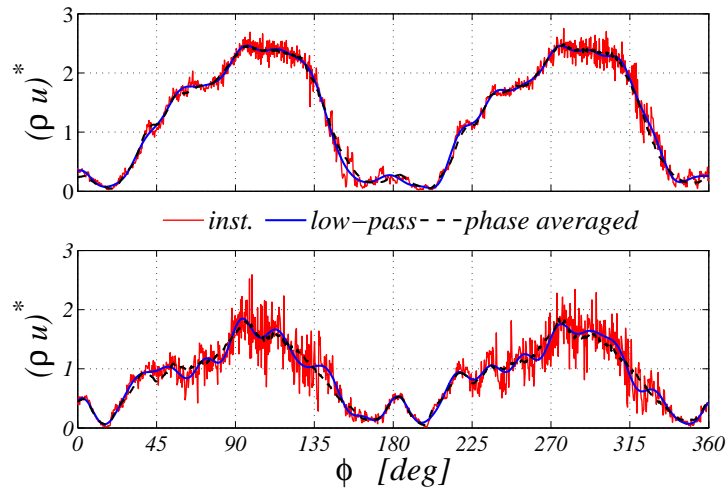


FIGURE 5. Instantaneous signal of the mass flow rate density at the exit of the pipe bend together with its low-pass filtered ($f_c = 400$ Hz) and phase-averaged (≈ 200 valve cycles) counterpart. *Top*: $y/R = 0$, *bottom*: $y/R = 0.87$.

While under steady conditions the instantaneous as well as low-pass filtered signals are unambiguously positive, the signals under pulsating conditions exhibit “reflections” at the abscissa, e.g. at around 160–200 and 340–20 degrees, which can be seen as an indication of back flow (cf. Bruun (1995); Chandran & Yearwood (1981)).

While the low-pass filtered and phase averaged signals for the straight pipe, shown in figure 3, demonstrate that both large-scale extraction techniques are equivalent, minor differences can be observed for the pipe bend, where the small-scale (high frequency) turbulence is more amplified compared to the straight pipe section. Here, the low-pass filtered representation of the instantaneous signal appears to be more representative than the phase averaged representation. Figure 6, on the other hand, demonstrates that phase averaging is a very robust method to extract the large-scale motion, while the low-pass filtered signal –as inherent in its definition– improves with increasing cut-off frequency, f_c . For the example shown in figure 6 the low-pass filtered signal approaches the phase averaged one at around 280 Hz and continues to improve further with increase in cut-off frequency. However, since the low-pass filtered signal for $f_c \rightarrow f_s/2$ approaches the instantaneous one, use of the low-pass filter requires pre-knowledge about the pulsatile motion (which albeit known here,

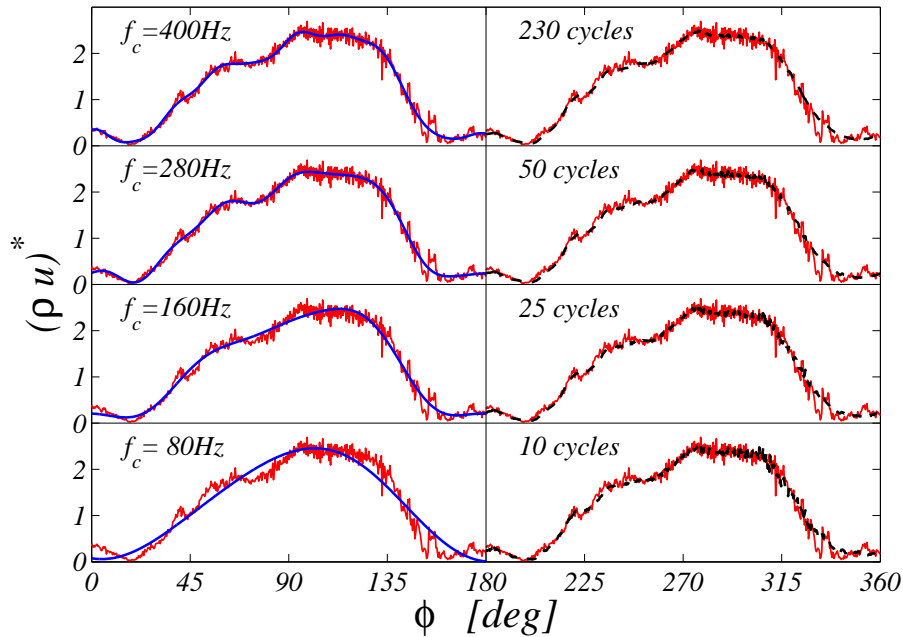


FIGURE 6. Same signal as in upper subplot of figure 3. Demonstration of the effect of different low-pass cut-off frequencies (shown in the region $0 \leq \phi \leq 180$) as well as the number of employed valve cycles for the phase averaging (shown in the region $180 \leq \phi \leq 360$).

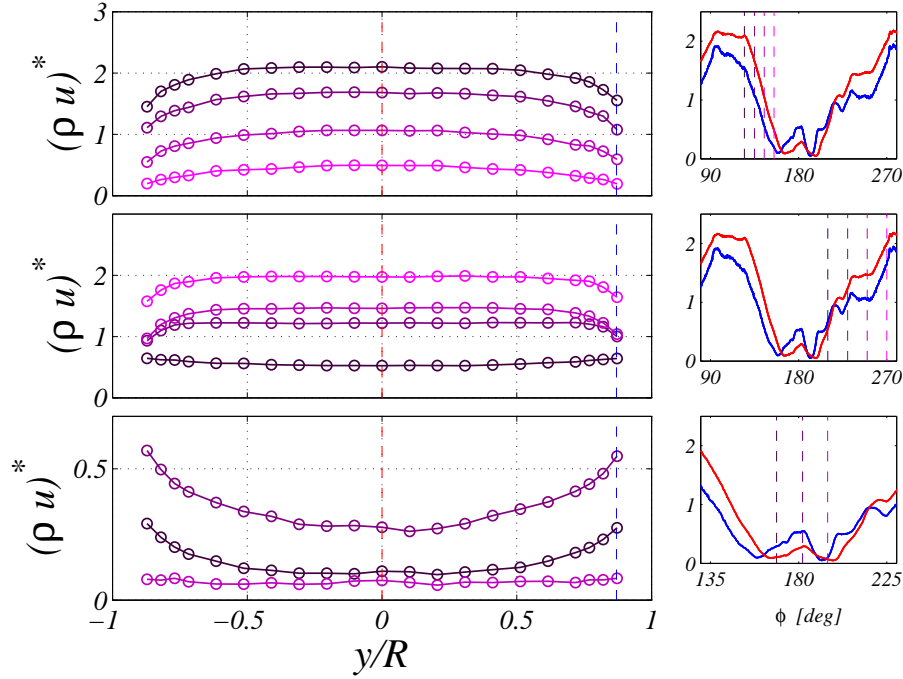


FIGURE 7. Ensemble averaged mean mass flow rate density profile along the y -axis for the straight pipe under pulsations for various phases. *Top*: deceleration phase, *middle*: acceleration phase, *bottom*: back flow region. Subplots on the right indicate the position in the phase averaged profile for $y/R = 0$ (red) and 0.87 (blue). Increasing phase positions are shown in progressively lighter shades of magenta. Note that the scale of the lower subplot is different.

is not always known in practise) in order to select a certain cut-off frequency. The phase averaging technique on the other hand appears to give a good and robust large-scale representation with as few as only 10 ensemble averages, in accordance with Chandran & Yearwood (1981). This also emphasises the excellent stability of the pulse generator.

3.2. Evidence of back flow

Back flow is a common phenomena in pulsating flows where the amplitude of the pulsations exceeds the bulk value, but even where this is not the case it can occur in curved pipes, due to secondary motions. As mentioned in the context of the pdfs shown in figure 2 and 4 and the instantaneous and phased-averaged signals depicted in figure 3 and 5, there are strong indications of back flow in both the straight and

curved pipe. To further illuminate the presence of back flow ensemble averaged mean profiles have been computed for the deceleration and acceleration phase as well as for the region in which back flow is suspected.

Figures 7 and 8 depict these ensemble averaged mean profiles for the straight and curved pipe, respectively. Considering the flow in the straight pipe, figure 7, it can be observed that the axi-symmetry is not only fulfilled in the long-time average, but throughout the pulsations. In particular for the deceleration and acceleration phase it becomes clear, that a flat turbulent pipe flow profile is present and appears to be carried on the large-scale pulsations. In accordance with Chandran & Yearwood (1981), the profiles for the acceleration phase are flat over a large part of the central region. Flows starting from rest depict an even more profound top-hat profile (Boiron *et al.* 2007) as evident from the middle subplots in figures 7 and 8 (see profile for $\phi \approx 200^\circ$).

At the end of the deceleration phase the profiles approach the zero level and suspicion of back flow is supported by the inversion of the profile shape, i.e. the velocity around the centre of the pipe appears to be lower than closer to the wall.

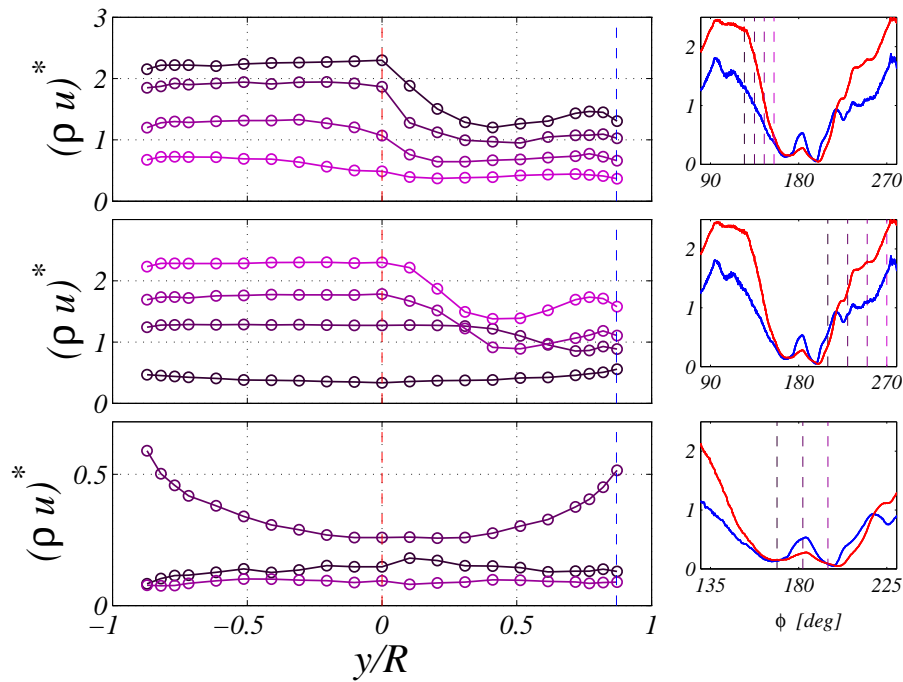


FIGURE 8. Ensemble averaged mean mass flow rate density profile along the y -axis for the pipe bend under pulsations for various phases. See caption of figure 7 for further details. Note that the scale of the lower subplot is different.

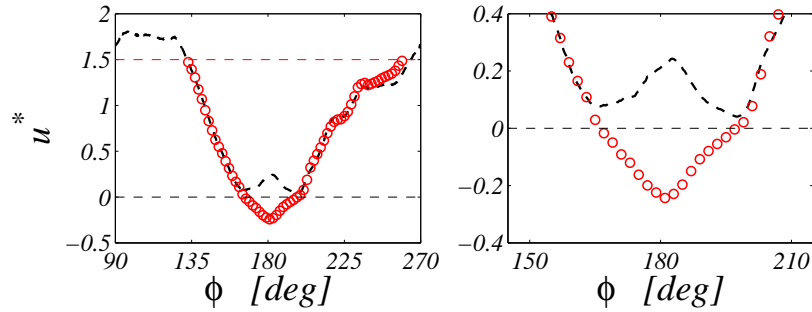


FIGURE 9. Comparison of phased-averaged mean streamwise velocity component at the exit at $y/R = 0$ for the straight pipe under pulsating conditions measured by means of hot-wire anemometry (dashed) and laser Doppler velocimetry (red circles). *Left*: Close-up of the deceleration and acceleration phase, *right*: close-up of the back flow region.

Similar observations can be made for the pipe bend, figure 8. However, here the strength of the back flow appears to be stronger.

The indication of back flow through the shown contour plots of the pdfs, figures 2–4, the phase-averaged signals, figures 3–6, as well as the ensemble averaged mean profiles, figures 7–8, was further substantiated by LDV measurements performed for the straight pipe under pulsating conditions to qualitatively confirm and quantitatively assess the presence of back flow. Due to the limitations of the optical arrangement of the present LDV settings velocity measurements were restricted to ± 100 m/s. In order to cover the back flow region this range was set to -50 to 150 m/s and hence leaves out the high speed phases. Figure 9 therefore depicts a comparison between the phase-averaged mean streamwise velocity component measured by means of the hot-wire and the laser Doppler system. The close-up of the back flow region clearly indicates the fraction of back flow between 165 and 195 degrees, coinciding with the anticipated range from figures 3–6. It is also interesting to note that, despite the inability of the hot-wire to measure near zero velocity or to indicate the direction, it measures the correct amplitude of the back flow.

3.3. Decomposition into pulsatile and turbulent motions

Having concluded that the large-scale pulsatile motion is merely superposed on the small-scale “background” turbulence consequently leads to the statement that these scale separated motions can be considered independently from each other. In turn, it should be possible to decompose – to a high degree independent of the (reasonably) chosen cut-off frequency – the pulsatile flow into two superposed scale-separated motions; one low-pass and one high-pass filtered signal, where the latter one gives very similar statistics to the one of the flow under steady conditions. To verify this, figure 10 depicts the rms distribution of both the steady and pulsed flow in the straight

and the bend pipe. As anticipated the large-scale pulsatile motion is mainly responsible for the rms value of the pulsatile flow. Interestingly, the high-pass filtered signal (i.e. the “background” turbulence) is not only qualitatively, but also to some degree quantitatively identical to the rms distribution of the steady flow. It is also shown that the choice of the cut-off frequency is a rather insensitive parameter, which again supports the view of a linear superposition of two independent motions. It should, however, be kept in mind, that the turbulence time scale is around two orders of magnitude smaller than the pulsation period, and hence the conclusions drawn here should not be carried over to cases where the time scales are of the same order of magnitude. Nevertheless, the scale separation found here is comparable to those that can be found in intake pipes of exhaust manifolds and the conclusions drawn should therefore be relevant in this context.

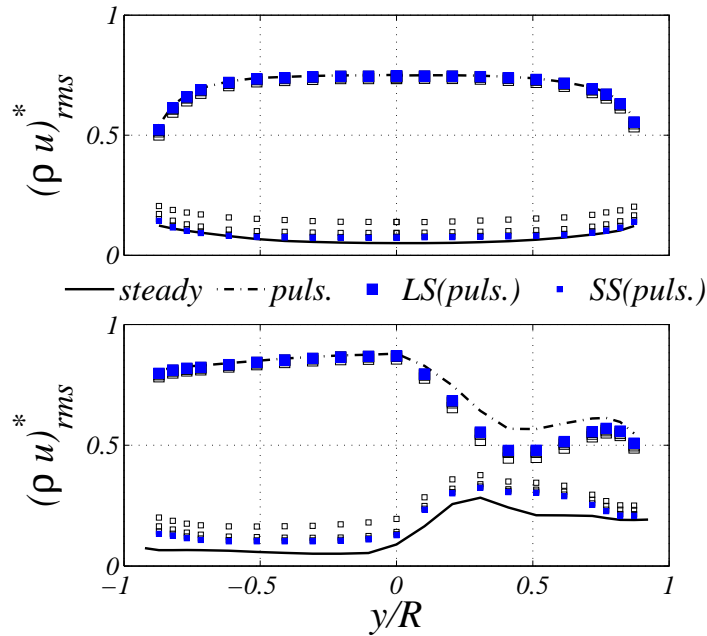


FIGURE 10. Root mean square distribution of the mass flow rate density along the y -axis for the steady (solid line) and pulsating (dash-dotted line) flow. Decomposition into a periodic large-scale (LS) and “background” small-scale (SS) contribution of the rms distribution by means of a filter with the cut-off frequencies employed in figure 6, viz. 80, 160, 280 (open symbols) and 400 (filled symbols) Hz. *Top*: straight pipe, *bottom*: pipe bend.

4. Summary & Conclusions

Hot-wire measurements of the mass flow rate density were performed in a newly developed flow rig for steady and pulsating flows. Mean and rms profiles, pdf distributions, time series, phase-averaged and low-pass filtered signals, as well as ensemble averaged phase evolution of the mean profiles have been presented for a straight pipe and a pipe bent at high Reynolds number. Due to the lack of studies for the parameter range covered here, these results provide unique, albeit preliminary, data in a parameter range related to the exhaust manifold of ICE.

Despite the complexity of the flow under pulsating conditions as well as in curved pipes, it has here been shown that a simple decomposition into a large-scale pulsating and a small-scale “background” turbulence is possible. In fact, the long-time statistics of the decomposed small-scale part of the pulsating flow resemble to a high degree qualitatively and quantitatively the statistics from the steady flow. This indicates, that the large-scale pulsating motion, due to the wide scale separation, is merely superposed on the turbulence.

Furthermore, a back flow region has been observed for the pulsatile flow, not only for the bend pipe section, but also for the straight pipe. In pulsatile flows the possibility of a non-negligible fraction of back flow should particularly be considered in light of its consequences for mass flow rate measurement techniques based on hot-wire/film anemometry, where the inability to detect the flow direction can lead to an overestimation of the mass flow rate. Nevertheless, it has also been demonstrated that hot-wire data can indicate back flow and even give its correct amplitude.

Acknowledgments

This research was done within KTH CICERO, a centre supported by the Swedish Energy Agency, Swedish Vehicle Industry and KTH. The first author acknowledges the travel grant from the *Erik Petersohns* foundation.

References

- BAUER, W.D., WENISCH, J. & HEYWOOD, J.B. 1998 Averaged and time-resolved heat transfer of steady and pulsating entry flow in intake manifold of a spark-ignition engine. *Int. J. Heat Mass Transfer* **19**, 1–9.
- BOIRON, O., DEPLANO, V. & PELISSIER, R. 2007 Experimental and numerical studies on the starting effect on the secondary flow in a bend. *J. Fluid Mech.* **574**, 109–129.
- BRUUN, H.H. 1995 Hot-wire anemometry. Principles and signal analysis. *Oxford University Press*.
- CAPOBIANCO, M., GAMBAROTTA, A. & NOCCHI, M. 1993 Unsteady Flow Phenomena and Volume Effects in Automotive Engines Manifolds. *SAE Tech. paper* pp. 1–13.
- CHANDRAN, K. B. & YEARWOOD, T. L. 1981 Experimental study of physiological pulsatile flow in a curved tube. *J. Fluid Mech.* **111**, 59–85.
- LAURANTZON, F., TILLMARK, N. & ALFREDSSON, P. H. 2010 A pulsating flow rig for analyzing turbocharger performance. *9th Int. Conf. on Turbochargers and Turbocharging (IMEchE)* pp. 363–372.
- MULLIN, T. & GREATED, C. A. 1980 Oscillatory flow in curved pipes. Part 2. The fully developed case. *J. Fluid Mech.* **98**, 397–416.
- SCHLICHTING, H. 1955 Boundary-layer theory. *McGraw-Hill*.
- SUDO, K., SUMIDA, M. & YAMANE, R. 1992 Secondary motion of fully developed oscillatory flow in a curved pipe. *J. Fluid Mech.* **237**, 189–208.
- SUMIDA, M. 2007 Pulsatile entrance flow in curved pipes: effect of various parameters. *Exp. Fluids* **43**, 949–958.

Paper 2

Pulsatile turbulent flow through pipe bends at high Dean and Womersley numbers

By Athanasia Kalpakli, Ramis Örlü, Nils Tillmark & P. Henrik Alfredsson

Linné Flow Centre & CCGEx, KTH Mechanics, SE-100 44 Stockholm, Sweden

Published in *J. Phys.: Conf. Ser.* **318**, 092023, 2011

Turbulent pulsatile flows through pipe bends are prevalent in internal combustion engine components which consist of bent pipe sections and branching conduits. Nonetheless, most of the studies related to pulsatile flows in pipe bends focus on incompressible, low Womersley and low Dean number flows, primarily because they aim in modeling blood flow, while internal combustion engine related flows have mainly been addressed in terms of integral quantities and consist of single point measurements. The present study aims at bridging the gap between these two fields by means of time-resolved stereoscopic particle image velocimetry measurements in a pipe bend with conditions that are close to those encountered in exhaust manifolds. The time/phase-resolved three-dimensional cross-sectional flow-field 3 pipe diameters downstream the pipe bend is captured and the interplay between different secondary motions throughout a pulse cycle is discussed.

1. Introduction

1.1. Background

The study of fluid flow through pipe bends is often associated with Dean (1927), who provided an analytical solution to this problem under steady and laminar conditions. His study revealed the existence of two symmetrical counter-rotating vortices located in the upper and lower half of the pipe. These unique structures, that have become the driving force for many research studies, are nowadays widely known as *Dean vortices*. While Dean's study as well as those following (McConalogue & Srivastava 1968; Greenspan 1973) were dealing with laminar and steady flows, the question whether the vortical picture found in steady flows would remain under more practical, i.e. unsteady or turbulent, conditions remained to a large extent untouched. Almost five decades after the seminal work by Dean, the problem of unsteadiness of a viscous fluid motion in a curved pipe was addressed by Lyne (1970), who revealed that the flow pattern can change drastically depending on the frequency of the oscillations. A series of studies, which confirmed and extended Lyne's work followed (Zalosh & Nelson 1973; Bertelsen 1975), but were still limited to smaller parameter values than

those met for example in the internal combustion engine environment, for which this study is aimed at. A great interest in pulsating flow through pipe bends was also shown by a number of authors due to its relevance to physiological mechanisms such as the causes of atherosclerosis and the blood flow in the aortic arch (Chandran & Yearwood 1981; Hamakiotes & Berger 1990) and consequently did not extend their investigation to high values of the parameters.

Up to now, the interest for pulsating flow through pipe bends remains vibrantly alive while no clear conclusion has been made yet on the structural picture of the flow field under turbulent, pulsating flow conditions. The most important parameters that control the flow under turbulent, pulsating conditions through pipe bends are the Dean and Womersley (or frequency parameter) number, which are defined respectively as: $De = \sqrt{\gamma} Re$ and $\alpha = D/2\sqrt{\omega\rho/\mu}$, where Re denotes the Reynolds number based on the pipe diameter D , γ the curvature ratio, ω the angular frequency, ρ the density and μ the dynamic viscosity of the fluid. The Reynolds number itself is of course also of importance, here we assume that it is high enough so that the flow is fully turbulent. The Womersley number can be said to be the ratio of the oscillatory inertial forces related to the pulsations and the viscous forces. Recently, Timité *et al.* (2010) performed both simulations and experiments in developing laminar pulsating flow, adding information on the evolution of the secondary flow under the effect of different, but low, Reynolds numbers and a wide range of the frequency parameter. In the same kind of flow, but for a slightly different parameter range, Jarrahi *et al.* (2010) performed Particle Image Velocimetry (PIV) measurements, revealing secondary flow patterns varying from a single dominating vortex to more complex constellations with up to four vortices.

1.2. Motivation

The aforementioned studies show that increasing the Dean and Womersley number has a large effect on the strength of the secondary motions and makes the flow field more complicated, varying between multiple vortex patterns at certain instances and no vortex patterns at other instances. Our motivation to study high Dean and Womersley number flows in curved pipes stems from the fact that such flows are widely met in internal combustion engines (for example in the exhaust manifold) and can strongly affect the engine performance, especially for turbo-charged engines.

Studies focusing on engine research often regard single point measurements (Szymko *et al.* 2005; Capobianco *et al.* 1993) which do not provide a full picture of the nature and structures of the turbulent pulsating flow field. The way for example the Dean vortices behave under harsh engine flow conditions (reportably of the 10^2 and 10^5 order for the Womersley and Dean number respectively) and how the three dimensional velocity field looks during the phases is to a large extent unknown. Some efforts have been reported in more recent years to show how the vortices behave under high Dean number conditions. Rütten *et al.* (2005) performed Large Eddy Simulation (LES) and comparing results with these from PIV measurements by Brücker (1998), confirmed the existence of the so-called “swirl switching” phenomenon first observed by Tunstall & Harvey (1968). This phenomenon exhibits one vortex that alternatively dominates the two different sides of the pipe, “switching” between the two positions with varying strength. The same phenomenon was depicted in the results from Stereoscopic PIV

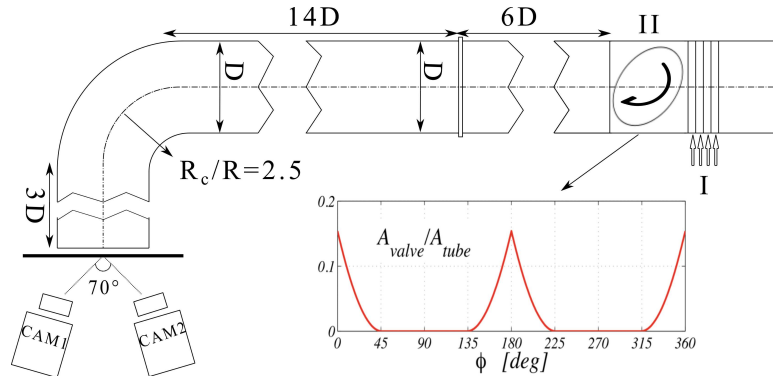


FIGURE 1. *Left:* Schematic of the pipe bend configuration and the set-up of the cameras for the TS-PIV measurements. $D = 40.5$ mm and $R_c = 51$ mm: I) smoke injection section, II) rotating valve. The insert depicts the relative open area change caused by the rotating valve as function of revolution angle.

measurements by Sakakibara *et al.* (2010) at a Reynolds number of $Re = 1.2 \times 10^5$. Sudo *et al.* (1998) on the other hand, presented results from hot-wire measurements providing information on the velocity field and Reynolds stresses distribution in a 90° pipe bend with long straight upstream and downstream pipes at $Re = 6 \times 10^4$. These studies, addressing the effect of the pipe bend, considered only steady flow conditions. Hellström (2010) computed the turbulent steady and pulsatile flow field by LES and Reynolds Averaged Navier-Stokes (RANS). The steady turbulent case at $De = 3 \times 10^4$ was computed in a single pipe bend while the pulsating case at $De = 6.3 \times 10^2$ and $\alpha = 8$ was calculated for the case of a double bended pipe revealing very complex secondary patterns during a cycle.

It is now made clear that studies need to be performed on high Dean and Womersley number flows in order to investigate the parameters that affect the performance of the engine but also to give useful information on the limitations of classical experimental techniques in highly unsteady, turbulent and three dimensional flows, as well as to provide a unique data base for the CFD community. Above all, these studies will give new insight into the complex flow field, during a cycle and its vortical structures.

2. Experimental set-up

2.1. Pulsating pipe flow rig

The experiments were conducted in a newly developed flow rig in the *CICERO Laboratory* at *KTH CCGEx*. The rig can be operated both under steady and pulsating flow conditions and the air is supplied through a compressor installation facility that can deliver up to 500 g/s at 6 bar. The pulses are obtained from a rotating valve located upstream of the pipe test section and its rotation rate can be set by a frequency controlled AC motor. The insert in Figure 1 depicts the relative open area change

caused by the rotating valve as function of the revolution angle. The flow rate is monitored for accuracy by means of a hot-film type mass flow meter (ABB Thermal Mass Flowmeter FMT500-IG) which is located around 10 m upstream from the measurement site. For details on the *CICERO rig* the reader is referred to Laurantzson *et al.* (2010).

For the present measurements, a 90° pipe bend of inner diameter $D = 40.5$ mm and curvature radius $R_c = 51$ mm was connected to the downstream end of a straight pipe section which provided a total entrance length of $20 D$ downstream of the pulse generator. All measurements were taken at the exit of an extension pipe with the same inner diameter and length $3 D$ downstream of the bend as depicted in Figure 1.

2.2. Measurement technique

Time-Resolved Stereoscopic Particle Image Velocimetry (TS-PIV) was employed in order to capture snapshots of the instantaneous in-plane velocity components as well as the streamwise velocity across the pipe cross-section. Two high-speed C-MOS cameras (Fastcam APX RS, 3000 fps at full resolution, 1024×1024 px, Photron) were positioned in backward-forward scattering mode at an angle of approximately 70° between the observation axes (see figure 1). The 105 mm camera lenses (Nikon Nikkor) mounted on the cameras were adjusted by means of a Scheimpflug adapter. The raw images from the measurements had a resolution of 1024×1024 px and a 10-bit dynamic range. For the steady flow measurements the images were taken at a sampling frequency of 1 kHz and for the pulsating flow measurements images were acquired at 1.5 kHz while the laser was additionally triggered externally by the valve rotation in order to enable phase averaging of the snapshots.

A laser light sheet of 1 mm thickness was produced by a Nd-YLF laser (Pegasus PIV-Laser, 10 kHz maximum frequency, New Wave) which was aligned 1 mm downstream from the exit of the pipe and oriented perpendicular to the main flow direction. For the *in-situ* calibration of the cameras, images were taken of a two-level calibration plate (#20, LaVision GmbH).

A water-based solution (Jem Pro Smoke Super ZR-Mix) was atomized using a high volume liquid seeding generator (10F03 Seeding Generator, DANTEC Dynamics). Smoke was injected homogeneously through 4 holes drilled symmetrically around a steel pipe section which was mounted upstream of the pulse generator in order to avoid effects on the smoke distribution from the valve rotation. The post-processing of the PIV data was performed using a commercial software (DaVis 7.2, LaVision GmbH). The vector fields were calculated by a multi-pass iteration procedure starting with a 64×64 px interrogation window and decreasing down to 16×16 px interrogation window with 50 % area overlapping.

3. Results & Discussion

3.1. Steady Turbulent Flow

Steady turbulent flow measurements were performed by means of TS-PIV at a downstream position of $3 D$ from the bend. Figure 2 shows snapshots of the streamwise velocity field and the in-plane velocity components. Nearly symmetrical structures at the upper and lower section of the pipe are observed at certain instances (*left*

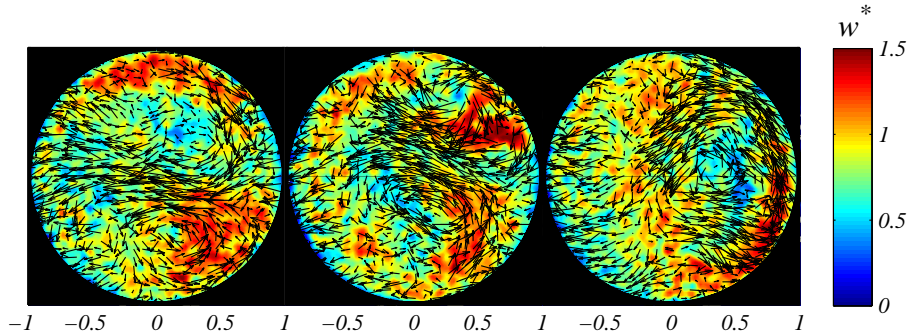


FIGURE 2. *Left, Middle & Right:* Snapshots of the streamwise and in-plane velocity field from TS-PIV measurements $3D$ downstream the 90° pipe bend. Streamwise (W) and in-plane (U and V) velocities are depicted through the contour map as well as vector field, respectively. The asterisk denotes scaling by the bulk velocity obtained from the ABB mass flow meter.

figure) while at other instances the vortices are seen to move either in clockwise (*middle figure*) or anti-clockwise (*right figure*) direction in varying strength. Similar observations were also made by Hellström (2010) who performed simulations on the experimental set-up by Sudo *et al.* (1998) in a 90° pipe bend, for $De = 3 \times 10^4$. Even though no direct comparison can be made due to the different flow and geometrical parameters between the two studies, the instantaneous results from the simulations show a behaviour of the vortical structures that can also be seen in the present study.

Figure 3 depicts the time-averaged flow field computed over 500 snapshots acquired at a sampling frequency of 1 kHz, which corresponds to about 400 integral time scales. In principle the figure should be symmetric around the centreline, however the difference between the lower and upper half is probably due to an insufficient number of independent snapshots.

The vortex structure is clearly illustrated by the streamlines in Figure 3, though the upper vortex is not captured entirely. Note also that the region $r/R > 0.95$ is excluded here due to reflections which cause spurious vectors. One observation in our study is that the streamwise velocity maxima is not at the outer wall but two maxima are found along the upper and lower sides, respectively. A similar effect was seen by Sudo *et al.* (1998) where the evolution of the flow field at different stations after the bend showed a tendency of the higher speed side slowly moving from the outer wall until the flow profile becomes fully symmetrical. Contour maps featuring the highest velocity located closer to the inner wall at downstream locations after the bend was also shown in Enayet *et al.* (1982), who studied developing turbulent flow by means of Laser-Doppler Velocimetry (LDV) in a 90° pipe bend at $Re = 43000$. For the present experimental configurations, additional measurements at further upstream locations (not presented here), showed the maximum velocity located closer to the outer wall revealing a tendency of the velocity maxima to move from the outer wall towards the

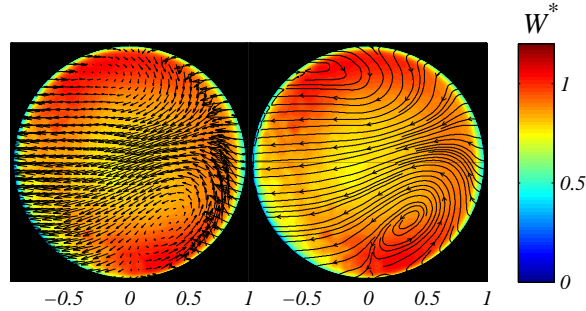


FIGURE 3. Time-averaged streamwise and in-plane velocity field from TS-PIV measurements $3D$ downstream the 90° pipe bend at $De = 1.5 \times 10^4$. *Left*: time-averaged vector field, and *Right*: time-averaged streamlines. The time-average was computed over 500 snapshots with $\Delta t = 1/1000$ s. The largest time-averaged in-plane velocity component is around 0.3 of the bulk velocity.

centre while under the effect of the secondary motions exhibiting a slight “overshoot” towards the inner wall at $3D$ distance from the bend.

3.2. Time/Phase-Resolved results: Pulsating turbulent flow

For a high Womersley number the unsteady inertia forces dominate in comparison with the viscous forces while interacting with the centrifugal forces under one cycle, providing more complicated and varying secondary flow structures than those seen in the steady flow case. TS-PIV measurements under pulsatile conditions were performed at $De = 1.5 \times 10^4$ and $\alpha = 72$. Snapshots of the streamwise and in-plane velocities are shown in Figure 4 for different phases of the pulse cycle. The phase averaged velocity at the centreline of the pipe is also shown as an indication of what instance during the pulse cycle each one of the figures represent. At the end of the first acceleration phase the highest velocity reaches 3.5 times the bulk speed, while at the end of the deceleration phase back flow with a magnitude of the bulk speed sets in.

During the whole acceleration phase (top of Figure 4) no clear cross flow structures can be seen, and at the beginning of the phase shown the highest streamwise velocity is at the inner half of the pipe whereas the flow becomes more uniform with time. Timité *et al.* (2010) showed that for laminar flow, as the frequency parameter increases, the secondary flow intensity decreases which can also be seen here for a large value of α , even though for a completely different type of flow.

A completely different vortical picture is shown during the deceleration phase (centre of Figure 4) where almost symmetrical vortical structures are seen and the position of the maximum streamwise velocity has switched to the outer wall, thereby

resembling a C-shaped velocity distribution similar to those observed in steady flows in the vicinity of the pipe bend.

Reversed flow is an often observed phenomenon under pulsating flow conditions (Timité *et al.* 2010; Hellström 2010). As the deceleration phase ends and back flow sets in (bottom of Figure 4), a pair of vortical structures can be distinguished which

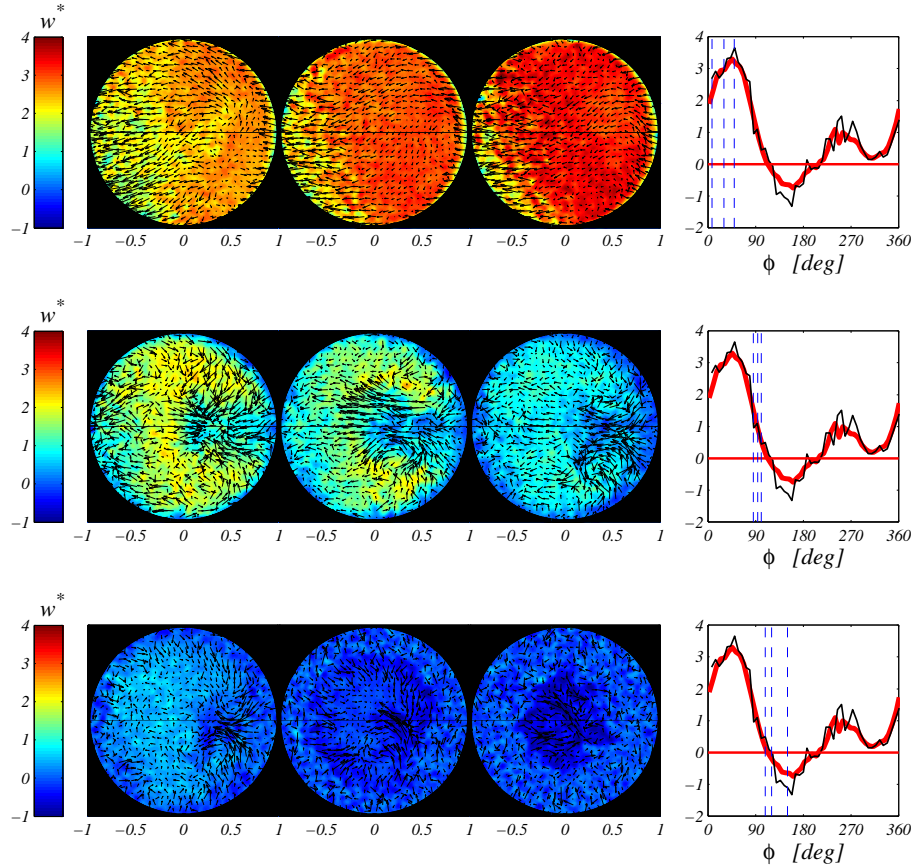


FIGURE 4. *Left:* Snapshots of the streamwise velocity and in-plane vector field at subsequent instances $3D$ downstream the 90° pipe bend at $De = 1.5 \times 10^4$ at a pulsating frequency of 30 Hz corresponding to $\alpha = 72$. *Right:* Instantaneous streamwise velocity (thin black line) and its phase average (thick red line) at the centreline of the pipe. The phase angle corresponding to the shown snapshots is indicated through the vertical dashed lines. *Top:* Acceleration phase, *middle:* Deceleration phase, *Bottom:* Back flow.

are seen later on being almost “squeezed” inside the back flow region until they are completely vanished.

The phase averaged streamwise and in-plane velocities are shown as contour and vector plots respectively in Figure 5 depicting a similar and smoother structural picture as in the instantaneous figures, as expected. During the acceleration phase, no vortical structures can be recognized even here, due probably to the dominant inertial forces. The almost symmetrical vortices observed in the instantaneous figures

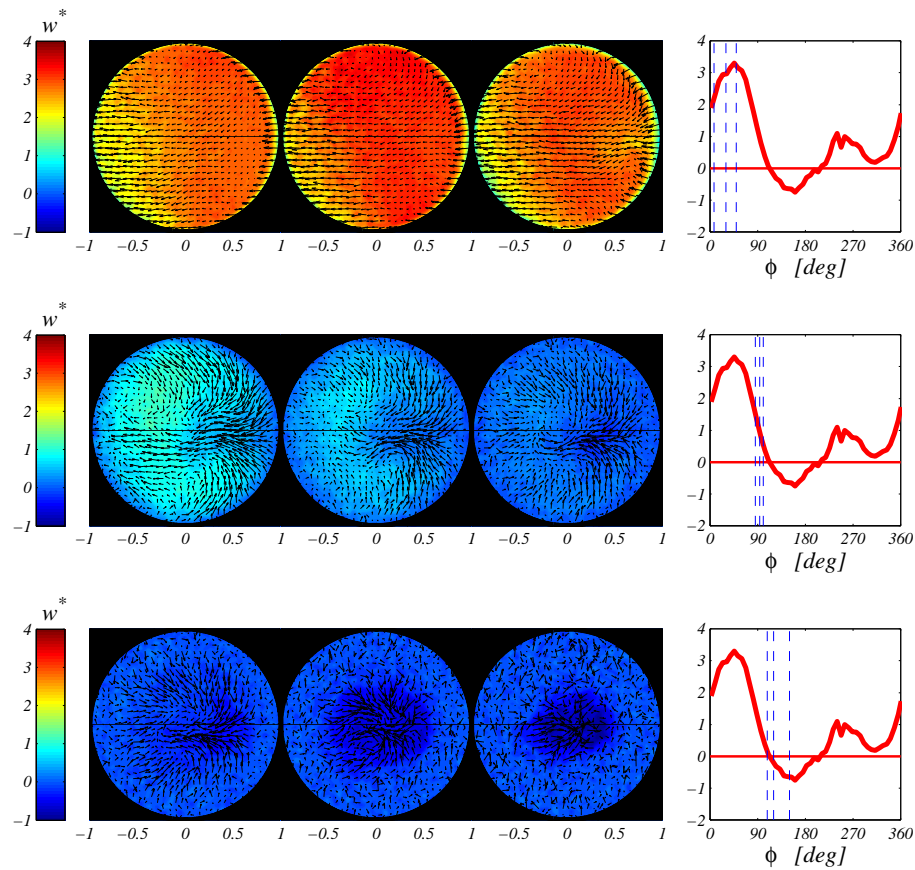


FIGURE 5. *Left:* Phase averaged streamwise velocity and in-plane vector field for the same case as in Figure 4. *Right:* Phase averaged streamwise velocity (thick red line) at the centreline of the pipe. The phase angle corresponding to the shown phase averages is indicated through the vertical dashed lines. *Top:* Acceleration phase, *middle:* Deceleration phase, *Bottom:* Back flow.

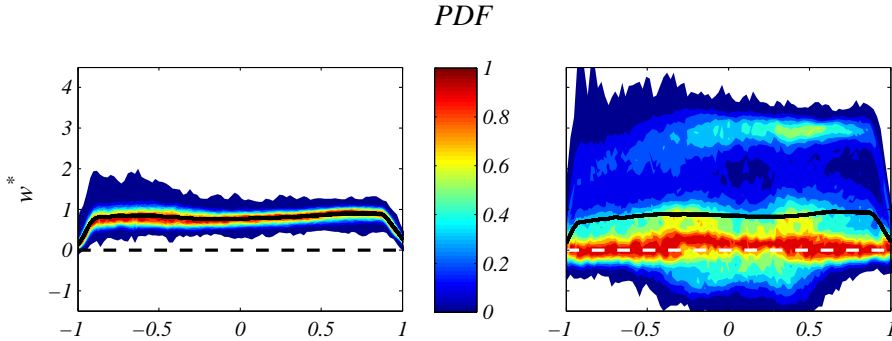


FIGURE 6. Contour plots of the probability density function of the streamwise velocity along the horizontal axis at $3D$ downstream distance from the pipe bend exit, plotted together with its mean value (thick black line) at $De = 1.5 \times 10^4$. *Left:* Steady flow *Right:* Pulsating flow ($\alpha = 72$). Note that the PDFs have been scaled to unity in order to ease comparison between the steady and pulsating flow case.

during the deceleration phase appear smoother now as a result of the phase averaging, though at the last considered phase angle here, the two vortices at the lower and upper part of the pipe appear to have been smoothed out. This effect can also be seen in the figure which corresponds to the onset of back flow, where the two small vortical structures positioned close to the inner pipe wall each one at one side of the pipe in the corresponding snapshot, have been filtered out. At the peak of the negative velocity region the vortices have already vanished and no significant feature can be observed.

Figure 6 shows the probability density function (PDF) of the streamwise velocity component for both the steady and the pulsating flow case together with its mean value along the horizontal axis. The time-averaged profiles between the two flow cases do not differ considerably from each other; i.e. both exhibit a “saddle”-like profile with a slightly larger amplitude on the inner side of the pipe (see also § 3.1). It is interesting to note, that for the steady flow case the PDF looks as expected, i.e. with the most frequent velocity appearing around its time-average value, while for the pulsating flow it is accumulated around zero velocity. The bimodal behaviour of the PDF (*Left Figure*) caused by the pulsatile motion, is apparent from the phase averaged signal at the centreline (thick red line) shown in Figure 5.

4. Summary & Conclusions

The present investigation aims at understanding the behaviour of the secondary motions and the distribution of the axial velocity under the effect of the pipe bend in a parameter range that is relevant to the flow environment for internal combustion engines. TS-PIV measurements have been conducted in a high Dean and Womersley number flow, through a 90° pipe bend.

It was shown that the flow has started to recover from the bend at a downstream distance of $3 D$, depicting the highest axial velocity located close to the inner wall. Measurements conducted in highly pulsating flow revealed that the secondary flow appeared to be very weak during the acceleration phase while the highest velocity reached 3.5 times the bulk speed. A different vortical picture was observed during the deceleration phase, where symmetrical structures were present at certain instances. The streamwise velocity was observed to have moved its maximum from the inner wall during the acceleration phase to the outer wall during deceleration. The almost symmetrical vortices were observed at the beginning of back flow, being quickly “squeezed” into the centre of the pipe until vanishing in the peak of the reversed flow region.

Acknowledgements

This research was done within KTH CCGEx, a centre supported by the Swedish Energy Agency, Swedish Vehicle Industry and KTH. The first author acknowledges the travel grant from the *Björns* foundation at KTH.

References

- BERTELSEN, A. F. 1975 An experimental investigation of low Reynolds number secondary streaming effects associated with an oscillating viscous flow in a curved pipe. *J. Fluid Mech.* **70**, 519–527.
- BRÜCKER, CH. 1998 A time-recording DPIV-Study of the swirl switching effect in a 90° bend flow. *Proc. 8th Int. Symp. Flow Vis., 1-4 Sept., Sorrento (NA), Italy* pp. 171.1–171.6.
- CAPOBIANCO, M., GAMBAROTTA, A. & NOCCHI, M. 1993 Unsteady Flow Phenomena and Volume Effects in Automotive Engines Manifolds. *SAE Tech. paper* pp. 1–13.
- CHANDRAN, K. B. & YEARWOOD, T. L. 1981 Experimental study of physiological pulsatile flow in a curved tube. *J. Fluid Mech.* **111**, 59–85.
- DEAN, W. R. 1927 Note on the motion of fluid in a curved pipe. *Phil. Mag.* **4**, 208–223.
- ENAYET, M. M., GIBSON, M. M., TAYLOR, A. & YIANNESKIS, M. 1982 Laser-doppler measurements of laminar and turbulent flow in a pipe bend. *Int. J. Heat Fluid Flow* **3**, 213–219.
- GREENSPAN, D. 1973 Secondary flow in a curved tube. *J. Fluid Mech.* **57**, 167–176.
- HAMAKIOTES, C. C. & BERGER, S. A. 1990 Periodic flows through curved tubes: the effect of the frequency parameter. *J. Fluid Mech.* **210**, 353–370.
- HELLSTRÖM, F. 2010 Numerical computations of the unsteady flow in turbochargers. *PhD thesis, KTH Mechanics, Sweden.*
- JARRAHI, M., CASTELAIN, C. & PEERHOSSAINI, H. 2010 Secondary flow patterns and mixing in laminar pulsating flow through a curved pipe. *Exp. Fluids* **50**, 1539–1558.
- LAURANTZON, F., TILLMARK, N. & ALFREDSSON, P. H. 2010 A pulsating flow rig for analyzing turbocharger performance. *9th Int. Conf. on Turbochargers and Turbocharging (IMEchE)* pp. 363–372.
- LYNE, W. H. 1970 Unsteady viscous flow in a curved pipe. *J. Fluid Mech.* **45**, 13–31.
- MCCONALOGUE, D. J. & SRIVASTAVA, R. S. 1968 Motion of a fluid in a curved tube. *Proc. Roy. Soc.* **307**, 37–53.
- RÜTTEN, F., SCHRÖDER, W. & MEINKE, M. 2005 Large-eddy simulation of low frequency oscillations of the Dean vortices in turbulent pipe bend flows. *Phys. Fluids* **17**, 035107.

- SAKAKIBARA, J., SONOBE, R., GOTO, H., TEZUKA, H., TADA, H. & TEZUKA, K. 2010 Stereo-PIV study of turbulent flow downstream of a bend in a round pipe. *14th Int. Symp. Flow Vis., 21-24 June, EXCO Daegu, Korea* pp. 1–11.
- SUDO, K., SUMIDA, M. & HIBARA, H. 1998 Experimental investigation on turbulent flow in a circular-sectioned 90-degree bend. *Exp. Fluids* **25**, 42–49.
- SZYMKO, S., MARTINEZ-BOTAS, R. F. & PULLEN, K. R. 2005 Experimental evaluation of turbocharger turbine performance under pulsating flow conditions. *Proc. GT2005: ASME TURBO EXPO* pp. 1–11.
- TIMITÉ, B., CASTELAIN, C. & PEERHOSSAINI, H. 2010 Pulsatile viscous flow in a curved pipe: Effects of pulsation on the development of secondary flow. *Int. J. Heat Fluid Flow* **31**, 879–896.
- TUNSTALL, M. J. & HARVEY, J. K. 1968 On the effect of a sharp bend in a fully developed turbulent pipe-flow. *J. Fluid Mech.* **34**, 595–608.
- ZALOSH, R. G. & NELSON, W. G. 1973 Pulsating flow in a curved tube. *J. Fluid Mech.* **59**, 693–705.

Paper 3

Dean vortices in turbulent flow: rocking or rolling?

By Athanasia Kalpakli, Ramis Örlü & P. Henrik Alfredsson

Linné Flow Centre & CCGEx, KTH Mechanics, SE-100 44 Stockholm, Sweden

Published in *J. Visualization* **15**, 37–38, 2011

Flows in pipe bends have been studied extensively over the last decades due to their occurrence both in the human respiratory and blood systems as well as in many technical applications. When a fluid flows through a pipe bend an adverse pressure gradient is generated forcing high velocity fluid towards the outer wall which is then replaced by low velocity fluid moving along the wall towards the inner side of the bend. The physical effect is that the high velocity fluid is experiencing a large centrifugal force, resulting in an unstable “stratification” making the high velocity fluid in the centre deflect outwards along the pipe bend, thereby forming two counter-rotating roll cells, so-called *Dean vortices*. While their behavior in laminar flows has been nicely visualized, the picture of their unsteady behavior in turbulent flows still remains rather blurry, and in fact the question “whether the Dean vortices stay symmetric with respect to the geometric plane of symmetry or whether the strength of the Dean vortices varies with time are hardly addressed” (Rütten et al. 2005).

In the present study stereoscopic particle image velocimetry has been employed to seize the unsteady behavior of the *Dean vortices* at the exit of a 90° pipe bend at a Reynolds number and Dean number of 34 000 and 19 000, respectively. While the time-averaged flow field shows two symmetrical roll cells, that can be observed both in the streamwise (Fig. 1a) and cross stream (Fig. 1b) velocities¹, as well as in the streamwise vorticity (Fig. 1c), the instantaneous snapshots reveal an unsteady behavior where the roll cells are pushing one another alternatively towards the lower or upper half of the pipe, in what could be described as a “rocking” motion of the high speed “stem” in between the roll cells (Fig. 2).

Hence the real question is not whether “*to be, or not to be*” in regards to the instantaneous existence of the *Dean vortices* in turbulent flows, but rather *why, when* and *how* they *roll* (as their time-averaged counterpart) or *rock* between the states caught in the presented snapshots.

Acknowledgements

Dr. Gabriele Bellani is acknowledged for valuable comments on the set-up of the PIV system and the post-processing of the PIV images.

¹In the original version there has been an error and the extension after the curvature was misprinted as $0.5 D$.

Reference

Rütten F., Schröder W. and Meinke M. (2005) Large-eddy simulation of low frequency oscillations of the Dean vortices in turbulent pipe bend flows. *Phys. Fluids* **17**, 035107.

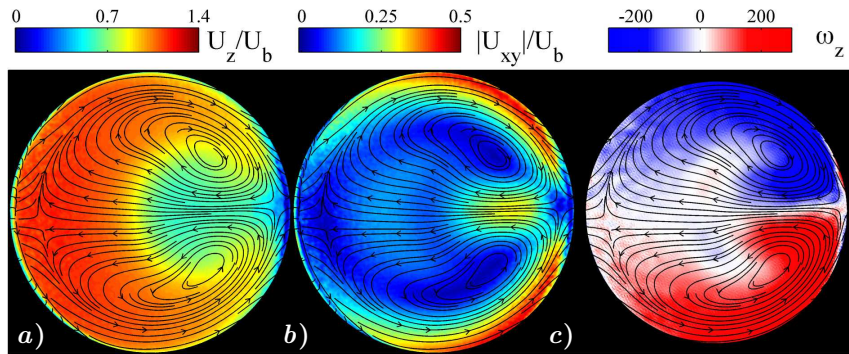


FIGURE 1. Time-averaged streamlines from stereoscopic particle image velocimetry measurements across the pipe cross section $0.67 D$ downstream the 90° pipe bend. The Reynolds number (based on bulk velocity $U_b = 8.5$ m/s and pipe diameter $D = 0.06$ m) and Dean number (Reynolds number \times square root of the curvature ratio) were 34 000 and 19 000, respectively. Contours denote the *a*) streamwise velocity component U_z , *b*) magnitude of the in-plane components $|U_{xy}|$, and *c*) streamwise vorticity ω_z . The averages were performed over 3000 snapshots with $\Delta t = 1$ ms. Note that the streamlines were smoothed by means of a spatial low-pass filter and that the region close to the wall in the vorticity map has been blinded out due to spurious vectors.

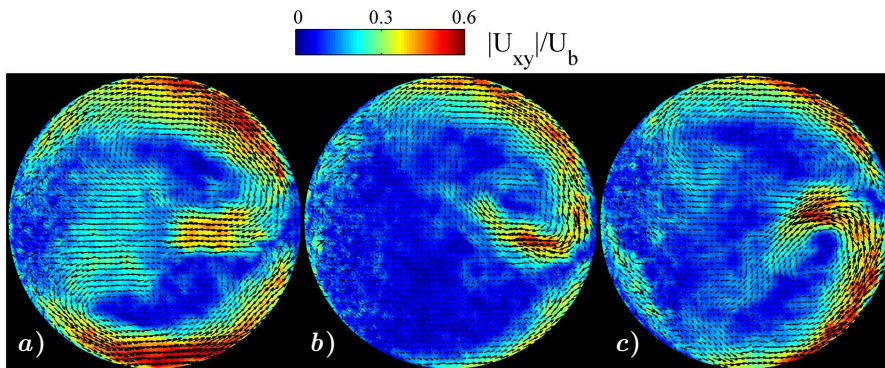


FIGURE 2. Snapshots of the in-plane vector field at three independent time instances for the same conditions as described in Fig. 1. The small-scale fluctuations have been suppressed through a moving average of $\Delta t = 2$ ms in time and a spatial low-pass filter. The instantaneous snapshots reveal the three states between which the two Dean vortices are switching, viz. *a)* symmetric, as well as dominant *b)* clockwise and *c)* counterclockwise Dean cell.

Paper 4

Experimental investigation on the effect of pulsations on exhaust manifold-related flows aiming at improved efficiency

By Athanasia Kalpakli, Ramis Örlü, Nils Tillmark & P. Henrik Alfredsson

Linné Flow Centre & CCGEx, KTH Mechanics, SE-100 44 Stockholm, Sweden

Accepted to *Proc. of 10th Int. Conf. on Turbochargers and Turbocharging* 2012

The gas flowing through the exhaust manifold of the internal combustion engine to the inlet of the turbine side of a turbocharger is highly pulsating and turbulent. The gas enters the turbine after travelling through a complex curved and branched pipe system where the effect of centrifugal (from the acute curvature), inertia and viscous forces result in a three-dimensional, non-symmetric flow field. Additionally, vortical structures are being formed and dissolved due to the co-existence of these forces that change in magnitude under a pulse period. This complex flow field, typical for the inflow condition to the turbine, is the focus of the present study. Instantaneous mass flow rate and pressure measurements that provide information on changes in the turbine map when a sharp bend is mounted at the inlet of the turbine are performed and complemented with time-resolved stereoscopic particle image velocimetry measurements of the pulsating turbulent flow downstream a 90° pipe bend. The results indicate, that the time-averaged operation point in a turbine map is only marginally affected by the inflow conditions and the pulsation frequency. The hysteresis loops, on the other hand, exhibit differences not only for different pulsation frequencies, but also for different inflow conditions as a comparison between a straight and a curved pipe section upstream the turbine shows.

1. Introduction

Flows through curved pipes are widely met in nature and in industry. Scientific interest on such flows is traced back to the 1800s (Thomson 1876) and up to this moment it remains vibrantly alive (Timité *et al.* 2011). Nevertheless, a lot of information about the behaviour of the various flow structures under the existence of a centrifugal force is still missing. The presence of non-ideal components in the internal combustion engine, such as sharp pipe bends comprising the exhaust manifold together with the highly pulsatile turbulent flow from the engine cylinders, leads to very complex flow phenomena that may affect the engines performance. Despite its

technical importance, not many studies through pipe bends have been conducted aimed at the engine flow environment, i.e. highly pulsatile turbulent flow, but most studies instead focus on laminar, low frequency pulsatile flows related to biological or natural mechanisms.

At KTH CCGEx (Competence Centre for Gas Exchange), a new approach to investigate the effect of pulsations and curved geometries on the flow field entering the turbine of a turbocharger and the pressure ratio across it has been undertaken. For that purpose, state of the art experimental techniques such as Time-resolved Stereoscopic Particle Image Velocimetry (TS-PIV), high frequency pressure transducers, and a time-resolved vortex shedding mass flow meter (Laurantzon *et al.* 2010a) have been implemented. This gives the possibility to obtain the instantaneous, phase-averaged and time-averaged velocity fields after a sharp pipe bend together with the phase-resolved turbine maps. The obtained results constitute valuable information on the effect of pulsations on the flow field resembling the inflow to an exhaust manifold under practically relevant conditions.

The present study aims at providing new insight into the flow field evolution with particular focus on the secondary motion behaviour in steady and highly pulsatile turbulent flow conditions through curved pipes, which –to the authors knowledge– has not been considered in the literature yet. § 2 gives the background and defines the relevant parameters, whereas § 3 describes the experimental set-up and the Time resolved Stereoscopic Particle Image Velocimetry (TS-PIV) system¹. § 4 describes and discusses the results and finally § 5 gives a short summary and some concluding remarks.

2. Pulsating flow through curved pipes

Laminar and steady flow through curved pipes has been studied extensively throughout the last decades. The main characteristic feature of such a flow is the development of a secondary flow due to the formation of two symmetrical counter-rotating vortices, the so called *Dean vortices*. Such flows have been considered in the literature with investigations initiated many years ago (Eustice 1911; Dean 1927). An important consequence of the vortices is that they shift high-speed fluid towards the outer pipe wall whereas a region of low velocity fluid develops at the inner wall.

Studies on turbulent steady flows (Rütten *et al.* 2005) or laminar pulsating flows (Jarrahi *et al.* 2010) through curved pipes have been conducted in recent years revealing a complicated flow field which is highly dependent on the value of certain flow parameters. On the other hand, studies of *highly pulsatile turbulent flows through curved pipes* with regard to the flow field evolution, and in particular the existence and importance of the secondary motion behaviour, is missing.

The most important parameters which convey the pulsatile flow through curved pipes are the Dean number ($De = \sqrt{\gamma}Re$, where $\gamma = D/(2R_c)$ is the curvature ratio and $Re = UD/\nu$ the Reynolds number with U the characteristic velocity, $D(= 2R)$ the pipe diameter and ν the kinematic viscosity) and the Womersley number or the so-called frequency parameter ($\alpha = D/2\sqrt{\omega\rho/\mu}$, where ω denotes the angular

¹Note that most of the figures in this paper are better viewed in colour therefore the reader is kindly redirected to the CD version of the proceedings.

frequency of the pulsation). These two parameters define the interplay between the centrifugal, inertial and viscous forces. The values of the parameters used in the current measurements are close to the ones found in a real engine environment, viz. the Dean and Womersley numbers that are of the order of 10^5 and 10^2 , respectively.

3. Experimental procedure

3.1. Set ups

The experiments were conducted at the CICERO laboratory at KTH CCGEx. compressor installation facility delivers air at a maximum mass flow rate of 500g/s at 6 bar while the flow rig can be operated under both steady and pulsating flow conditions. A rotating valve generates pulses where the rotation rate is set by a frequency controlled AC motor. In order to ensure steady flow conditions, the mass flow rate is additionally monitored by a hot-film type mass flow meter (ABB Thermal Mass Flow meter FMT500-IG). For details on the CICERO rig the reader is referred to Laurantzson *et al.* (2010b). Two different set-ups were used: one was used to study the details of flow downstream a pipe bend under steady and pulsating conditions, whereas the second was used to investigate how the pipe bend itself affected the turbine characteristics.

For the pipe bend measurements, a 90° pipe bend of inner diameter $D = 40.5$ mm and curvature radius of $Rc = 51$ mm is mounted downstream a $20 D$ long straight pipe. The bend used for the present investigation was chosen to be sharp ($\gamma = 0.4$), since the aim of the study was to consider typical geometries met in engines where curved sections usually are sharp due to packaging constraints. Straight pipes of different lengths can be mounted at the exit of the curved pipe in order to study the flow evolution downstream the bend. For the results presented here the measurements were made with time resolved stereoscopic PIV (TS-PIV) at three downstream stations at $0.2 D$, $1 D$, and $2 D$ (see figure 1).

The second set up (figure 2) was used in order to study how the turbine map is affected by a pulsating inlet flow using the same pipe bend geometry as for the flow measurements (with the shortest downstream station i.e. $0.2 D$ mounted). For that purpose, measurements by means of high frequency response pressure transducers (Kistler) and an in-house developed vortex shedding mass flow meter (Laurantzson *et al.* 2010a, 2012) were made in order to obtain the instantaneous pressure and mass flow rate across the turbine. In these experiments the mass flow rate was higher than that used for the flow measurements due to certain limitations of the TS-PIV system. Nevertheless, the two set ups is believed to complement well each other and the reader should bear in mind that the aim of the present study is not to compare them but exploit the unique features that each one offers in order to get as much information as possible of the flow conditions into the turbine.

3.2. Time-resolved Stereoscopic Particle Image Velocimetry (TS-PIV)

Time-resolved stereoscopic particle image velocimetry measurements were performed in order to obtain instantaneous snapshots of the three-dimensional velocity field after a 90° pipe bend and examine the behaviour of the secondary flow structures. To seed the flow an alcohol-based solution (Jem Pro Smoke Super ZR-Mix) was atomized

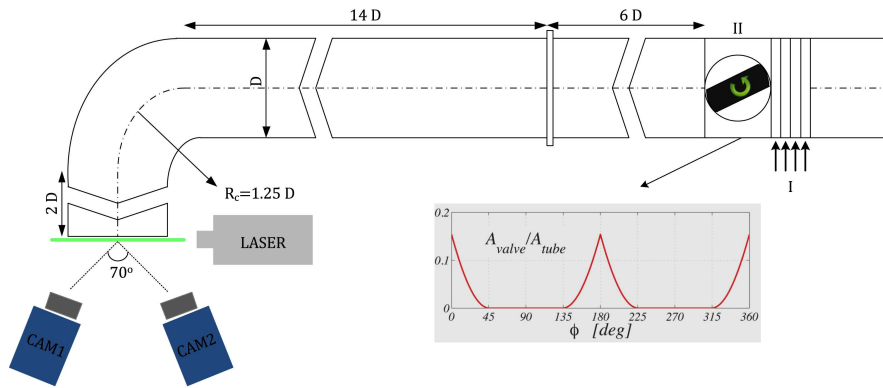


FIGURE 1. Geometrical configuration used in the experiments and camera set up for the TS-PIV measurements (*top view*). $D = 40.5$ mm, $R_c = 51$ mm, I) smoke injection inlet, II) rotating valve. The insert depicts the relative open valve area change as function of the revolution angle.



FIGURE 2. Set up for the instantaneous pressure and mass flow rate measurements across the turbocharger (Garrett).

using a high volume liquid seeding generator (10F03 Seeding Generator, DANTEC Dynamics). The resulting smoke was injected homogeneously through 4 holes drilled symmetrically around a steel pipe section mounted upstream of the pulse generator in order to avoid effects on the smoke distribution from the valve rotation.

A laser light sheet of 1 mm thickness was produced by an Nd-YLF laser (Pegasus, 10kHz maximum frequency, New Wave Research). The laser was externally triggered by the valve rotation in order to enable phase averaging of the snapshots.

Two high-speed C-MOS cameras (Fastcam APX RS, Photron, 3000 fps at full resolution 1024×1024 pixels) were positioned at an angle of approximately 70° between their viewing axes (Figure 1). The 105 mm Nikon Nikkor lenses of the cameras were adjusted using a Scheimpflug adapter so that the image plane, lens plane and object plane for each camera intersect along a common line. For the in-situ calibration of the cameras, images were taken of a two-level calibration plate (#20, LaVision, GmbH). Small discrepancies between the object and image planes due to vibrations during the measurements were eliminated by means of a disparity correction.

The number of acquired images was 1000 for each case and was taken with a sampling frequency of 1 kHz and 1.5 kHz for the steady and pulsating flow cases, respectively. The post-processing of the data was performed with a commercial software (DaVis 7.2, LaVision GmbH). The vector fields were calculated with a multi-pass iteration procedure for increased resolution (starting with an interrogation window of 64×64 pixels and decreasing to 16×16 pixels with an overlapping area of 50%). Information about the principal of PIV and data evaluation methods along with examples of applications can be found in Raffel *et al.* (2007).

4. Results & discussion

4.1. Flow field under steady turbulent conditions

In the following section time-averaged and instantaneous results from the TS-PIV measurements from the steady flow downstream the pipe bend will be presented to discuss the evolution of the three-dimensional flow field. Figure 3 shows the time-averaged flow field with the streamwise component shown as a (coloured) contour map and the in-plane components as streamlines at the three downstream stations for a Dean number of $De = 1.5 \times 10^4$.

The well-known flow field formed through curved pipes with two symmetrical vortices at the lower and upper parts of the pipe are clearly seen at $0.2 D$ downstream from the bend. This is due to the centrifugal effects and as expected the vortices give rise to a high streamwise velocity at the outer wall and low velocity at the inner wall.

Following the development of both the secondary and primary flow at the other two downstream planes, the flow attempts to overcome the effects from the curvature with the high speed moving consequently towards the inner wall as the distance from the bend increases. Symmetrical vortical structures are evident, changing shape from “bean”-like (at $1 D$) to almost round (at $2 D$) structures. The magnitude of the largest in-plane component throughout the development process is 0.3 times the bulk velocity.

While for laminar flow symmetrical counter-rotating cells, i.e. Dean vortices, appear, under turbulent flow conditions, the behaviour of the vortices remains unclear both on average as well as instantaneously (Rütten *et al.* 2005). Snapshots of the secondary flow field are shown in figure 4 for the different downstream stations. An interesting feature is that for the $0.2 D$ station, the vortices that appear on average at the lower and upper part of the pipe cross section, appear similarly instantaneously, exhibiting a behaviour similar to that known for laminar flows. No additional vortical structures can be seen in that case, as for the other two stations where up to three cells can be captured at certain instants (see figure 4c *middle*). This can probably be

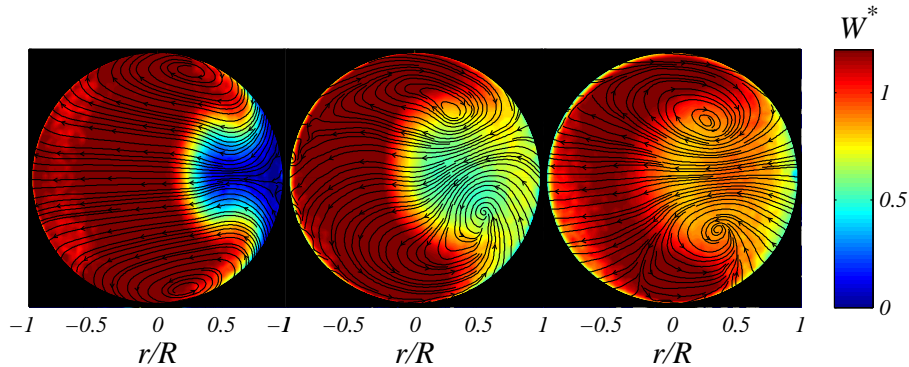


FIGURE 3. Time-averaged velocity flow field at $0.2 D$ (left), $1 D$ (middle) and $2 D$ (right) downstream the 90° pipe bend at $De = 1.5 \times 10^4$. The streamwise component is shown as the background contour map while the in-plane components as streamlines. Quantities with asterisk indicate scaling by the bulk velocity obtained from the ABB mass flow meter. View from the exit plane, whereas the flow comes from the right side.

explained by the interaction between the centrifugal forces introduced by the sharp bend which is the dominating factor in that case.

A different and highly unsteady behaviour is observed for the $1 D$ and $2 D$ downstream stations. Symmetrical vortices resembling the ones seen on average (Figures 4b & 4c, left) as well as dominating “bean”-like shaped vortices following a clockwise or anti-clockwise rotation of the plane of symmetry (Figure 4b *middle & right* and Figure 4c, *right*) and vortices breaking up in smaller cells are depicted (Figure 4b, *middle*). An explanation of the reason of the existence of dominating vortices and their change of position is given in Brücker (1998), even though the exact mechanism that creates the phenomenon remains unclear. The switching between dominating vortices in the pipe cross section for a fully developed turbulent pipe flow into a 90° pipe bend has also been visualized experimentally in Kalpakli *et al.* (2011). To be able to predict such a phenomenon is of great importance due to the low frequency oscillations it creates (Rütten *et al.* 2005) and the fatigue that can be caused in systems comprised of pipe bends.

4.2. Flow field under pulsatile conditions

Results from TS-PIV measurements conducted in a pulsating turbulent flow at the same Dean number as the one in the steady flow case ($De = 1.5 \times 10^4$) and a Womersley number of $\alpha = 30$ (corresponding to a pulsation frequency of 20 Hz) are presented for the same cross-planes as described in § 4.1.

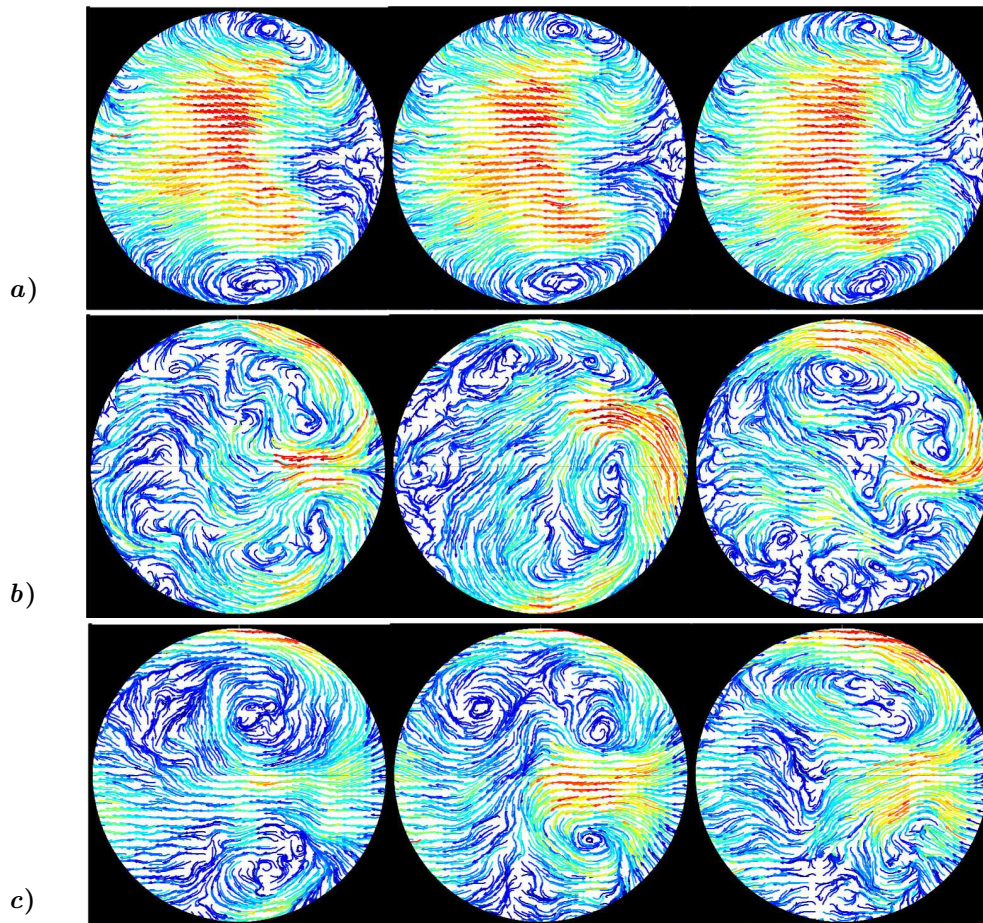


FIGURE 4. Snapshots at various time instances of the in-plane velocity vector field at three instances for the: $0.2 D$ (*a*), $1 D$ (*b*) & $2 D$ (*c*) downstream stations from the pipe bend. The small-scale fluctuations have been subtracted using a moving average of 3 ms and spatial low pass filtering. The magnitude of the largest in-plane component (red vectors) is 0.3 times the bulk velocity.

Figure 5 shows the phase-averaged flow field plotted with the streamwise component as the background contour map and in-plane components as vectors, for the three downstream stations. As a reference, the phase-averaged streamwise velocity at the centreline of the pipe is plotted for each of the three cross plane cases to indicate the phase angle to which each of the shown phase averages belongs.

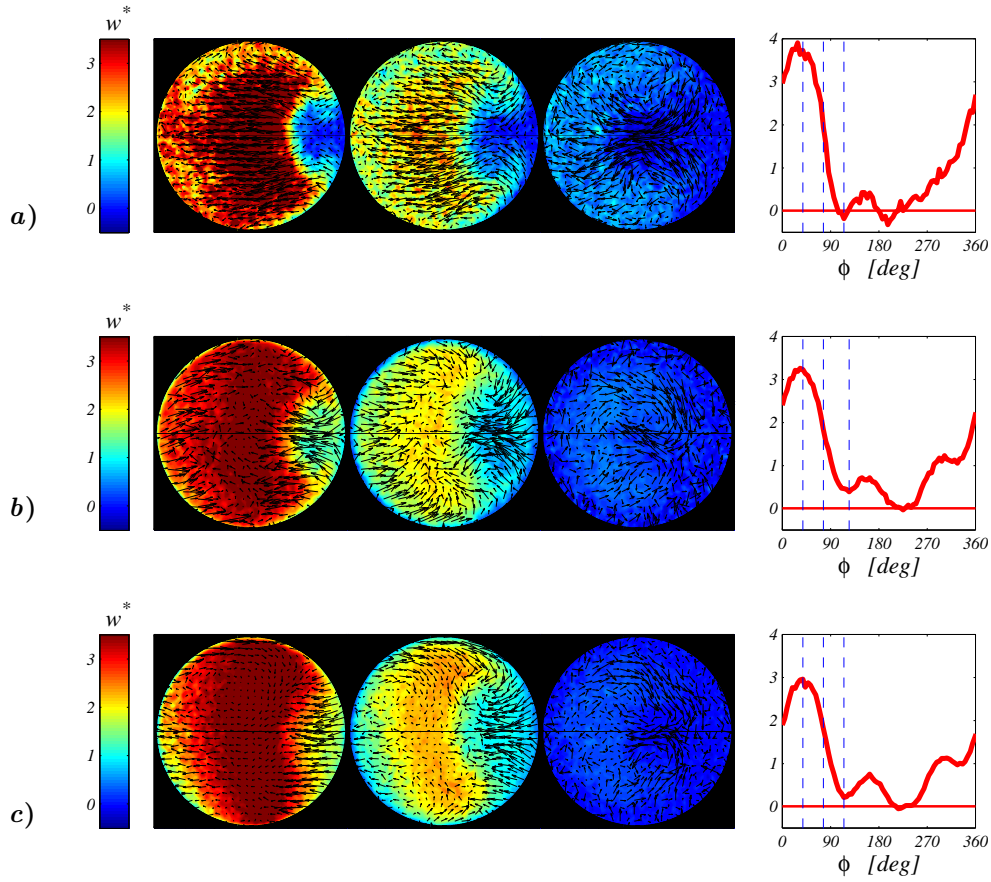


FIGURE 5. *Left:* Phase averaged flow field at $\alpha = 30$ and $De = 1.5 \times 10^4$ for the $0.2 D$ (a) $1 D$ (b) & $2 D$ (c) station. *Right:* Phase averaged streamwise velocity (red line) at the centreline of the pipe. The phase angle corresponding to the shown phase averages is indicated through the dashed lines.

For the $0.2 D$ downstream station the stagnation region at the inner side of the pipe, which was observed under steady flow conditions, appears here as well during the acceleration and deceleration phases. At the end of the deceleration phase, a zone with substantially lower velocity around the centreline than that at the outer wall is depicted. Comparing the flow field evolution under the different phases between the three cross planes, it can be seen that the effects of pulsations are much larger directly after the bend. Here (i.e. at $0.2 D$) the mass flow rate varies from 4 times the bulk velocity down to zero (and slightly negative) within a fraction of a pulse.

Such drastic changes may affect the performance of the turbine and will be discussed within the context of turbine maps in the next section (cf. § 4.3).

Numerical studies have indicated that vortical structures appearing at the inlet of the turbocharger strongly affect the performance of the turbine (Hellström 2010), therefore an assessment of their behaviour is also of great importance for the flow characterization of the engine. At the end of the acceleration phase, one of the two symmetrical vortices, which were evident under steady flow conditions (§ 4.1), appears at the upper part of the pipe while during deceleration both of the vortices are captured. The persistence of these vortices is explained merely by the highly skewed velocity profile and the co-existence of the near zero-velocity region close to the inner wall and high velocity region at the core region. This is further supported by the way they deform at the end of deceleration phase where the flow seems more “relaxed” with the minimum possible flow rate in the pipe and the higher velocity region confined to a small C-shaped area close to the wall. The two vortices expand in bigger, almost round-shaped structures covering the cross section area between the upper and lower walls and the centre of the pipe. Their existence in combination with almost no flow entering the turbine during this phase, should be further investigated for efficiency effects.

At the 1 D station no large scale vortices are observed at the peak of acceleration, due to the dominance of the inertia forces from the pulsations. During deceleration, small vortical structures start to form, as the flow inside the pipe decreases, until the valve closes and two roll cells move towards the centre of the pipe, accumulated around its circumference. When the valve closes and there is almost no mass flow, the centrifugal effects are favored causing the cells to whirl at the centre of the pipe where the velocity is close to zero. At the end of the deceleration phase the same vortex pattern at the centre of the pipe, is also observed for the far most downstream station considered here.

4.3. Turbine maps

One of the most important parameters that affect the efficiency of the turbocharger is the ratio between the inlet stagnation pressure and the outlet static pressure, i.e. the pressure ratio. It is known that large pressure drops can occur along a bend depending on its curvature as well as the flow conditions. Having already obtained a quantitative and qualitative picture of the flow (§ 4.2) entering the turbine, the next step is to connect this information to the pressure changes across the turbocharger due to the presence of a sharp bend. This will provide an overall estimation of the bend effects on the turbocharger performance.

In Figure 6 the instantaneous pressure ratio and mass flow rate measured with fast response transducers and the vortex flow meter respectively, are plotted for four different mass flows. The 55 g/s case corresponds to a Dean number equal to $De = 2.0 \times 10^5$ and 40Hz pulsating frequency gives $\alpha \approx 10^2$. In order to check the accuracy of the vortex shedding technique to estimate the instantaneous mass flow rate, the same data are plotted compared to values given by the ABB mass flow meter and it is shown that the results from both devices agree satisfactorily well (for details on the accuracy as well as limitations and appliance of the technique, the reader is referred to Laurantzou *et al.* (2010a, 2012)).

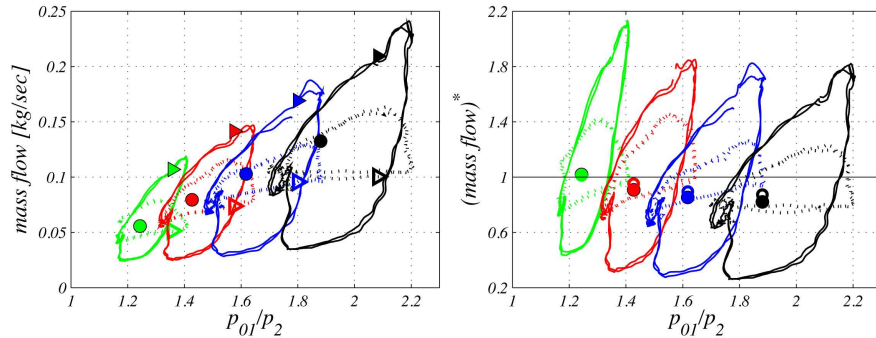


FIGURE 6. *Left*: Turbine map for 55 (green), 80 (red) 105 (blue) & 130 g/sec (black) at 40 Hz pulsation frequency. *Solid lines*: inflow, dashed lines: outflow. *Right*: The same data as in the left figure with the mass flow scaled by the value obtained by the ABB mass flow meter. Circles indicate time-averaged results, where the mass flow rate is based on the ABB reference mass flow meter; filled and open symbols denote inflow and outflow, respectively.

As already mentioned in § 4.2, the pulsating flow after a bend varies rapidly from very high to very low mass flow rates which causes a filling and emptying effect into the turbine leading to a hysteresis loop around the steady flow results which is observed in the above figures. With the increase in mass flow rate the pressure ratio increases, as it is expected but the interesting feature is that the hysteresis loop at higher mass flow rates, expands to larger ranges. It has been shown previously (Marelli & Capobianco 2009) that the magnitude of the loop increases with the pulse frequency and average mass flow level. In Piscaglia *et al.* (2007) instantaneous pressure and mass flow rate measurements across a turbocharger were compared with results from simulations. The instantaneous quantities were measured after a curved pipe section, though effects from secondary motions on the inflow conditions to the turbine were not investigated. Significant hysteresis was observed also in those results due to the tendency of the flow to accumulate in the volume of the turbine casing, which increases the pressure inside it. The weakness of these studies lies on the fact that instantaneous temperature measurements could not be performed due to the fast response rates needed for such flow conditions. This can lead to substantial errors in the mass flow rate estimation using hot-wires under highly pulsating flows (Laurantzon *et al.* 2010*b*), therefore correction of the hot-wire readings for temperature fluctuations is essential.

Figure 7 shows turbine maps for the same conditions as in Figure 6 but only for the 55 and 105 g/s mass flow cases together with results from Laurantzon *et al.* (2012), which were performed in the same set-up under the same operational conditions, but with a straight pipe instead of the bend pipe as its inflow geometry. By matching the same operational conditions in the same experimental rig, it is possible to relate the observed differences to the used inflow geometry, viz. straight versus

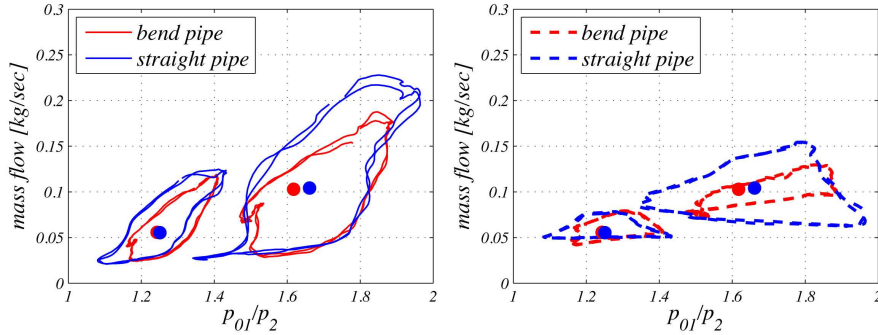


FIGURE 7. Turbine maps for 55 and 105 g/sec at 40 Hz pulsation frequency for a straight and bend pipe configuration at the inlet of the turbocharger. *Left*: inflow. *Right*: outflow. Circles indicate time-averaged results, where the mass flow rate is based on the ABB reference mass flow meter; filled and open symbols denote inflow and outflow, respectively.

bend pipe section. While the trends look similar for the 55 g/s case, the magnitude of the hysteresis loop appears to be damped in the case of the pipe bend, while the general trend of the hysteresis seems to be similar during the deceleration phase, when considering the 105 g/s run. The hysteresis loops based on the mass flow rate from the outlet depict quite different pictures. Here the flow from the bend pipe appears to be damped considerably stronger than that from the straight pipe. Despite these differences for the higher mass flow rate and in particular for the outflow, the time-averaged operational points (indicated by the circles) do not exhibit any significant differences. Consequently, turbine maps based on steady operational conditions need to be considered with great caution when taken as reference for pulsating flows. As apparent from these results, a good agreement of the two different time-averaged operation points does not imply that the hysteresis loops are similar.

5. Summary & conclusions

Time-resolved stereoscopic particle image velocimetry measurements were performed downstream of a 90° pipe bend for a highly pulsatile turbulent flow in order to investigate flow conditions similar to those entering a turbine. A complex flow field, showing rapid velocity changes as well as peculiar vortical patterns during one pulse period, was captured. Velocity magnitudes four times the bulk speed were recorded as well as negative velocities at the end of the deceleration phase.

To investigate the influence of curved, pulsating inflow on the turbine performance, instantaneous pressure and mass flow measurements were made upstream and downstream the turbine with a sharp bend mounted at its inlet and compared with a straight pipe inlet. For the estimation of the instantaneous mass flow rate, a vortex flow meter was used, from which the time signal was extracted by means of a novel post-processing technique introduced in Laurantzson *et al.* (2010a). The pressure ratio-mass flow loop due to the filling and emptying of the turbine during

a pulse period, was observed to expand to greater magnitudes as the mass flow rate increased. Moreover, only a slight effect of the presence of the bend at the inlet of the turbine was shown on the average quantities but a significant change was observed in the instantaneous results with the hysteresis loop significantly damped in case of the bend pipe.

Acknowledgements

This research was done within KTH CCGEx, a centre supported by the Swedish Energy Agency, Swedish Vehicle Industry and KTH. TeknL. Fredrik Laurantzon is acknowledged for valuable help on the experimental set up as well as for providing data from his measurements for comparative purposes in the current study.

References

- BRÜCKER, CH. 1998 A time-recording DPIV-Study of the swirl switching effect in a 90° bend flow. *Proc. 8th Int. Symp. Flow Vis., 1-4 Sept., Sorrento (NA), Italy* pp. 171.1–171.6.
- DEAN, W. R. 1927 Note on the motion of fluid in a curved pipe. *Phil. Mag.* **4**, 208–223.
- EUSTICE, J. 1911 Experiments on stream-line motion in curved pipes. *Proc. Roy. Soc.* **85**, 119–131.
- HELLSTRÖM, F. 2010 Numerical computations of the unsteady flow in turbochargers. *PhD thesis, KTH Mechanics, Stockholm, Sweden.*
- JARRAHI, M., CASTELAIN, C. & PEERHOSSAINI, H. 2010 Secondary flow patterns and mixing in laminar pulsating flow through a curved pipe. *Exp. Fluids* **50**, 1539–1558.
- KALPAKLI, A., ÖRLÜ, R. & ALFREDSSON, P. H. 2011 Dean vortices in turbulent flows: rocking or rolling? *J. Visualization* **15**, 37–38.
- LAURANTZON, F., ÖRLÜ, R., SEGALINI, A. & ALFREDSSON, P. H. 2010a Time-resolved measurements with a vortex flowmeter in a pulsating turbulent flow using wavelet analysis. *Meas. Sci. Technol.* **21**, 123001.
- LAURANTZON, F., SEGALINI, A., ÖRLÜ, R., TILLMARK, N. & ALFREDSON, P. H. 2012 Experimental analysis of turbocharger interaction with a pulsatile flow through time-resolved flow measurements upstream and downstream the turbine. *10th Int. Conf. on Turbochargers and Turbocharging (IMEchE), UK.*
- LAURANTZON, F., TILLMARK, N. & ALFREDSSON, P. H. 2010b A pulsating flow rig for analyzing turbocharger performance. *9th Int. Conf. on Turbochargers and Turbocharging (IMEchE)* pp. 363–372.
- MARELLI, S. & CAPOBIANCO, M. 2009 Measurement of instantaneous fluid-dynamic parameters in automotive turbocharging circuit. *SAE Tech. paper.*
- PISCAGLIA, F., ONORATI, A., MARELLI, S. & CAPOBIANCO, M. 2007 Unsteady behavior in turbocharger turbines: experimental analysis and numerical simulation. *SAE Tech. paper* pp. 1–13.
- RAFFEL, M., WILLERT, C., WERELEY, S. & KOMPENHANS, J. 2007 Particle image velocimetry. A practical guide. *Springer Verlag, 2nd ed.*
- RÜTTEN, F., SCHRÖDER, W. & MEINKE, M. 2005 Large-eddy simulation of low

frequency oscillations of the Dean vortices in turbulent pipe bend flows. *Phys. Fluids* **17**, 035107.

THOMSON, J. 1876 On the origin of windings of rivers in alluvial plains with remarks on the flow of water round bends in pipes. *Proc. Roy. Soc.* **25**, 5–8.

TIMITÉ, B., CASTELAIN, C. & PEERHOSSAINI, H. 2011 Mass transfer and mixing by pulsatile three-dimensional chaotic flow in alternating curved pipes. *Int. J. Heat Mass Transfer* **54**, 3933–3950.

Paper 5

POD analysis of stereoscopic PIV data from swirling turbulent flow through a pipe bend

By Athanasia Kalpakli

CCGEx & Linné Flow Centre, KTH Mechanics, SE-100 44 Stockholm, Sweden

Internal report

Coherent structures in turbulent swirling flow through a pipe bend are investigated experimentally by means of stereoscopic particle image velocimetry. In particular, the effect of the imposed swirling motion on the Dean vortices as well as the very-large-scale structures is examined for a wide range of swirl numbers. Proper orthogonal decomposition is employed to rank the spatial modes by energy content and extract the underlying secondary swirling motion as well as the large-scale structures present in the flow field. Moreover the original snapshots are reconstructed by using only a few of the most energetic modes and ease visualization of the structures by inhomogeneously filtering the flow fields. Phenomena such as the unsteady motion of the Dean vortices, the so called swirl switching, in the non-swirling turbulent flow case and the tilting of the very-large-scale structures in a highly swirling turbulent flow are captured and presented. The results presented here are preliminary and further analysis is planned in the future. Nevertheless, this work is believed to provide unique data as the first experimental study on swirling flows through a pipe bend which is not restricted to single-point measurements.

1. Introduction

Two types of body forces are of particular interest due to their occurrence both in nature and industry, namely the centrifugal and Coriolis forces which may result from curved geometries and rotating elements being present, for example in the atmosphere, cyclone separators, combustion chambers etc. The flow through bends is associated with the formation of counter rotating cells, the so-called *Dean vortices* (Dean 1927), created due to the imbalance between centrifugal effects and pressure while the additional presence of rotation can lead to perturbations of the vortices. Such a flow characterized both by streamline curvature and three dimensionality is considered to be complex. Commonly employed point-wise techniques for their study might be contaminated by the strong secondary motions. Moreover, measuring the three velocity components covering a whole pipe cross-section by means of single-point methods such as 3 D Laser Doppler Velocimetry (LDV) or multiple hot-wire probes, is both time consuming and limited to statistical quantities. It is therefore important

for the study of such flows, where both vortical structures and out-of-plane motion are predominant, to employ time-resolved whole-field measurements, e.g. by means of Time-resolved Stereoscopic Particle Image Velocimetry (TS-PIV), which can provide simultaneously the three dimensional velocity field across a pipe cross-section.

Turbulent flow through curved pipes has been studied mainly with focus on the behavior of the vortical structures which can be unsteady under turbulent flow conditions. Particularly the phenomenon which has been investigated the most, starting with the study by Tunstall & Harvey (1968), is the so-called “swirl switching” phenomenon describing an unsteady motion consisting of a single (dominating in strength) vortex oscillating in clockwise and counter-clockwise directions. A number of scientists have been intrigued to investigate the phenomenon and it has been illustrated both through PIV measurements (Brücker 1998; Sakakibara *et al.* 2010; Hellström *et al.* 2011b; Kalpakli *et al.* 2012) and computations, e.g. *Large-Eddy Simulations* (LES) or *Reynolds Averaged Navier Stokes* (RANS) (Rütten *et al.* 2005; Hellström 2010). The phenomenon has also recently attracted the interest of the community in the nuclear sector due to the fatigue that the unsteady motion of the vortices can cause in the piping of the cooling system of a nuclear reactor (i.e. “hot-leg” and “cold-leg” pipings) but also the increase in soundness that can be caused in the surrounded equipment by the unsteady secondary motion (Ono *et al.* 2010; Yuki *et al.* 2011; Takamura *et al.* 2011). Nevertheless, the mechanism which triggers such a motion is not fully understood yet. The pioneering study by Tunstall & Harvey explained it as a result of the asymmetry of the inner wall separation and the turbulent axial circulation generated in the upstream flow. However, the simulations by Rütten *et al.* (2005) performed in two different curved pipes, a sharp one where separation occurred and a smooth one, showed that the “swirl switching” can occur also in flow cases where separation is not present. In the aforementioned studies different ways of finding the frequency of this oscillating motion are pursued including spectral analysis of the time series of the in-plane velocity components (Brücker 1998; Rütten *et al.* 2005; Takamura *et al.* 2011) or spectral analysis of the POD (*Proper Orthogonal Decomposition*) coefficients (Sakakibara *et al.* 2010) and auto-correlation of the tangential velocity component at the centre of one of the vortices (Hellström *et al.* 2011b). The identification and reconstruction of the swirl switching through POD analysis will be applied on the present experimental data and the outcome will be discussed in the present study.

Swirling turbulent flow through straight pipes and its effect on turbulent quantities has been studied to some extent both experimentally (Imao *et al.* 1996; Facciolo *et al.* 2007) and numerically (Orlandi & Fatica 1997; Malin & Younis 1997). Here we separate for easiness the studies which generated swirling flows by axially rotating pipes (the method used in the present study) from the other techniques. A short description on the different methods to generate swirling motions can be found in Örlü (2009). Since different swirl generating methods result in substantially different flow fields (Facciolo *et al.* 2007), only the studies using the same swirl generating technique as the present one are mentioned here. It has been shown that turbulent fluctuations decrease with an increase in swirl rate while the flatness factor of radial velocity fluctuations increases due to a stabilizing effect (Imao *et al.* 1996). For the same experimental set up as the one used in the present study it was illustrated that the axial profile changes towards a parabolic shape while the azimuthal profile depicts

a close to parabolic shape independent of Reynolds number when rotation is applied (Facciolo 2006).

Among the works that have been conducted on the interaction between the Dean vortices and the swirling motion most relevant to the case studied here (both flow- and set up-wise), are the experimental study by Anwer & So (1993) and the computational study by Pruvost *et al.* (2004). In Anwer & So (1993) the turbulent swirling flow for different angles along a 180° pipe bend and for one swirl intensity was measured by means of single-point measurement techniques. The results were used later on by Pruvost *et al.* in order to validate the models used by the simulations at the same swirl number. In that study different swirl intensities were applied both in a 90° and 180° bend and it was shown that as the swirl intensity increases a complex interaction between the secondary motions exists with the tendency of the counter-rotating vortices to merge and fully diminish at even higher swirl rates.

The aim of the present study is to examine experimentally the combined effect of centrifugal forces in a fully developed turbulent pipe flow and for increasing swirl intensities including the case where the motion is swirl dominated. In order to fully assess the characteristics of the flow and visualize as well as quantify the vortical patterns in a three dimensional flow field, TS-PIV measurements have been performed and results are presented here.

The paper is organised as follows: § 2 provides the details of the pipe flow facility and the PIV system. § 3 introduces the notation for the employed snapshot POD, while § 4 and § 5 present and discuss the results from the non-swirling and swirling flow at the exit of a 90° pipe bend, respectively. The work is summarized and concluded in § 6.

2. Experimental set up & techniques

2.1. The rotating pipe facility

The measurements for the current study were conducted at the *rotating pipe facility* located at the *Fluid Physics Laboratory* at *KTH Mechanics*. The air is provided by a centrifugal fan and the mass flow rate can be controlled by means of a butterfly valve monitored through the pressure drop across an orifice plate. A distribution chamber is implemented in order to minimize the vibrations created by the fan while a honeycomb installed inside a stagnation chamber, where the air is fed into, distributes the air evenly. The air is first led into a one meter long stationary section which is connected to the rotating pipe, which has at its entrance a 12 cm long honeycomb and brings the flow into more or less solid body rotation. The circular pipe can rotate to speeds up to 2000 rpm by means of DC motor which is connected to the pipe through a belt (figure 1). The total length of the pipe section is $100 D$ where D denotes the inner diameter of the pipe, equal to 60 mm (c.f. Facciolo (2006) and Örlü (2009) for further details). In Sattarzadeh (2011) the mean velocity profiles for different swirl intensities at a Reynolds number based on the pipe diameter of $Re_D = 24000$ at the exit of the pipe are documented and it is shown that the profile for the non-swirling case, adheres to what is known for fully-developed turbulent flow while as the swirl number increases the profile shape approaches that of the laminar pipe flow, i.e. becomes more parabolic. This constitutes also the inflow condition for the flow which is fed into the bent pipe (figure 2). Note that while the straight pipe is rotating, the

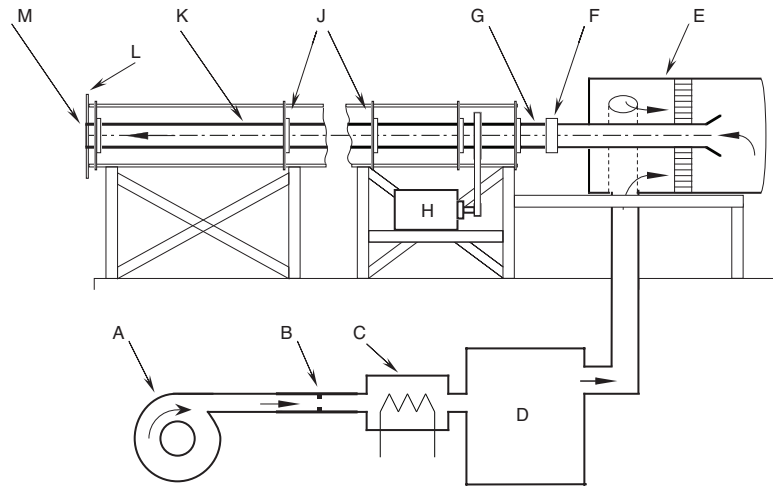


FIGURE 1. Schematic of the experimental set up. **A)** Centrifugal fan, **B)** flow meter, **C)** electrical heater, **D)** distribution chamber, **E)** stagnation chamber, **F)** coupling between stationary and rotating pipe, **G)** honeycomb, **H)** DC motor, **J)** ball bearings, **K)** rotating pipe, **L)** circular end plate, **M)** pipe outlet to which the pipe bend (figure 2) has been mounted.



FIGURE 2. *a)* Pipe bend that was mounted at the exit of the $100 D$ long straight pipe. *b)* Dimensional details of the pipe bend.

bend is remaining still. The curved pipe has an inner diameter of $D = 60.3$ mm (with a small junction to the straight pipe to avoid flow disturbances) and curvature radius of $R_c = 95.3$ mm, giving a curvature ratio R/R_c of 0.31. The length of the straight section after the 90° curvature is $0.67 D$.

With the present experimental set up the mean velocity both in axial and tangential direction are well defined by rotating the whole pipe, therefore the *integral*

TABLE 1. Parameter range for the experiments.

$Re \times 10^3$	$De \times 10^3$	S
14	8	0.85, 1.2
24	13	0, 0.1, 0.3, 0.5
34	19	0

swirl number (Gupta *et al.* 1985) which is defined as the ratio of axial flux of swirl momentum to the axial flux of axial momentum:

$$S_{int} = \frac{\int_0^R \int_0^{2\pi} W U_\theta r^2 dr d\theta}{R \int_0^R \int_0^{2\pi} W^2 r dr d\theta}, \quad (1)$$

can be interchanged with the *Swirl number*:

$$S = \frac{U_w}{W_b}, \quad (2)$$

where W and U_θ are the mean axial and circumferential velocity components, r and θ the radial and angular coordinates respectively, U_w the angular speed of the pipe wall and W_b the bulk speed. This is a convenient way to define the swirl number since the wall velocity can be directly obtained by the rotational speed of the pipe which is monitored in the present experimental apparatus. The swirl numbers investigated in the present study are listed in table 1. The parameter marked as De denotes the *Dean number* which is defined as:

$$De = \frac{\rho W_b D}{\mu} \sqrt{\frac{R}{R_c}}, \quad (3)$$

where ρ denotes density and μ the dynamic viscosity of the fluid medium (air). From equation (3) it is obvious that the Dean number is a composition of the *Reynolds number*, $Re = \rho W_b D / \mu$ and the curvature ratio. It should be noted here that the curvature ratio has been the same for all the cases which will be presented here, therefore Reynolds number effects are examined. Also, in order to avoid confusion it should be stated at this point that results from $Re = 34 \times 10^3$ are presented only in § 4 while for the rest sections where results from swirling flow are presented, the pairs of Reynolds-swirl numbers as listed in the above table have been used.

2.2. Measurement technique and post-processing of the data

The experimental technique employed in order to acquire the entire flow field at a pipe cross-section is Time-resolved Stereoscopic Particle Image Velocimetry. A schematic of the experimental configuration along with the cameras and laser light sheet aligned at the immediate vicinity of the pipe bend exit (approximately 0.5 mm downstream the pipe exit) is shown in figure 3.

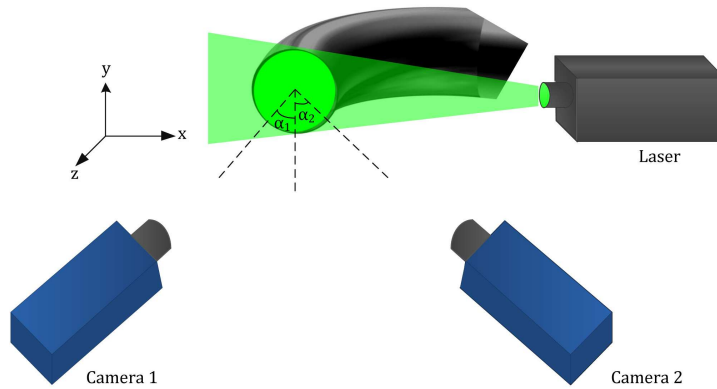


FIGURE 3. TS-PIV set up with the cameras and the laser light sheet aligned at the exit of the curved pipe and the coordinate system used with z being the streamwise, x the horizontal and y the vertical directions corresponding to W , U and V velocity components, respectively. The angles in between the viewing axes of the cameras, α_1 and α_2 were 45° each.

Two high-speed C-MOS cameras (Fastcam APX RS, Photron, 3000 fps at 1024×1024 pixels) were positioned at an angle of approximately 90° and at forward-backward scatter mode and 105 mm Nikon Nikkor lenses were adjusted using a Scheimpflug adapter (Prasad & Jensen 1995). A laser light sheet of approximately 1 mm thickness was produced by a Nd-YLF laser (Pegasus, 10 kHz maximum frequency, New Wave Research) and a water-based solution (Jem Pro Smoke Super ZR-Mix) was atomized using a high volume liquid seeding generator (10F03 Seeding Generator, DANTEC). For the *in-situ* calibration of the cameras, images were taken of a two-level calibration plate and the pinhole model (Willert 2006) was used in order to fit the dewarping mapping function to the marks found in each image, with the commercial software *DaVis 7.2* from *LaVision GmbH*. A self-calibration procedure has also been applied to eliminate errors from misalignment of the laser light sheet with the calibration target (Wieneke 2005).

The raw images from the measurements had a resolution of 1024×1024 px at 10-bit while the field of view (FOV) was equal to $80 \times 80 \text{ mm}^2$ in physical space. $N_s = 3000$ images were acquired for the non-swirling cases at $Re = 14$ and 34×10^3 and 1000 images for the rest of the cases at a sampling frequency, f_s , of 1 kHz. It should be underlined here that the aim of the present study is the characterization

and identification of large scale structures under the effect of different flow conditions and it is believed that the sampling conditions under which the data were acquired are sufficient to resolve those in time. Nevertheless the definition of time-resolved data usually calls for time-resolving the smallest turbulent scales which is not the case here (Sattarzadeh 2011). Within the context of the present paper time-resolved implies that the most energetic structures are resolved in time and this should be kept in mind while interpreting the results.

The post-processing of the PIV data was performed using DaVis 7.2 (LaVision GmbH). The vector fields were calculated through a multi-pass correlation iteration procedure in order to increase resolution, starting with a 64×64 px interrogation window and decreasing to 16×16 px interrogation (which sets also the lower limit for the spatial resolution) window with 50 % area overlapping. The percentage of accepted vectors was more than 95 %. In all the cases a median test (Westerweel 1994) has been used to detect outliers and replaced by a linear interpolation of the neighboring vectors.

3. Proper Orthogonal Decomposition (POD)

Proper Orthogonal Decomposition is a technique for analyzing multi-dimensional data and is mostly known in fluid dynamics as a method to “extract” modes, sorted by energy content which are believed to be the structures that contribute mostly to the total energy of the flow. The principal of POD lies on finding an optimal—in a least squares sense—representation of a stochastic process as an infinite linear combination of orthogonal functions. Due to its strong relation (and resemblance) to other statistical methods (Karhunen-Loève theorem, singular-value decomposition as two examples) it can be considered that POD has been known for quite a long time but it was only in the late 60’s that it was introduced for the study of turbulent flow signals (Lumley 1971). In fluid dynamics it has been applied greatly after the development of whole-field measurement techniques (e.g. PIV) which provide three-dimensional data for the identification and visualization of coherent structures (Graftieux *et al.* 2001; Gurka *et al.* 2006; Hellström *et al.* 2011a) which were obtainable before only numerically.

In the present study *snapshot* POD has been used which was first introduced in Sirovich (1987). The procedure followed for the analysis of the current PIV data is similar to the one described in Meyer *et al.* (2007) and it is as follows:

Considering an ensemble of velocity fields: $\{\mathbf{u}_1, \mathbf{u}_2, \dots, \mathbf{u}_N\}$ where \mathbf{u}_N the n -th snapshot (or instantaneous flow field captured with the PIV camera) and by reorganizing all velocity components (without subtracting the mean) for each snapshot in a column of a matrix as:

$$\mathbf{U} = \begin{bmatrix} u_1^1 & u_1^2 & \dots & u_1^N \\ \vdots & \vdots & \vdots & \vdots \\ u_M^1 & u_M^2 & \dots & u_M^N \\ v_1^1 & v_1^2 & \dots & v_1^N \\ \vdots & \vdots & \vdots & \vdots \\ v_M^1 & v_M^2 & \dots & v_M^N \\ w_1^1 & w_1^2 & \dots & w_1^N \\ \vdots & \vdots & \vdots & \vdots \\ w_M^1 & w_M^2 & \dots & w_M^N \end{bmatrix}, \quad (4)$$

where u , v and w denote the velocity components at the x -, y - and z -direction, respectively as defined in figure 3.

Thereafter the covariance matrix $\mathbf{U}^T \mathbf{U}$ is created and the eigenvalue problem is considered:

$$\mathbf{U}^T \mathbf{U} A^i = \lambda^i A^i, \quad (5)$$

where λ the eigenvalues which are real and positive and are related to the energy content of the flow and are sorted in a descending order: $\lambda^1 > \lambda^2 \dots > \lambda^N$. Hence, the first modes are the most important in terms of energy content (with the first mode representing the mean field and referred to as the 0-mode) and are most likely those corresponding to the large scale structures in the flow field. The eigenvectors A are also real valued and can be used to construct the POD modes, ϕ :

$$\phi_i = \frac{\sum_{n=1}^N A_i^n u^n}{\left\| \sum_{n=1}^N A_i^n u^n \right\|}. \quad (6)$$

It is also possible to recover the temporal information of the modes (*chronomodes* or POD coefficients) by projecting the snapshots on the obtained basis. These can later be used in order to reconstruct a snapshot n as:

$$u^n = \sum_{i=1}^N \alpha_i^n \phi^i, \quad (7)$$

where α^n the POD coefficients obtained.

The importance of testing the autocovariance matrix for convergence in order to obtain physically meaningful modes was addressed in Semeraro (2011) pointing out that the modes extracted are the optimal representation of a stochastic process but are not necessarily a true representation of it. Therefore the selection of the number

of snapshots and time interval between them is very important in POD analysis in order to guarantee enough independent samples for converged statistics. Semeraro (2011) showed that while the spatial modes i.e. *topo-modes* are not very sensitive to the selection of the time interval between the snapshots Δt_s , the chrono-modes are greatly influenced. Therefore, a convergence test has been proposed concluding that the criteria of statistical convergence of the autocovariance matrix $\mathbf{U}^T \mathbf{U}$ are sufficient to guarantee convergence of the modes. For the selection of the number of snapshots and the time resolution in the current study the guidelines proposed in Semeraro (2011) and Meyer *et al.* (2007) have been followed. For details the reader is referred to § 4.3.

4. Non-swirling flow

4.1. Validation of measurement tactic

As mentioned in § 2.2, the images were acquired at the immediate vicinity of the pipe bend exit, i.e. approximately 0.5 mm downstream the exit of the pipe. This was preferred to be the measurement procedure due to the difficulties imposed from performing stereo-PIV measurements in air flows through optical distortions and in order to avoid reducing the accessible cross-sectional area due to reflections from the pipe walls. Nevertheless, the flow in focus is deemed representative of the flow within the pipe, therefore a comparison between hot-wire data obtained at the same

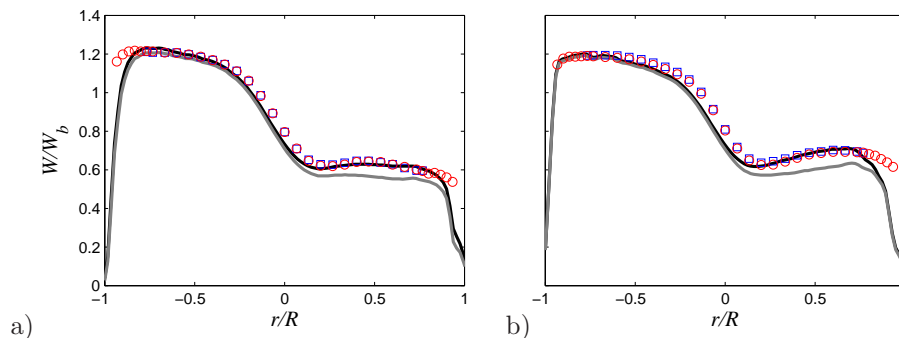


FIGURE 4. Comparison of mean streamwise velocity component along the horizontal plane from the present PIV experiments under no-swirl flow conditions with hot-wire data obtained in the same facility and under the same flow conditions and parameters. *a)* $De = 8 \times 10^3$ and *b)* $De = 19 \times 10^3$. Black lines denote the effective cooling velocity calculated from the PIV data, grey lines the PIV data, blue square (\square) the hot-wire data acquired at $z/D = 0.67$ and red square (\square) the hot-wire data acquired at $z/D = 0.67$ but with a $1.5 D$ extension mounted downstream the measurement plane. The hot-wire data are from Sattarzadeh (2011).

experimental facility and with the exact same geometrical and flow parameters as the current PIV data was performed in order to assess measurement discrepancies due to this choice of measurement tactic.

Figure 4 shows the mean velocity profile of the streamwise velocity component along the horizontal axis obtained by means of hot-wire anemometry (Sattarzadeh 2011) plotted together with the PIV data acquired within the context of the present work. In order to consider for errors on the (single) hot-wire readings due to the strong in-plane motion, the PIV data have also been plotted by calculating the effective cooling velocity ($W_{eff} = \sqrt{W^2 + U^2}$), which is the velocity that the hot-wire senses¹. Two sets of data have been taken by Sattarzadeh (2011): one set acquired with the hot-wire placed at the exit of the $z/D = 0.67$ extension pipe, downstream the bend and a second set acquired with the hot-wire placed at $z/D = 0.67$ but having a straight pipe section equal to $1.5D$ length downstream the measurement plane.

The results from the hot-wire/PIV comparison agree satisfactorily well which confirms that the measurement tactic followed gives results which resemble very closely data taken within a pipe.

4.2. Velocity fields & streamwise vorticity maps

In the present section both instantaneous and time-averaged velocity and vorticity fields will be presented for Dean numbers of $De = 8 \times 10^3$ and 19×10^3 in order to introduce the reader to the flow field which will be considered in the coming sections for further analysis and discuss Reynolds number effects, at least for the ranges considered here.

Figure 5 shows the time-averaged velocity field for the two Dean numbers considered here, with the streamwise velocity component plotted as the background contour map and the secondary motion, i.e. in-plane, as the streamlines. The outer pipe wall is to the left and the inner is to the right of the figure, as seen by the PIV cameras.

In both cases, the formed flow field bears the characteristics of flows through pipe bends. In such a geometrical configuration, i.e. curved pipe, the high velocity fluid is greatly affected by centrifugal forces and is pushed towards the outer wall of the pipe while the slower moving fluid is deflected towards the opposite side creating a C-shaped flow field. This behavior results in the formation of the Dean vortices, as seen also in figure 5. The highest in-plane velocity component here is 0.3 times the bulk velocity. For the considered Reynolds numbers ($Re = 14$ and 34×10^3) no significant influence on the mean field, regarding also the shape of the vortical structures, can be observed.

Considering the mean streamwise vorticity maps and the field of the magnitude of the in-plane components for the two cases in figures 6 and 7, respectively it can be seen that there is a slight effect on the strength of the secondary motion with the higher Reynolds number case depicting higher vorticity levels and magnitudes of the in-plane velocities. Nevertheless, the differences between the two cases remain small and therefore in the following sections only the case of the higher Reynolds number

¹The single hot wire probe was mounted vertically and traversed horizontally, therefore the velocity component it senses besides the streamwise velocity, W , is predominantly the horizontal i.e. U component.

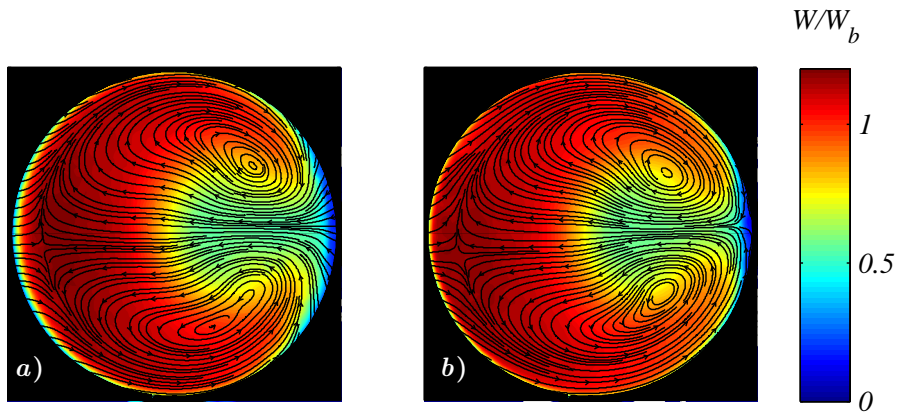


FIGURE 5. Time-averaged velocity field across a pipe cross-section for *a*) $De = 8 \times 10^3$ and *b*) $De = 1.9 \times 10^4$. The background contour map denotes the streamwise velocity component distribution scaled by the bulk speed and the in-plane components (largest mean value $0.3 \times W_b$) are shown as the streamlines.

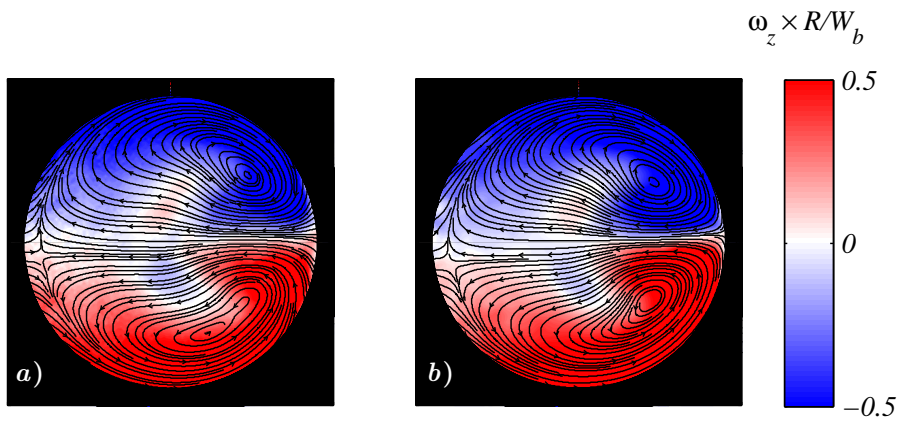


FIGURE 6. Mean streamwise vorticity maps for *a*) $De = 8 \times 10^3$ and *b*) $De = 19 \times 10^3$. The vorticity has been scaled here with W_b/R to ease comparison between the two cases.

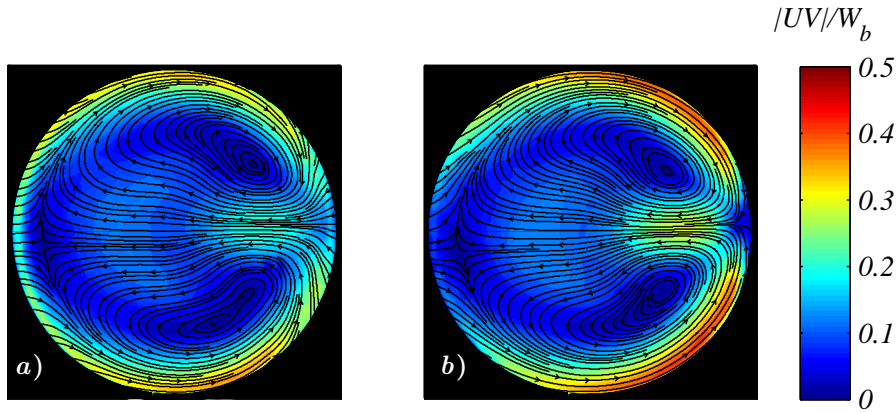


FIGURE 7. Time-averaged velocity field across pipe cross-section for *a)* $De = 8 \times 10^3$ and *b)* $De = 19 \times 10^3$. The magnitude of the in-plane components scaled by the bulk speed ($\sqrt{U^2 + V^2}/W_b$) is shown as the background contour map while the secondary motion is shown with the streamlines.

($Re = 34 \times 10^3$ corresponding to $De = 19 \times 10^3$) will be considered for further analysis in § 4.3.

4.3. Dean vortices in turbulent flow

In the following section the unsteady behavior of the Dean vortices that has been illustrated also in a previous study by the present author (Kalpakli *et al.* 2012) will be discussed. Figure 8 shows the instantaneous vector field of the in-plane components and three states between which the vortices alter can be observed: a symmetrical one (*middle subfigure*) where two vortices resembling highly the ones seen in the time-averaged field (figure 5) are shaped and two where one of the vortices dominates the cross-section and rotates in reference to the plane of symmetry either to the clockwise or counter-clockwise direction.

This unsteady motion matches the description of what is known in the literature as “swirl switching”, even though here the dominance of one of the vortices is more predominant as, for example, in Brücker (1998) and Sakakibara *et al.* (2010) and is more similar to what is seen in Ono *et al.* (2010). Nevertheless the exact shape the vortices take, their highly unsteady behavior under turbulent flow conditions is of great importance due to the fatigue their oscillatory motion can cause in the piping systems. Therefore the further study of how and under which conditions their unsteady motion initiates is crucial.

In the first study on the “swirl switching” (Tunstall & Harvey 1968) it was concluded that the necessary conditions for the switching of the vortices to happen was that the pipe should be circular and sharp and the flow turbulent. In the experimental

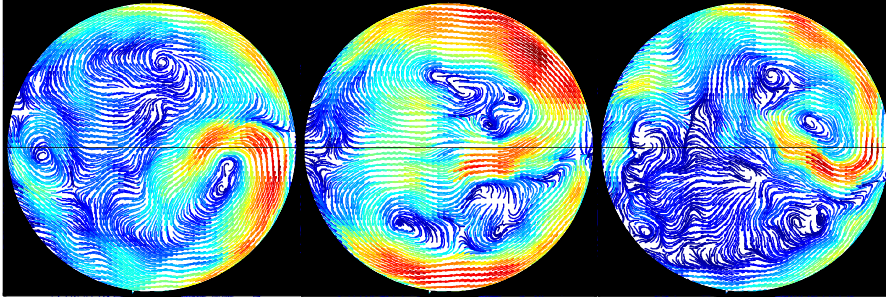


FIGURE 8. Snapshots of the in-plane vector field at three independent time instances. The small-scale fluctuations have been suppressed through a moving average of $\delta t = 2$ ms in time and a spatial low-pass filter. The instantaneous snapshots reveal three states between which the two Dean vortices are switching. The highest in-plane velocity ($0.3 \times W_b$) is denoted with red vectors and the lowest with blue vectors.

studies which were conducted thereafter mostly sharp pipe bends were used with $R_c/D = 1$ (Brücker 1998; Ono *et al.* 2010) or $R_c/D = 1.5$ (Sakakibara *et al.* 2010) while in the present study the ratio of the radius of the center line of the bend to the pipe diameter was 1.6 (see figure 2). The Reynolds number in all cases was high enough to ensure turbulence. In the simulations by Rütten *et al.* (2005) the additional case of $R_c/D = 3$ was considered and it was shown that even when the pipe bend is not sharp, the behavior of the vortices is still unsteady. Therefore, the conclusive remarks by Tunstall & Harvey (1968) are still open for discussion.

As a first approach that has been used in literature in order to explore and understand the behavior of the vortices was to find out at which frequency the two vortices oscillate. Different techniques have been applied for that with the most obvious one i.e. spectral analysis of the time series of the in-plane components as e.g. done by Brücker (1998). In the present study where the time resolution is not considered to be enough (also due to the hardware limitations of the PIV (Agrawal 2005)) to provide fully resolved PSD (note here that the fluid medium was air while most of the aforementioned studies on turbulent flows through pipe bends have been conducted in water), therefore a post processing of the data was necessary in order to suppress high frequency fluctuations and noise and detect periodicities in the flow structures. POD has been chosen to be tested as a possible way to obtain more detailed information on the unsteady behavior of the Dean vortices, constituting the most energetic structures in the flow. It is expected that the snapshot-based POD which has been used here, will capture the large scale structures, as the most energetic features in the flow field and they will be represented satisfactorily using only a few of the first POD modes (Meyer *et al.* 2007).

A total number of $N_s = 3000$ snapshots acquired with a sampling frequency of 1 kHz was available for the present analysis and following, as a first test, the example

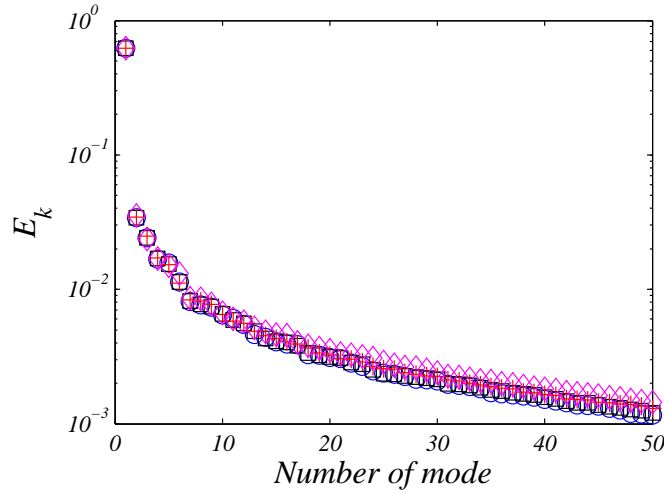


FIGURE 9. Eigenvalue spectrum for four data sets and for the first 50 modes: $\Delta t_s = 1/1000$ (\circ), $\Delta t_s = 1/500$ (\square), $\Delta t_s = 1/250$ ($+$) and $\Delta t_s = 1/125$ (\diamond).

by Meyer *et al.* (2007) different numbers of snapshots $\{3000, 1000, 500\}$ were tested which gave qualitatively the same results but for the least number of snapshots tested, the structures appeared slightly asymmetrical in comparison to the other two cases, therefore the sampling time in that case was deemed insufficient to obtain converged statistics. Additionally a convergence test as proposed in Semeraro (2011) for different Δt_s of $\{1/1000, 1/500, 1/250, 1/125\}$ corresponding to the total number snapshots of: $\{3000, 1500, 750, 375\}$ respectively for a total sampling time of $T_s = 3$ sec has been performed. The eigenvalue spectrum for the first 5 decades of modes is shown in figure 9 and it can be seen that for the first three pairs of Δt_s - N_s , the agreement is good while for $\Delta t_s = 1/125$, the eigenvalue cascade starts to diverge. Taking into consideration all the aforementioned observations the following POD analysis was decided to be performed for $\Delta t_s = 1/500$ s and $N_s = 1500$ which corresponds to a sampling frequency of 500 Hz.

Regarding the spatial modes the 0-mode provides the mean field as expected and since the structures in focus, i.e. the Dean vortices are already included in the mean field no further discussion on the spatial modes will be made. The interesting possibility that POD analysis offers here is that by using just the first few of the extracted topo-modes, the flow field can be reconstructed. Due to the ranking of the modes by energy content the more dominant and interesting features of the flow field will therefore appear. Consequently POD acts as an inhomogeneous filter which helps to visualize the large scale structures and it is expected in that case to serve as a tool for the identification of the vortices' motion.

Figure 10 shows the reconstructed field by using only the first six modes. The selection of the number of the modes for the reconstruction has been done by first

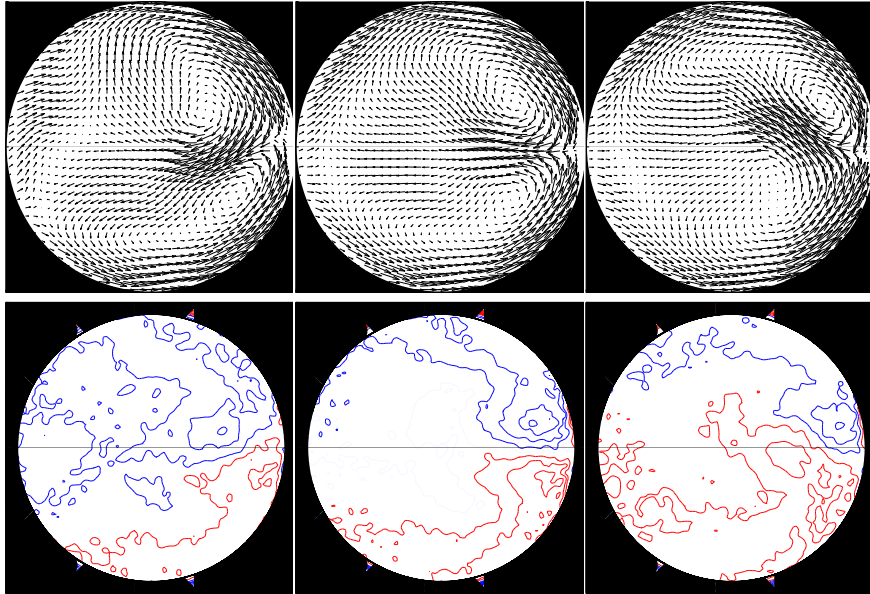


FIGURE 10. Vector field and streamwise vorticity maps reconstructed from the first six POD modes. The vorticity maps are shown as contour lines with red color indicating positive and blue color negative values, respectively.

setting a threshold range of energy amount captured e.g. 60-70% by the total number of modes considered for the reconstruction. Additionally, an iterative test was performed by observing the changes in the flow fields and how well the original snapshots are represented by increasing the number of modes. Six modes, capturing about 70% of the total energy, were deemed to be sufficient in order to approximate satisfactorily the large scale structures without adding noise and fluctuations into the flow field.

The unsteady motion of the vortices is clearly depicted interchanging between the three states as mentioned before for the instantaneous snapshots (figure 8). Here only the in-plane components are shown to emphasize the focal point of this section, i.e. the motion of the vortices. Additionally streamwise vorticity maps support the aforementioned behavior of the vortical structures. For the vorticity plots the filtered data the POD provides, deem particularly useful since the vorticity is quite sensitive to fluctuations and noise.

In order to detect the frequency of the swirl switching, the flow field has been monitored in time in order to see at which point the two vortices switch position. Figure 11) shows the region (marked in a rectangular box) of two reconstructed snapshots which was considered for the spectral analysis. In that region the vectors can be seen to change direction in time and they have been observed to continue like this in a periodic manner. PSD of the circumferential velocity component was calculated at different points in that region giving the same quantitative results and

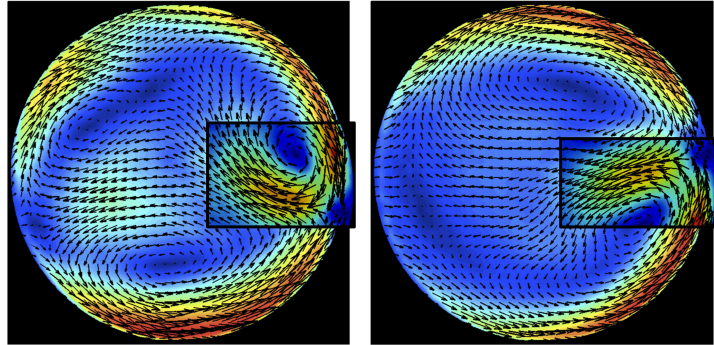


FIGURE 11. Reconstructed velocity field at two instants showing the magnitude of the in-plane components as contour map and their direction as vectors. The region where the PSD of figure 12 was calculated is marked with a rectangular box. Comparing the two figures and the area-in-focus a change in the direction of the vectors can be observed which is believed to be related to the swirl switching mechanism.

the outcome for one point ($x = 0.1R, y = 0.2R$) is shown in figure 12d along with the corresponding time series (12c). The spectra was computed from an average of the spectra of 10 subsets of the whole data sequence in order to reduce the random error whereas the data were smoothed by means of a moving average of degree 5. In order to highlight and appreciate the possibilities that the POD offers, the time series and the corresponding spectra of the original snapshots have been plotted in figure 12a and 12b for the same point as for the reconstructed flow fields. A comparison between the figures is revealing, showing a scattered spectra in the case of the original time series, from which it is hard to draw any conclusions for a dominating frequency. POD smooths out the high frequency fluctuations in the time series and which appear as “noisy peaks” in the spectra.

The signal of the reconstructed time series depicts a periodical behavior with large fluctuations of the tangential velocity. The signal has been additionally filtered in order to highlight the periodic motion and the low frequency variations (shown with blue in figure 12c). A dominant peak at a Strouhal number of around 0.1 as well as two at lower ($St \approx 0.03$) and higher frequencies ($St \approx 0.18$) can be observed in the corresponding spectra. The Strouhal number is defined as: $St = f \times D/W_b$ based on the diameter of the pipe and the bulk speed. The low Strouhal number peak can be considered as an indication of the low frequency variation of the velocity (shown with blue) while the higher Strouhal numbers indicate the imposed high frequency fluctuations on the low frequency variations.

In Semeraro (2011) it was shown that characteristic frequencies in the flow field are depicted in the spectral of the temporal modes as in the spectra of the original time-series whereas the high-energy modes can be associated to high periodicity and

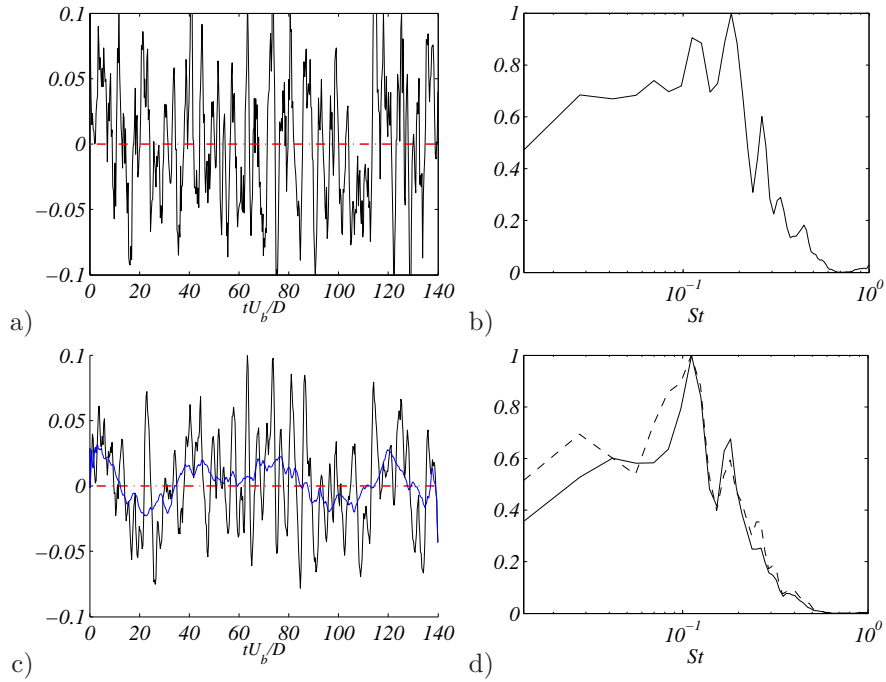


FIGURE 12. a) Time series of the circumferential velocity component at $x = 0.1R, y = 0.2R$ of the original signal. b) Power spectrum of the signal shown to the left. c) Time series of the circumferential velocity component at $x = 0.1R, y = 0.2R$, reconstructed using the first six POD modes. The signal has been filtered additionally and it is shown with blue color in order to highlight the low frequency variation at $St \approx 0.03$ d) Power spectrum of the reconstructed signal shown to the left (—) and the first POD coefficient (---). The power spectra have been scaled to their maximum values.

periodic coherent structures. The spectral analysis of the POD coefficients has been adopted previously by Sakakibara *et al.* (2010) for the determination of the swirl switching frequency. Here, to additionally examine and support the aforementioned observations on the swirl switching frequency and exploit the possibilities that POD offers, the spectra of the first POD coefficient has been calculated and plotted together with the spectra from the reconstructed time series in figure 12b.

The spectra of the first chrono-mode not only agrees well with the spectra of the time-series but depicts additionally more clearly the low-frequency peak at Strouhal number of about 0.03. The spectra of the third and fourth POD coefficients have also been computed (not shown here) and for the second mode peaks at the same Strouhal numbers are depicted but have a larger amplitude whereas the spectra of the

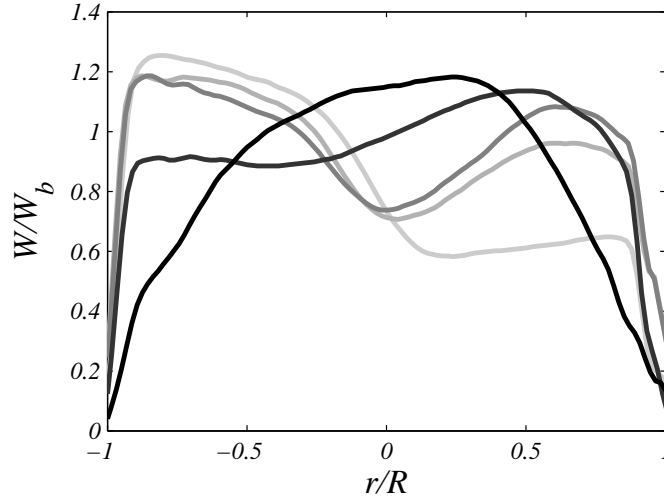


FIGURE 13. Mean streamwise velocity profiles across the horizontal axis for: $S = 0, 0.3, 0.5, 0.85$ and 1.2 . Increasing color intensity denotes increasing swirl number.

rest of the modes become scattered with the peaks becoming wider and with lower amplitudes. This has been shown also in Sakakibara *et al.* (2010) and it is explained due to the fact that the swirl switching is expected to be one of the most energetic features in the flow field, therefore it should be indicated in the first modes (both in the spatial and temporal domain).

5. Swirling flow

5.1. Visualizing the vortical structures

In the present study the main focus is the investigation of the interaction between the Dean vortices and a superposed swirling motion on the primary flow by axially rotating a long pipe connected to the pipe bend. Previous studies (Anwer & So 1993; Pruvost *et al.* 2004; Sattarzadeh 2011) have shown that by increasing the swirl intensity the centrifugal effects of the bend decrease and the symmetrical roll cells tend to merge until full axi-symmetry is achieved at a sufficiently high swirl number, S . The experimental studies which have been conducted so far in swirling flows through bends (Shimizu & Sugino 1980; Anwer & So 1993; So & Anwer 1993; Sattarzadeh 2011) are limited to point-wise techniques (pitot-tubes, hot-wires) which provide long-time series and are therefore very useful for statistical analysis of the flow but are limited to that.

Here, by means of TS-PIV, we provide both quantitatively and qualitatively the flow field at a pipe cross-section under the influence of centrifugal and Coriolis forces and for different swirl intensities. The swirl numbers (see equation (2)) studied with the present experimental set up are $S = 0, 0.1, 0.3, 0.5, 0.85$ and 1.2 with the

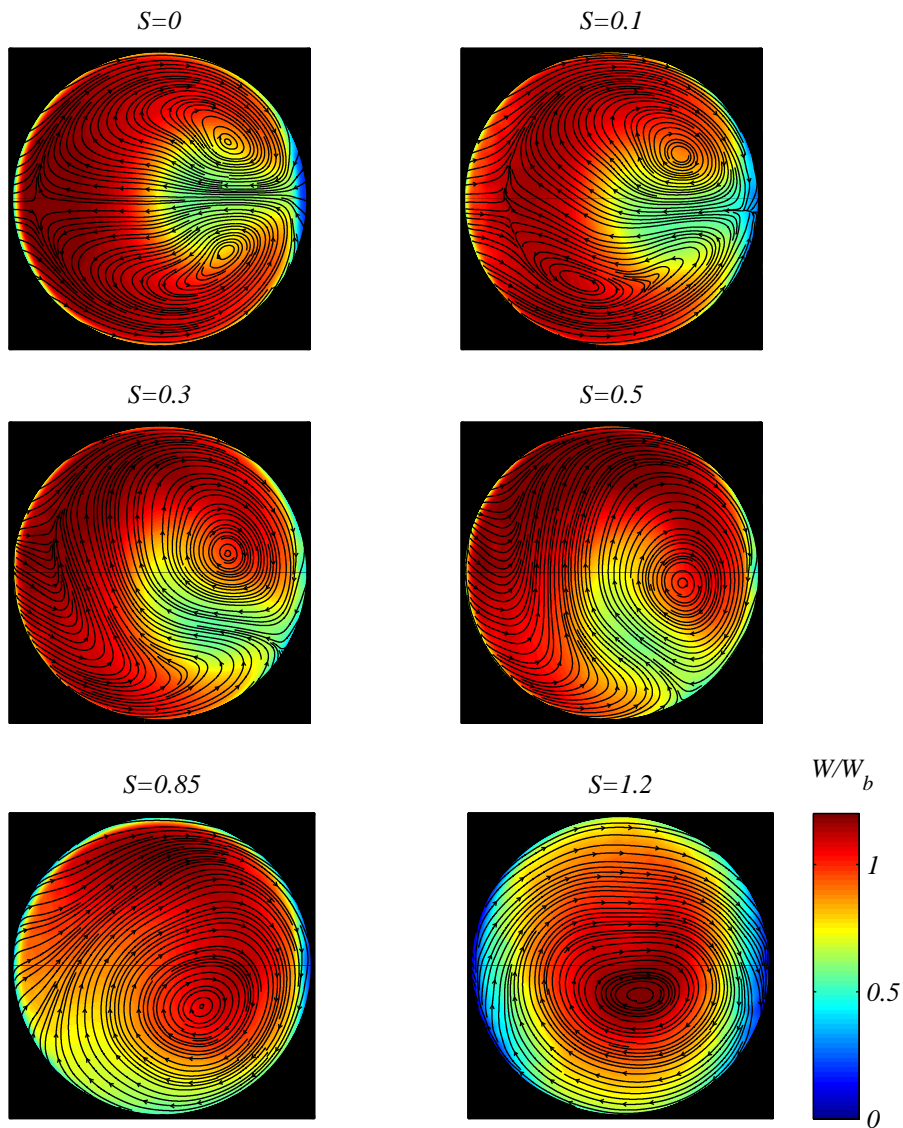


FIGURE 14. Mean velocity fields for different swirl numbers: $S = 0, 0.1, 0.3, 0.5, 0.85$ and 1.2 (swirl dominated motion). Streamwise velocity component scaled by the bulk speed is shown as the background contour map while the secondary motion is plotted as the streamlines.

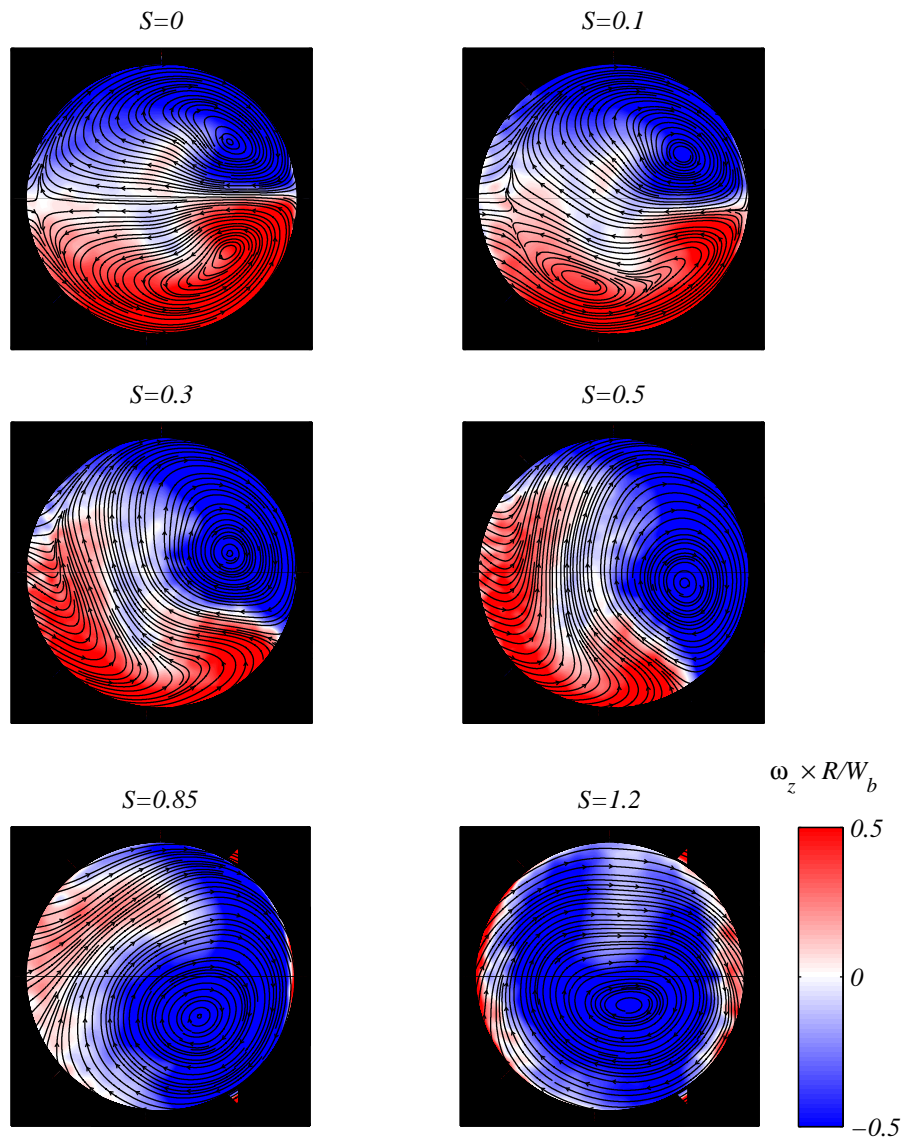


FIGURE 15. Mean streamwise vorticity maps scaled by R/W_b corresponding to the velocity fields shown in the previous figure. Secondary motion is shown as the streamlines for clarity.

latter one denoting swirl dominated motion. Figure 13 shows the profiles of the streamwise velocity across the horizontal plane while figure 14 shows the flow field for the aforementioned swirl numbers starting from the non-swirling case with the streamwise component shown as the background contour map scaled by the bulk speed and the secondary motion as streamlines. The results here show a behavior which is probably not unexpected but for the first time -to the author's knowledge- visualized and quantitatively assessed simultaneously through experiments. A description of the flow evolution as a function of the swirl number can be given as follows: for the non-swirling case the two well-known symmetrical Dean vortices occupying the upper and lower side of the pipe are shaped. With even a slight increase in swirl intensity ($S = 0.1$), a perturbation of the symmetry of the vortices can clearly be observed. The vortices move towards the center due to the solid-body-kind motion that is being applied on the flow, though one of the vortices (the lower one) seems to be more sensitive in the swirl effect, probably due to the direction of the swirl motion which is applied in the clockwise direction (which is the angular direction at which the $100 D$ pipe upstream the bend was rotating). As the swirl intensity increases further to $S = 0.5$ the vortices continue to change location and the flow starts to take a more stabilized and structured form even though two structures can still be seen until a swirl number of $S = 0.85$ where only one structure remains closer to the center of the pipe and moves to the center at $S = 1.2$ resulting in a well-structured and symmetric flow field with the bottom vortex being completely vanished. The dominance of a vortex across the pipe cross section rotating at one direction (clockwise) can be seen also in the mean streamwise vorticity maps in figure 15 with the vorticity level also slightly decreasing with increase of swirl number.

The above description matches well what has been predicted in the simulations by Pruvost *et al.* (2004) even though there exist differences between the two studies regarding the set up and flow parameters and no direct comparison can be made but the general trend of the vortices' behavior under swirl motion seems to be similar and show how the centrifugal and pressure gradient effects from the presence of the bend are modified when a swirling motion is applied on the flow. In that study a "swirl intensity drop criterion" was introduced (as the ratio of the difference between the swirl number at the bend outlet and the swirl number at the inlet to the swirl number at the outlet) and comparisons with a straight pipe were made, to further support his observations on the decrease of centrifugal effects with increase in swirl number and the dominance of swirl motion at some swirl rate.

The question though of whether coherent structures, similar to the Dean vortices in the non-swirling flow, are lying under the large-scale swirl still remains. Here, an effort to answer this question is being made by decomposing the flow field by means of POD introduced in § 3.

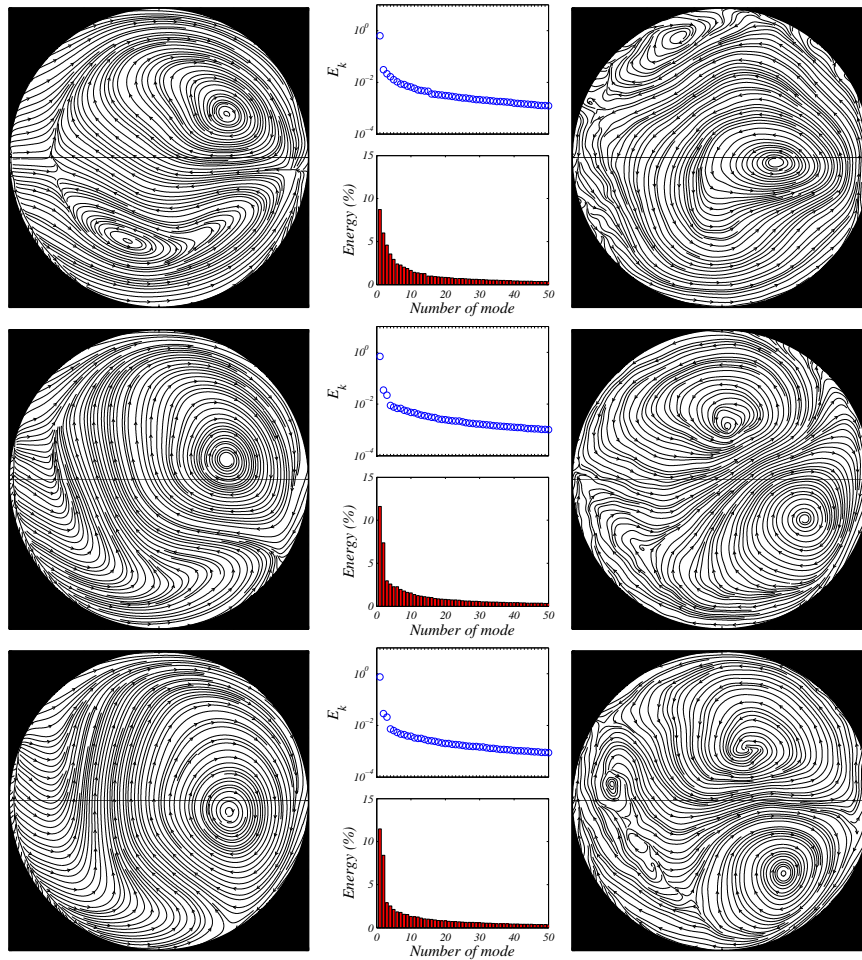


FIGURE 16. The first two POD modes for the: $S = 0.1, 0.3, 0.5$ swirl flow cases from top to bottom with the secondary motion shown as streamlines. The subplots in the middle of each mode show the eigenvalues (*top*) and the relative energy excluding the 0-mode (*bottom*) of the first 50 modes.

5.2. Decomposition of the swirling flow field

In this section results from POD analysis on a turbulent swirling pipe flow will be presented and discussed. The aim is to check whether the Dean vortices merely lay under the imposed swirling motion or if the Coriolis force is so large as to completely diminish any other existing structure. Dealing with large scale structures, with the

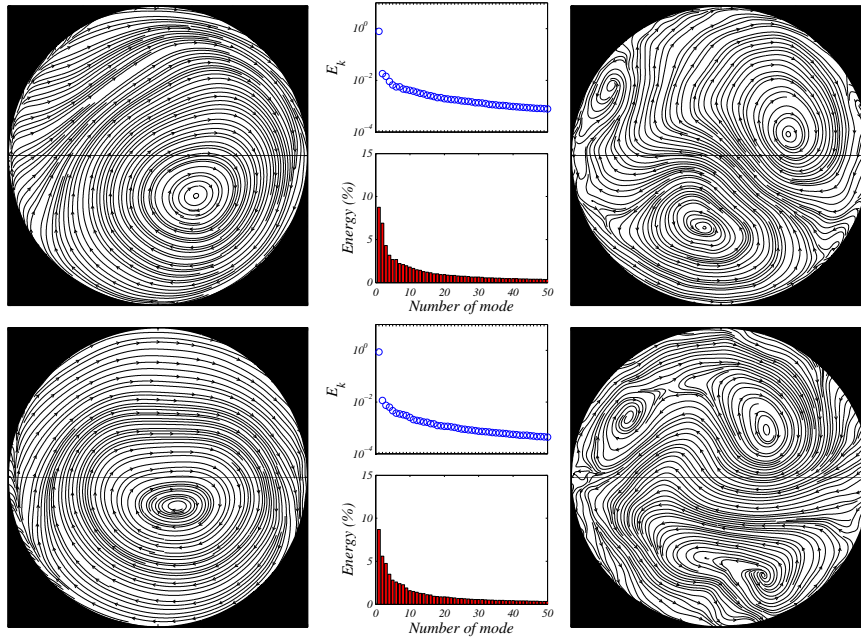


FIGURE 17. The first two POD modes for the: $S = 0.85, 1.2$ swirl flow cases from top to bottom with the secondary motion shown as streamlines. The subplots in the middle of each mode show the eigenvalues (*top*) and the relative energy excluding the 0-mode (*bottom*) of the first 50 modes.

swirling motion being substantially more dominant than the Dean vortices (as can be seen in the mean velocity and vorticity fields in figures 14, 15) POD was thought to be a useful tool in order to decompose the flow field and rank the obtained topo-modes by energy content. It is expected, that the swirling motion –as the most energetic structure– will be the dominating feature in the 0-mode which represents the mean field and any other coherent structure –if existing– should be depicted in the following modes which represent the fluctuating part of the flow.

Figures 16 & 17 show both the 0-mode and the first mode for each one of the swirl flow cases introduced in § 5.1. Additionally the eigenvalues are plotted for the first 50 modes as well as the relative energy content of the fluctuating part of the flow field (excluding the 0-mode). This represents also the relative turbulent kinetic energy (TKE) scaled by the total. In all cases it can be seen that the mean field is represented well by the 0-mode. Regarding the energy content, it is not unexpected that this mode contains most of the energy, with substantial difference from the other modes and it can be seen that by increasing the swirl rate, the energy content of the respective 0-mode increases. It can be mentioned that the relative energy content for

the $S = 0.1$ case was 70%, rising to 90% for the $S = 1.2$ case. Moreover, the number of modes needed to reach 95% of the total energy was found to be significantly lower for that swirl rate, with a difference of 200 modes between the lowest and highest swirl number flow cases. That shows that the swirling motion contributes greatly to the total energy of the flow field, constituting also the most energetic structure.

For the second topo-mode, various vortical structures appear in all the swirling flow cases, showing first that coherent structures seem to exist in the flow field other than the swirl but have been drifted by the large scale motion. Those structures have a relative TKE of 8 – 13%, depending on the swirl case. The structures resemble shape-wise, in most of the cases, the Dean vortices even though they are not as well structured. Moreover in most of the cases the vortices seem to have been rotated in reference to the plane of symmetry either in the clockwise or anti-clockwise direction.

5.3. Visualizing the very-large-scale motion (VLSM) in swirling turbulent bent pipe flow

Large structures of wavelengths more than $8R$ have been reported in literature for turbulent pipe flows (Guala *et al.* 2006). Those structures are highly energetic and previous work (Hellström *et al.* 2011a) has shown that POD can be used as a tool for the identification and visualization of the very-large-structures from PIV data of turbulent pipe flow.

Here, the same procedure as proposed in (Hellström *et al.* 2011a) is applied on the data in order to examine the effect of the imposed swirling motion on the long meandering structures. Figure 18 shows contour plots of both the instantaneous and reconstructed streamwise velocity fluctuations for different swirl numbers, constructed by using Taylor's hypothesis of frozen turbulence. The velocity fluctuations are captured at a wall distance of $1 - r/R = 0.15$. The cylindrical plane is unrolled in order to view the velocity fluctuations in cartesian coordinates. The distances are scaled with the pipe radius, and the velocity fluctuations are scaled with the bulk speed.

The structures for the non-swirling case are long spanning a streamwise distance of about $5R$ and their characteristics can be captured by superposition of only the 15 most energetic modes. Comparing the present data with those from turbulent flow in a straight pipe (Hellström *et al.* 2011a) it can be observed that the structures are slightly inclined. In Hellström *et al.* (2011b) no significant differences between the straight and pipe bend case were reported, but it should be kept in mind that the two studies (the present one and Hellström *et al.* (2011b)) were taken at different downstream distances from the bend. The data shown here consider a shorter distance from the bend than in the results shown in (Hellström *et al.* 2011b), therefore the centrifugal effects are expected to act stronger on the different flow features. To highlight the high energy of the streaky patterns as well as visualize more clearly the curvature effects on the them, the velocity fluctuations have been reconstructed by using decreasing number of modes. Figure 19a shows the VLSM reconstructed from six modes. Their motion has been captured even in that case which agrees with the conclusions drawn in Hellström *et al.* (2011b) where it was shown that when the most energetic modes are superimposed, a meandering character is revealed even with few modes. Figure 19b shows in conjunction with what has been mentioned in this

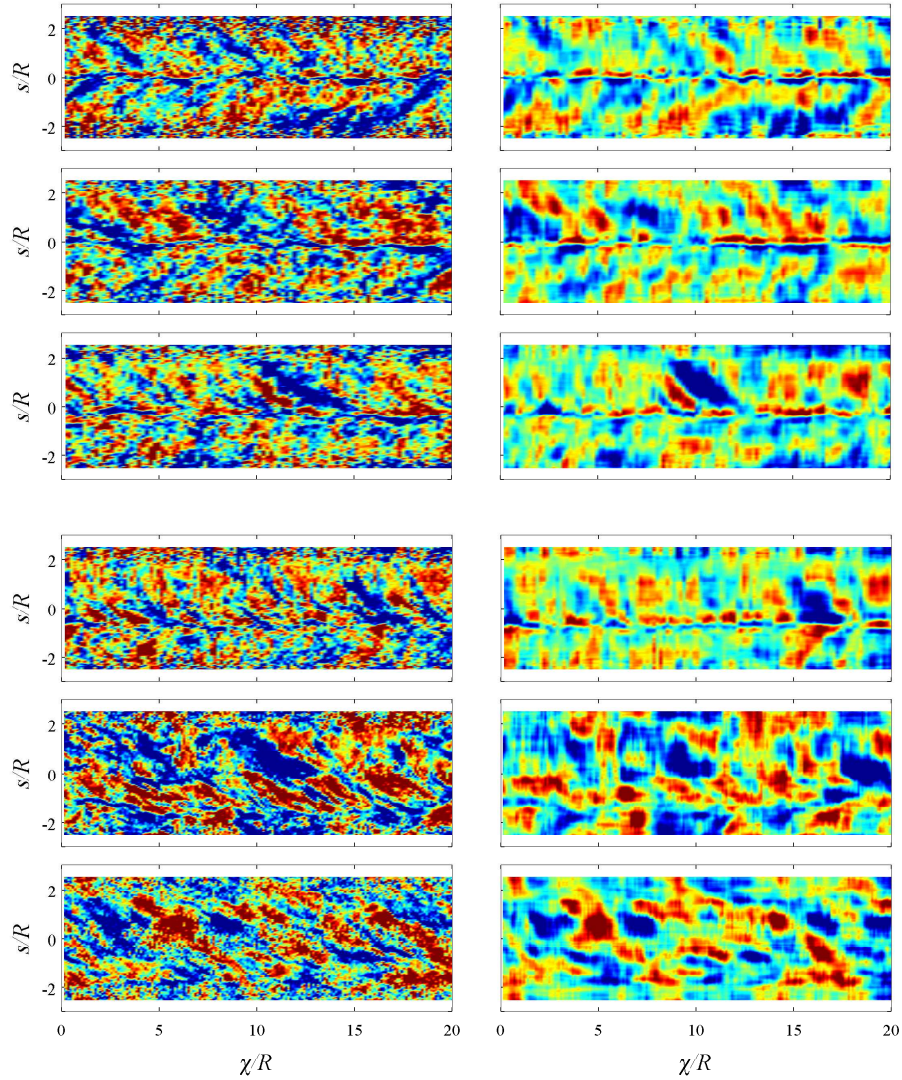


FIGURE 18. Contour plots of the instantaneous streamwise velocity fluctuations (*left subplots*) and the reconstructed ones using 15 POD modes (*right subplots*) at $1 - r/R = 0.15$ scaled by the bulk speed, for $S = 0, 0.1, 0.3, 0.5, 0.85$ and 1.2 (*from top to bottom*) constructed using Taylor's hypothesis.

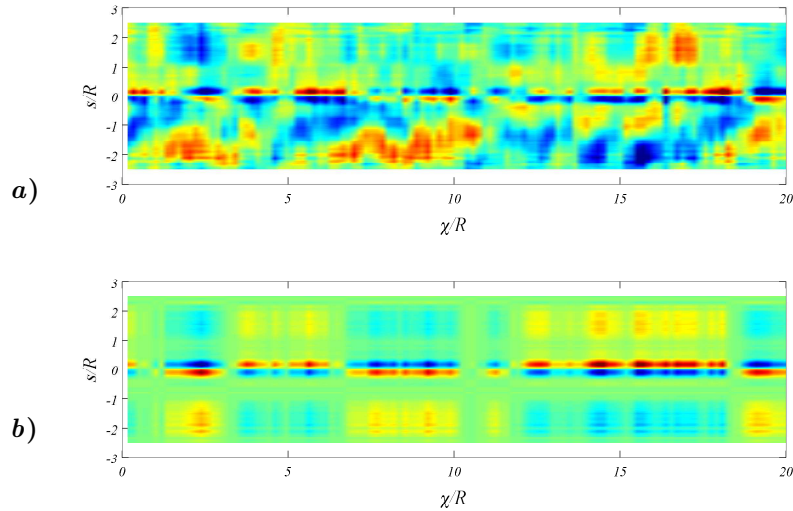


FIGURE 19. Contour plots of the streamwise velocity fluctuations at $1 - r/R = 0.15$ scaled by the bulk speed, for $S = 0$ and using a) 6 modes and b) the first POD mode for the reconstruction.

paragraph, the structures reconstructed by using only the first (and most energetic) mode. Here, the structures do not appear as horizontally-oriented as in a straight pipe flow (Hellström *et al.* 2011b; Guala *et al.* 2006) but are inclined. This can be an effect from the curvature which causes the structures to change direction of motion. Further analysis on this matter will be performed in the future and it is of specific interest to examine how the structures develop from a downstream distance from the bend.

For the swirling flow cases the structures are observed to exhibit an increasing tilting character with increasing swirl number which is caused by the change in the mean flow direction (see also figure 14). As the swirl intensity increases slightly ($S = 0.1$) no significant changes are evident with only a slight tilting effect on them. On the other hand, the streaks are seen to significantly reduce in length and increase in width for the two higher swirl numbers, indicating that the swirl motion is tearing up the elongated structures. Similar observations have been reported also in the numerical analysis by Nygård & Andersson (2009) where the effects of swirl on turbulent flow in a straight pipe were investigated.

While there have been observed changes in the structures' orientation due to the centrifugal effects (see also figure 19), as the swirl number increases the results resemble closely those reported for a straight pipe flow (Nygård & Andersson 2009). This underlines also the stabilizing effect of the swirling motion on the flow which has

been also observed in the mean field results of straight and bent pipe flows (Facciolo 2006; Sattarzadeh 2011).

6. Summary & Conclusions

Results from turbulent swirling flow at the exit of a 90° curved pipe have been presented for a wide range of swirl numbers. The effect of the swirling motion on the Dean vortices has been examined by combining TS-PIV data and POD analysis. POD has been used as a powerful tool to extract the most energetic structures in the flow field and succeeded to reveal both the unsteady behavior of the vortices under turbulent non-swirling flow conditions and the coherent structures underlying the swirling motion.

In particular, for the non-swirling turbulent flow case, similar behavior to that of the so-called “swirl-switching” phenomenon was captured by reconstructing the original snapshots with only few of the most energetic modes. The frequency at which the two vortices switch position alternatively could be determined by combining spectral analysis of the reconstructed time series and the POD coefficient which has been shown to detect periodicities in the flow in a previous work (Semeraro 2011). A dominant peak at about $St = 0.1$ was depicted in both spectra, indicating the high frequency fluctuations in the tangential velocity time-series while a lower Strouhal number was found to be associated with the low velocity variations resembling a periodic motion.

For the swirling turbulent flow, three approaches to investigate the effects of it on different features of the flow field were presented. First, results from mean velocity and streamwise vorticity fields were illustrated in order to visualize and quantify the effect of the swirl on the flow field. Even for the lowest swirl number shown here, the stabilizing effect of the swirl is evident, moving the high speed fluid from the outer wall to the centre of the pipe. Axi-symmetry of the flow field is gradually achieved with increasing swirl number, as one of the Dean vortices with the same rotational direction as the imposed motion, drifts away and merges with the other vortex resulting in a single large scale motion located almost at the centre of the pipe for the swirl dominated flow field.

As a second approach, the existence of underlying coherent structures in the swirling flow field was investigated by analyzing the most energetic POD modes. Last, the VLSM in turbulent swirling flow through a bend were visualized and their shape and behavior were explained in conjunction to works in turbulent, mainly straight, pipe flows existing in literature (Nygård & Andersson 2009; Hellström *et al.* 2011*b,a*). An effect of the pipe bend can be seen as an inclination of the structures due to the change in the direction of the fluid motion. The effect of increasing swirl intensity is seen to mainly concentrate on the tearing up of the elongated structures which has also been reported for DNS in swirling flow in a straight pipe (Nygård & Andersson 2009).

The present work constitutes a preliminary investigation into the dynamics of turbulent swirling flow through pipe bends which is apparent both in industry and nature. POD has been deemed a powerful tool for the characterization of the large scale structures in such a flow and will be used for further analysis in the future.

The data and results are further aimed to serve as a unique database for future collaborations with numerical simulations.

Acknowledgements

Dr. Ramis Örlü is greatly acknowledged for comments on the manuscript. The author would also like to thank Tekn.Lic. Onofrio Semeraro for the fruitful discussions on modal analysis and for pointing out the convergence test of the autocovariance matrix.

References

- AGRAWAL, A. 2005 Measurement of spectrum with particle image velocimetry. *Exp. Fluids* **39**, 836–840.
- ANWER, M. & SO, R. M. C. 1993 Swirling turbulent flow through a curved pipe. Part 1: Effect of swirl and bend curvature. *Exp. Fluids* **14**, 85–96.
- BRÜCKER, C. 1998 A time-recording DPIV-Study of the swirl switching effect in a 90° bend flow. *Proc. 8th Int. Symp. Flow Vis., 1-4 Sept., Sorrento (NA), Italy* pp. 171.1–171.6.
- DEAN, W. R. 1927 Note on the motion of fluid in a curved pipe. *Phil. Mag.* **4**, 208–223.
- FACCIOLO, L. 2006 A study on axially rotating pipe and swirling jet flows. *PhD thesis, KTH Mechanics, Stockholm, Sweden.*
- FACCIOLO, L., TILLMARK, N., TALAMELLI, A. & ALFREDSSON, P. H. 2007 A study of swirling turbulent pipe and jet flows. *Phys. Fluids* **19**, 035105.
- GRAFTIEAUX, L., MICHARD, M. & GROSJEAN, N. 2001 Combining PIV, POD and vortex identification algorithms for the study of unsteady turbulent swirling flows. *Meas. Sci. Technol.* **12**, 1422–1429.
- GUALA, M., HOMMEMA, S. E. & ADRIAN, R. J. 2006 Large-scale and very-large-scale motions in turbulent pipe flow. *J. Fluid Mech.* **554**, 521–542.
- GUPTA, A. K., LILLEY, D. G. & SYRED, N. 1985 Swirl flows. *ABACUS Press, Cambridge, USA.*
- GURKA, R., LIBERZON, A. & HETSRONI, G. 2006 POD of vorticity fields: A method for spatial characterization of coherent structures. *Int. J. Heat Fluid Flow* **27**, 416–423.
- HELLSTRÖM, F. 2010 Numerical computations of the unsteady flow in turbochargers. *PhD thesis, KTH Mechanics, Stockholm, Sweden.*
- HELLSTRÖM, L. H. O., SINHA, A. & SMITS, A. 2011a Visualizing the very-large-scale motions in turbulent pipe flow. *Phys. Fluids* **23**, 011703.
- HELLSTRÖM, L. H. O., ZLATINOV, M. & SMITS, A. 2011b Turbulent pipe flow through a 90° bend. *7th Int. Symp. on Turbulence and Shear Flow Phenomena, 28-31 July, Ottawa, Canada.*
- IMAO, S., ITOH, M. & HARADA, T. 1996 Turbulent characteristics of the flow in an axially rotating pipe. *Int. J. Heat Fluid Flow* **17**, 444–451.

- KALPAKLI, A., ÖRLÜ, R. & ALFREDSSON, P. H. 2011 Dean vortices in turbulent flows: rocking or rolling? *J. Vis.* **15**, 37–38.
- LUMLEY, J. L. 1971 Stochastic tools in turbulence. *Academic Press, New York*.
- MALIN, M. R. & YOUNIS, B. A. 1997 The prediction of turbulent transport in an axially rotating pipe. *Int. Comm. Heat Mass Transfer* **24**, 89–98.
- MCKEON, B. J., ZAGAROLA, M. V. & SMITS, A. 2005 A new friction factor relationship for fully developed pipe flow. *J. Fluid Mech.* **538**, 429–443.
- MEYER, K., PEDERSEN, J. M. & ÖZCAN, O. 2007 A turbulent jet in crossflow analysed with proper orthogonal decomposition. *J. Fluid Mech.* **583**, 199–227.
- NYGÅRD, F. & ANDERSSON, H. I. 2009 DNS of swirling turbulent pipe flow. *International Journal for Numerical Methods in Fluids* **64**, 945–972.
- ONO, A., KIMURA, N., KAMIDE, H. & TOBITA, A. 2010 Influence of elbow curvature on flow structure at elbow outlet under high Reynolds number condition. *Nuclear Eng. Design* **241**, 4409–4419.
- ORLANDI, P. & FATICA, M. 1997 Direct simulations of turbulent flow in a pipe rotating about its axis. *J. Fluid Mech.* **343**, 43–72.
- ÖRLÜ, R. 2009 Experimental studies in jet flows and zero pressure-gradient turbulent boundary layers. *PhD thesis, KTH Mechanics, Stockholm, Sweden*.
- PRASAD, A. K. & JENSEN, K. 1995 Scheimpflug stereocamera for particle image velocimetry in liquid flows. *Appl. Optics* **34**, 7092–7099.
- PRUVOST, J., LEGRAND, J. & LEGENTILHOMME, P. 2004 Numerical investigation of bend and torus flows, part I: effect of swirl motion on flow structure in U-bend. *Chem. Eng. Sc.* **59**, 3345–3357.
- RÜTTEN, F., SCHRÖDER, W. & MEINKE, M. 2005 Large-eddy simulation of low frequency oscillations of the Dean vortices in turbulent pipe bend flows. *Phys. Fluids* **17**, 035107.
- SAKAKIBARA, J., SONOBE, R., GOTO, H., TEZUKA, H., TADA, H. & TEZUKA, K. 2010 Stereo-PIV study of turbulent flow downstream of a bend in a round pipe. *14th Int. Symp. Flow Vis., 21-24 June, EXCO Daegu, Korea* pp. 1–11.
- SATTARZADEH, S. S. 2011 Experimental study of complex pipe flows. *Master thesis, KTH Mechanics, Stockholm, Sweden*.
- SEMERARO, O. 2011 Feedback control and modal structures in transitional shear flows. *Licentiate thesis, KTH Mechanics, Stockholm, Sweden*.
- SHIMIZU, Y. & SUGINO, K. 1980 Hydraulic losses and flow patterns of a swirling flow in U-bends. *JSME* **23**, 1443–1450.
- SIROVICH, L. 1987 Turbulence and the dynamics of coherent structures. Part 1: Coherent structures. *Quart. Appl. Math.* **45**, 561–571.
- SO, R. M. C. & ANWER, M. 1993 Swirling turbulent flow through a curved pipe. Part 2: Recovery from swirl and bend curvature. *Exp. Fluids* **14**, 169–177.
- TAKAMURA, H., KONNO, H., HASHIZUME, H., AIZAWA, K. & YAMANO, H. 2011 PIV measurements of a complex turbulent flow in a short elbow piping under a high Reynolds number condition. *9th Int. Symposium on Particle Image Velocimetry, July 21-23, Kobe, Japan*.
- TUNSTALL, M. J. & HARVEY, J. K. 1968 On the effect of a sharp bend in a fully developed turbulent pipe-flow. *J. Fluid Mech.* **34**, 595–608.

- WESTERWEEL, J. 1994 Efficient detection of spurious vectors in particle image velocimetry data. *Exp. Fluids* **16**, 236–247.
- WIENEKE, B. 2005 Stereo-PIV using self-calibration on particle images. *Exp. Fluids* **39**, 267–280.
- WILLERT, C. E. 2006 Assessment of camera models for use in planar velocimetry calibration. *Exp. Fluids* **41**, 135–143.
- YUKI, K., HASEGAWA, S., SATO, T., HASHIZUME, H., AIZAWA, K. & YAMANO, H. 2011 Matched refractive-index PIV visualization of complex flow structure in a three-dimensionally connected dual elbow. *Nuclear Eng. Design* **241**, 4544–4550.